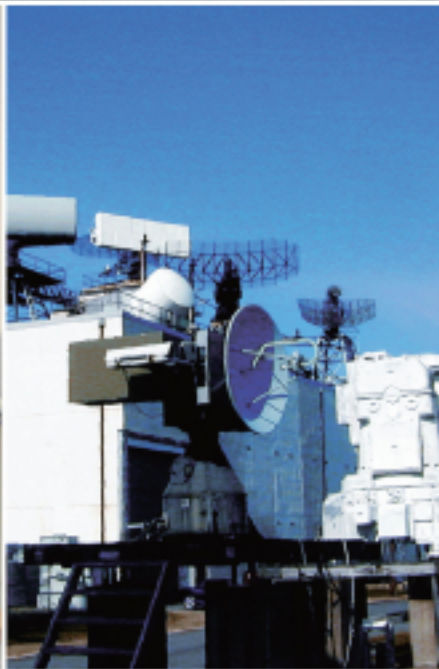
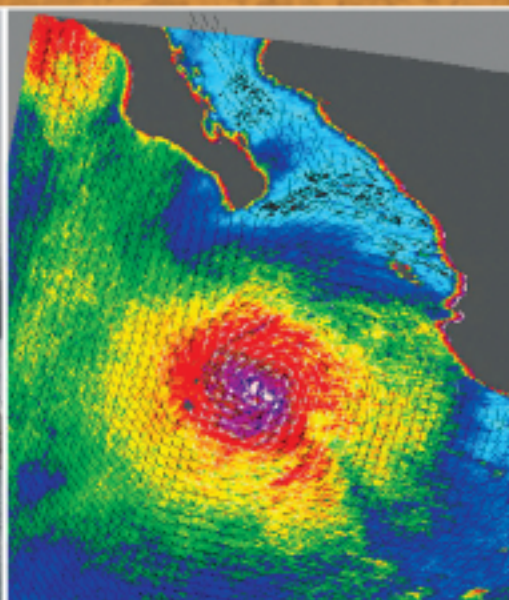


# PRINCIPLES OF MODERN RADAR

## BASIC PRINCIPLES



Mark A. Richards, James A. Scheer, William A. Holm (Editors)

# **Principles of Modern Radar**



# Principles of Modern Radar

## Vol. I: Basic Principles

Mark A. Richards  
Georgia Institute of Technology

James A. Scheer  
Georgia Institute of Technology

William A. Holm  
Georgia Institute of Technology



Raleigh, NC  
[scitechpub.com](http://scitechpub.com)



Published by SciTech Publishing, Inc.  
911 Paverstone Drive, Suite B  
Raleigh, NC 27615  
(919) 847-2434, fax (919) 847-2568  
scitechpublishing.com

Copyright © 2010 by SciTech Publishing, Raleigh, NC. All rights reserved.

No part of this publication may be reproduced, stored in a retrieval system or transmitted in any form or by any means, electronic, mechanical, photocopying, recording, scanning or otherwise, except as permitted under Sections 107 or 108 of the 1976 United States Copyright Act, without either the prior written permission of the Publisher, or authorization through payment of the appropriate per-copy fee to the Copyright Clearance Center, 222 Rosewood Drive, Danvers, MA 01923, (978) 750-8400, fax (978) 646-8600, or on the web at [copyright.com](http://copyright.com). Requests to the Publisher for permission should be addressed to the Publisher, SciTech Publishing, Inc., 911 Paverstone Drive, Suite B, Raleigh, NC 27615, (919) 847-2434, fax (919) 847-2568, or email [editor@scitechpub.com](mailto:editor@scitechpub.com).

The publisher and the author make no representations or warranties with respect to the accuracy or completeness of the contents of this work and specifically disclaim all warranties, including without limitation warranties of fitness for a particular purpose.

Editor: Dudley R. Kay  
Editorial Assistant: Katie Janelle  
Production Manager: Robert Lawless  
Typesetting: MPS Limited, A Macmillan Company  
Cover Design: Brent Beckley  
Printer: Sheridan Books, Inc., Chelsea, MI

This book is available at special quantity discounts to use as premiums and sales promotions, or for use in corporate training programs. For more information and quotes, please contact the publisher.

Printed in the United States of America  
10 9 8 7 6 5 4 3 2 1

ISBN: 978-1-891121-52-4

**Library of Congress Cataloging-in-Publication Data**

Richards, M. A. (Mark A.), 1952-  
Principles of modern radar / Mark A. Richards, James A. Scheer, William A. Holm.  
p. cm.  
Includes bibliographical references and index.  
ISBN 978-1-891121-52-4 (hardcover : alk. paper)  
I. Scheer, Jim, 1944- II. Holm, William A. III. Title.  
TK6575.R473 2010  
621.3848-dc22

2010013808

Dedicated to the many students of Georgia Tech's professional education course *Principles of Modern Radar*, who inspired this book's development;  
and  
to our wives, Theresa, Ruby, and Kathleen, who inspire us.



# Brief Contents

**Preface xvii**

**Publisher Acknowledgments xxiv**

**Editors and Contributors xxvii**

**List of Acronyms xxxi**

**List of Common Symbols xxxiv**

## **PART I Overview**

- 1 Introduction and Radar Overview 3**
- 2 The Radar Range Equation 59**
- 3 Radar Search and Overview of Detection in Interference 87**

## **PART II External Factors**

- 4 Propagation Effects and Mechanisms 117**
- 5 Characteristics of Clutter 165**
- 6 Target Reflectivity 211**
- 7 Target Fluctuation Models 247**
- 8 Doppler Phenomenology and Data Acquisition 273**

## **PART III Subsystems**

- 9 Radar Antennas 309**
- 10 Radar Transmitters 347**
- 11 Radar Receivers 391**
- 12 Radar Exciters 417**
- 13 The Radar Signal Processor 459**

## **PART IV Signal and Data Processing**

- 14 Digital Signal Processing Fundamentals for Radar 495**
- 15 Threshold Detection of Radar Targets 547**
- 16 Constant False Alarm Rate Detectors 589**
- 17 Doppler Processing 625**
- 18 Radar Measurements 677**
- 19 Radar Tracking Algorithms 713**
- 20 Fundamentals of Pulse Compression Waveforms 773**
- 21 An Overview of Radar Imaging 835**

**Appendix A: Maxwell's Equations and Decibel Notation 893**

**Appendix B: Answers to Selected Problems 899**

**Index 905**



# Contents

Preface	xvii
Publisher Acknowledgments	xxiv
Editors and Contributors	xxvii
List of Acronyms	xxxii
List of Common Symbols	xxxiv

## **PART I** Overview

---

<b>1</b>	Introduction and Radar Overview	3
1.1	Introduction	3
1.2	The Radar Concept	4
1.3	The Physics of EM Waves	5
1.4	Interaction of EM Waves with Matter	11
1.5	Basic Radar Configurations and Waveforms	18
1.6	Noise, Signal-to-Noise Ratio, and Detection	25
1.7	Basic Radar Measurements	27
1.8	Basic Radar Functions	33
1.9	Radar Applications	36
1.10	Organization of This Text	54
1.11	Further Reading	55
1.12	References	55
1.13	Problems	56
<hr/>		
<b>2</b>	The Radar Range Equation	59
2.1	Introduction	59
2.2	Power Density at a Distance $R$	61
2.3	Received Power from a Target	62
2.4	Receiver Thermal Noise	64
2.5	Signal-to-Noise Ratio and the Radar Range Equation	66
2.6	Multiple-Pulse Effects	66
2.7	Summary of Losses	67
2.8	Solving for Other Variables	72

2.9	Decibel Form of the Radar Range Equation	72
2.10	Average Power Form of the Radar Range Equation	73
2.11	Pulse Compression: Intrapulse Modulation	74
2.12	A Graphical Example	75
2.13	Clutter as the Target	76
2.14	One-Way (Link) Equation	78
2.15	Search Form of the Radar Range Equation	79
2.16	Track Form of the Radar Range Equation	80
2.17	Some Implications of the Radar Range Equation	83
2.18	Further Reading	84
2.19	References	84
2.20	Problems	85

---

3	Radar Search and Overview of Detection in Interference	87
3.1	Introduction	87
3.2	Search Mode Fundamentals	89
3.3	Overview of Detection Fundamentals	95
3.4	Further Reading	111
3.5	References	111
3.6	Problems	112

---

**PART II**    **External Factors**

---

4	Propagation Effects and Mechanisms	117
4.1	Introduction	117
4.2	Propagation Factor	118
4.3	Propagation Paths and Regions	119
4.4	Atmospheric Attenuation and Absorption	121
4.5	Atmospheric Refraction	130
4.6	Turbulence	137
4.7	Exploiting the Ionosphere	138
4.8	Diffraction	140
4.9	Multipath	142
4.10	Skin Depth and Penetration: Transmitting Through Walls	156
4.11	Commercial Simulations	158
4.12	Summary and Further Reading	160
4.13	References	161
4.14	Problems	163

---

<b>5</b>	<b>Characteristics of Clutter</b>	<b>165</b>
<b>5.1</b>	Introduction and Definitions	165
<b>5.2</b>	General Characteristics of Clutter	172
<b>5.3</b>	Clutter Modeling	202
<b>5.4</b>	Concluding Remarks	206
<b>5.5</b>	Further Reading	207
<b>5.6</b>	References	207
<b>5.7</b>	Problems	210

---

<b>6</b>	<b>Target Reflectivity</b>	<b>211</b>
<b>6.1</b>	Introduction	211
<b>6.2</b>	Basic Reflection Physics	212
<b>6.3</b>	Radar Cross Section Definition	219
<b>6.4</b>	Three Scattering Regimes	224
<b>6.5</b>	High-Frequency Scattering	227
<b>6.6</b>	Examples	236
<b>6.7</b>	Further Reading	244
<b>6.8</b>	References	244
<b>6.9</b>	Problems	245

---

<b>7</b>	<b>Target Fluctuation Models</b>	<b>247</b>
<b>7.1</b>	Introduction	247
<b>7.2</b>	Radar Cross Section of Simple Targets	248
<b>7.3</b>	Radar Cross Section of Complex Targets	251
<b>7.4</b>	Statistical Characteristics of the RCS of Complex Targets	253
<b>7.5</b>	Target Fluctuation Models	263
<b>7.6</b>	Doppler Spectrum of Fluctuating Targets	267
<b>7.7</b>	Further Reading	269
<b>7.8</b>	References	269
<b>7.9</b>	Problems	270

---

<b>8</b>	<b>Doppler Phenomenology and Data Acquisition</b>	<b>273</b>
<b>8.1</b>	Introduction	273
<b>8.2</b>	Doppler Shift	274
<b>8.3</b>	The Fourier Transform	276
<b>8.4</b>	Spectrum of a Pulsed Radar Signal	277
<b>8.5</b>	Why Multiple Pulses?	286

- 8.6 Pulsed Radar Data Acquisition 287
- 8.7 Doppler Signal Model 291
- 8.8 Range-Doppler Spectrum for a Stationary Radar 293
- 8.9 Range-Doppler Spectrum for a Moving Radar 296
- 8.10 Further Reading 303
- 8.11 References 303
- 8.12 Problems 303

---

**PART III Subsystems**

---

**9 Radar Antennas 309**

- 9.1 Introduction 309
- 9.2 Basic Antenna Concepts 310
- 9.3 Aperture Tapers 314
- 9.4 Effect of the Antenna on Radar Performance 317
- 9.5 Monopulse 320
- 9.6 Reflector Antennas 322
- 9.7 Phased Array Antennas 326
- 9.8 Array Architectures 339
- 9.9 Further Reading 343
- 9.10 References 343
- 9.11 Problems 345

---

**10 Radar Transmitters 347**

- 10.1 Introduction 347
- 10.2 Transmitter Configurations 351
- 10.3 Power Sources and Amplifiers 356
- 10.4 Modulators 371
- 10.5 Power Supplies 373
- 10.6 Transmitter Impacts on the Electromagnetic Environment 375
- 10.7 Operational Considerations 381
- 10.8 Summary and Future Trends 384
- 10.9 Further Reading 385
- 10.10 References 385
- 10.11 Problems 388

---

**11 Radar Receivers 391**

- 11.1 Introduction 391
- 11.2 Summary of Receiver Types 392

- 11.3 Major Receiver Functions 396
  - 11.4 Demodulation 400
  - 11.5 Receiver Noise Power 404
  - 11.6 Receiver Dynamic Range 406
  - 11.7 Analog-to-Digital Data Conversion 409
  - 11.8 Further Reading 414
  - 11.9 References 414
  - 11.10 Problems 415
- 

## 12 Radar Exciters 417

- 12.1 Introduction 417
  - 12.2 Exciter-Related Radar System Performance Issues 418
  - 12.3 Exciter Design Considerations 429
  - 12.4 Exciter Components 440
  - 12.5 Timing and Control Circuits 452
  - 12.6 Further Reading 454
  - 12.7 References 454
  - 12.8 Problems 455
- 

## 13 The Radar Signal Processor 459

- 13.1 Introduction 459
  - 13.2 Radar Processor Structure 460
  - 13.3 Signal Processor Metrics 462
  - 13.4 Counting FLOPS: Estimating Algorithm Computational Requirements 464
  - 13.5 Implementation Technology 472
  - 13.6 Fixed Point versus Floating Point 480
  - 13.7 Signal Processor Sizing 482
  - 13.8 Further Reading 488
  - 13.9 References 488
  - 13.10 Problems 491
- 

## **PART IV** Signal and Data Processing

---

## 14 Digital Signal Processing Fundamentals for Radar 495

- 14.1 Introduction 495
- 14.2 Sampling 496
- 14.3 Quantization 504
- 14.4 Fourier Analysis 506

<b>14.5</b>	The $z$ Transform	522
<b>14.6</b>	Digital Filtering	523
<b>14.7</b>	Random Signals	532
<b>14.8</b>	Integration	536
<b>14.9</b>	Correlation as a Signal Processing Operation	538
<b>14.10</b>	Matched Filters	540
<b>14.11</b>	Further Reading	543
<b>14.12</b>	References	543
<b>14.13</b>	Problems	544
<hr/>		
<b>15</b>	Threshold Detection of Radar Targets	547
<b>15.1</b>	Introduction	547
<b>15.2</b>	Detection Strategies for Multiple Measurements	548
<b>15.3</b>	Introduction to Optimal Detection	552
<b>15.4</b>	Statistical Models for Noise and Target RCS in Radar	557
<b>15.5</b>	Threshold Detection of Radar Signals	560
<b>15.6</b>	Further Reading	584
<b>15.7</b>	References	584
<b>15.8</b>	Problems	585
<hr/>		
<b>16</b>	Constant False Alarm Rate Detectors	589
<b>16.1</b>	Introduction	589
<b>16.2</b>	Overview of Detection Theory	590
<b>16.3</b>	False Alarm Impact and Sensitivity	592
<b>16.4</b>	CFAR Detectors	593
<b>16.5</b>	Cell Averaging CFAR	597
<b>16.6</b>	Robust CFARs	607
<b>16.7</b>	Algorithm Comparison	616
<b>16.8</b>	Adaptive CFARs	618
<b>16.9</b>	Additional Comments	619
<b>16.10</b>	Further Reading	620
<b>16.11</b>	References	620
<b>16.12</b>	Problems	622
<hr/>		
<b>17</b>	Doppler Processing	625
<b>17.1</b>	Introduction	625
<b>17.2</b>	Review of Doppler Shift and Pulsed Radar Data	626
<b>17.3</b>	Pulsed Radar Doppler Data Acquisition and Characteristics	627

- 17.4 Moving Target Indication 629
- 17.5 Pulse-Doppler Processing 644
- 17.6 Clutter Mapping and the Moving Target Detector 665
- 17.7 Pulse Pair Processing 668
- 17.8 Further Reading 673
- 17.9 References 673
- 17.10 Problems 674

---

## 18 Radar Measurements 677

- 18.1 Introduction 677
- 18.2 Precision and Accuracy in Radar Measurements 678
- 18.3 Radar Signal Model 683
- 18.4 Parameter Estimation 685
- 18.5 Range Measurements 690
- 18.6 Phase Measurement 695
- 18.7 Doppler and Range Rate Measurements 696
- 18.8 RCS Estimation 699
- 18.9 Angle Measurements 700
- 18.10 Coordinate Systems 709
- 18.11 Further Reading 710
- 18.12 References 710
- 18.13 Problems 711

---

## 19 Radar Tracking Algorithms 713

- 19.1 Introduction 713
- 19.2 Basics of Track Filtering 719
- 19.3 Kinematic Motion Models 746
- 19.4 Measurement Models 751
- 19.5 Radar Track Filtering 757
- 19.6 Measurement-to-Track Data Association 760
- 19.7 Performance Assessment of Tracking Algorithms 766
- 19.8 Further Reading 767
- 19.9 References 768
- 19.10 Problems 770

---

## 20 Fundamentals of Pulse Compression Waveforms 773

- 20.1 Introduction 773
- 20.2 Matched Filters 774
- 20.3 Range Resolution 782

20.4	Straddle Loss	786
20.5	Pulse Compression Waveforms	787
20.6	Pulse Compression Gain	788
20.7	Linear Frequency Modulated Waveforms	789
20.8	Matched Filter Implementations	794
20.9	Sidelobe Reduction in an LFM Waveform	797
20.10	Ambiguity Functions	800
20.11	LFM Summary	808
20.12	Phase-Coded Waveforms	808
20.13	Biphase Codes	817
20.14	Polyphase Codes	824
20.15	Phase-Code Summary	829
20.16	Further Reading	830
20.17	References	830
20.18	Problems	833

---

<b>21</b>	<b>An Overview of Radar Imaging</b>	<b>835</b>
21.1	Introduction	835
21.2	General Imaging Considerations	837
21.3	Resolution Relationships and Sampling Requirements	843
21.4	Data Collection	852
21.5	Image Formation	856
21.6	Image Phenomenology	875
21.7	Summary	888
21.8	Further Reading	888
21.9	References	889
21.10	Problems	890

<b>Appendix A:</b>	<b>Maxwell's Equations and Decibel Notation</b>	<b>893</b>
A.1	Maxwell's Equations	893
A.2	The Ubiquitous dB	895
A.3	Reference	897

<b>Appendix B:</b>	<b>Answers to Selected Problems</b>	<b>899</b>
<b>Index</b>		<b>905</b>

# Preface

## Goals of the Book

As the editors of *Principles of Modern Radar: Basic Principles (POMR)*, we had two primary goals in mind when this book was conceived. Our first goal was to design *POMR* to become the “Radar 101” textbook of choice for the next generation of radar engineers, whether students in graduate engineering courses, new hires on the job, or retraining professionals in government and industry. Our second goal was to provide a breadth of topics and modern approach that would make *POMR* the most convenient and valuable starting point for today’s professionals needing to study or review a particular subject. To accomplish these twin goals, we needed to make several key trade-offs in designing the book:

1. Focus on modern techniques and systems from the start rather than historical background and legacy systems.
2. Strike a careful balance between quantitative mathematical models and tools and qualitative motivation and insight.
3. Carefully proportion the breadth of topics versus the depth of coverage of systems and external phenomenology.
4. Draw on the knowledge of a range of subject experts—and accept the intense editing effort needed to integrate their contributions into a coherent whole—versus the less comprehensive coverage but inherently consistent style and notation of just one or two authors.

What follows is a description of how these trade-offs were struck to achieve our goals.

Many in the radar community will recognize that *POMR* has evolved from the professional education short course of the same name taught to thousands of students by Georgia Tech research faculty since 1969. Some may even remember that the short course produced an earlier book, now out of print, by the same name.<sup>1</sup> This book is a completely new text, developed from scratch by 15 scientists and engineers working today with the most modern systems and techniques in radar technology. Each of these contributing authors brings a wealth of research and teaching experience to bear in explaining the fundamental concepts underlying all radar systems.

There are, of course, several very good books currently in use for college- and professional-level courses in radar systems and technology, so it is fair to ask why one should consider *POMR*. We believe the answer is fourfold:

- Comprehensiveness.
- Qualitative versus quantitative balance.
- Emphasis on the most modern topics and methods.
- Radar community support.

---

<sup>1</sup>Eaves, J.L., and Reedy, E.K., *Principles of Modern Radar*. Van Nostrand Reinhold, New York, 1987.

Most importantly, *POMR* provides a breadth of coverage unmatched by currently available introductory radar textbooks: chapters on fundamental concepts, propagation and echo phenomenology for targets and interference, all major subsystems of a modern radar, and all basic signal processing functions so important to modern practice. Second, these topics are presented both qualitatively and quantitatively, at a consistent level appropriate for advanced undergraduate and beginning graduate students and readers. No competing book of which we are aware strikes such a carefully constructed balance. Some competitors provide the traditional fundamental concepts but offer little on modern signal processing. Some are almost entirely descriptive, lacking the mathematical analysis students need to undertake their own analysis and modeling. A few others are highly mathematical but have limited coverage and lack the qualitative interpretation needed to develop the understanding of students new to the field. *POMR* not only provides the basic mathematical tools but also supports those tools with the explanations and insights of its experienced authors.

*POMR*'s focus on *modern* radar is evident in its choice of topics. For example, extensive coverage is given to increasingly popular phased array antennas due to their advanced capabilities. Coherent systems, a prerequisite to most interesting signal processing, are strongly emphasized throughout the text. Last and most importantly, because so much functionality in modern systems lies in the signal processing, a significant portion of the book is devoted to methods enabled by digital radar signal processing, from pulse compression and Doppler processing to tracking and imaging. This topic choice and organization results in coverage superior to any other "Radar 101" textbook, so that *POMR* provides the most solid foundation for students progressing to "Radar 102" texts on more advanced and specialized topics.

Finally, *POMR* benefits from an extraordinary vetting by the modern radar community. It is a joint effort among the text's highly experienced authors and editors; the publisher SciTech, with its radar focus and resulting contacts; and the volunteering global community of radar experts, mostly fellow radar instructors and radar authors. As a result, the 21 chapters have been reviewed for content and style by more than 50 radar professionals representing academia, the government and military, and commercial companies. Chapters were reviewed first in their draft versions and then again after revisions. *POMR*'s editors were assisted in integrating the many reviewer suggestions by "master reviewers," each of whom read most or all of the chapters and also "reviewed the reviews" to help coordinate the improvements and perfect the emphasis, topical flow, and consistency across chapters. This extensive process of peer review iterations within the radar community ensures that *POMR* meets the needs of students, educators, and professionals everywhere.

## Organization of Content

*POMR* is organized into four major parts: *Overview*, *The Radar Environment*, *Radar Subsystems*, and *Signal and Data Processing*. In teaching a technology area as broad as radar, it is difficult to design a topical sequence that proceeds in a straight line from start to finish without looking ahead or doubling back. The *Overview* section solves this problem by taking readers through a high-level first pass that familiarizes them with a range of fundamental radar concepts and issues, setting the stage for a more detailed examination in the remaining parts. Chapter 1 introduces basic concepts such as properties of electromagnetic waves, target and clutter echoes, monostatic and bistatic radar, and detection in noise. It

also illustrates the scope of radar technology by describing a wide range of military and commercial applications. Finally, Chapter 1 introduces some radar cultural information such as the “band” terminology (e.g., L-band, X-band) and the AN Nomenclature for U.S. military systems. Chapter 2 delves into that most fundamental mathematical model in radar, the radar range equation. The basic point target range equation is derived, and its implications are explored. The chapter then develops several of the common variants tailored to specific radar modes. Chapter 3 provides a closer look at the most fundamental radar task of search and detection, describing search processes and introducing the idea of statistical detection and the resulting importance of probabilities in evaluating radar performance.

Part 2, *The Radar Environment*, is one of the truly distinguishing features of *POMR*. Few, if any, introductory radar texts provide the breadth and depth of discussion of propagation effects and target and clutter characteristics found here. Chapter 4 introduces all major electromagnetic propagation phenomenology of importance to radar, from simple attenuation in various weather conditions to more complex issues such as refraction, diffraction, multipath, ducting, and over-the-horizon propagation. Chapter 5 summarizes the extensive data on modeling the reflectivity and Doppler characteristics of atmospheric, land, and sea clutter and presents many of the common mean reflectivity and statistical models needed for clutter analysis. Chapter 6 introduces the mechanisms of scattering and reflection and the concept of radar cross section for targets, while Chapter 7 describes the common statistical models for radar cross section needed to evaluate detection performance. Chapter 8 delves more deeply into Doppler shift, concentrating on typical characteristics of Doppler spectra for stationary and moving targets and radar platforms.

Part 3, *Radar Subsystems*, describes each of the major subsystems of a typical modern radar system. Chapter 9 describes radar antenna technology, starting with basic antenna concepts and relations and then describing classic monopulse and mechanically scanned antennas. Half of this chapter is devoted to modern phased arrays, with detailed discussion of array patterns, wideband effects, and array architectures. Chapter 10 describes radar transmitter technology, including high-powered thermionic (tube-type) noncoherent and coherent transmitters, as well as solid-state transmitter technology. Again, significant coverage is devoted to transmitter modules and feed architectures for modern phased arrays. This chapter also addresses spectrum allocation and transmitter reliability issues, topics not found in other introductory textbooks. Chapter 11 presents radar receiver technology, beginning with the most basic types and extending to multistage superheterodyne receivers. Noise and dynamic range issues are discussed, and both classical analog synchronous detectors as well as the increasingly popular direct sampling digital receiver techniques for coherent systems are described. The coverage of coherent exciters in Chapter 12 is unique in an introductory textbook but important in understanding the architecture of modern systems. Exciter performance issues are presented, followed by a discussion of the technology available to implement modern coherent radar exciters. The importance of maintaining low phase noise for pulse-Doppler systems is also explained. Another topic unique to this textbook is Chapter 13, which discusses radar digital signal processor technology. Metrics and procedures for estimating processor loading are introduced, followed by discussion of alternative implementation technologies such as custom integrated circuits, reconfigurable hardware, and exciting new techniques such as the use of graphical processing units for real-time signal processing.

Part 4, *Signal and Data Processing*, concentrates on the increasingly sophisticated techniques used to extract ever more information from radar signals using advanced digital signal and data processing. The first half of Part 4 deals with signal processing basics, detection, and clutter rejection. It begins in Chapter 14 with a succinct summary of digital signal processor fundamentals such as sampling, quantization, and data acquisition, followed by a thorough review of discrete Fourier analysis, including windowing and interpolation. Other sections refresh the reader on digital filters, properties of random signals, and the all-important matched filter concept and its connection to data integration. Chapter 15 returns to the topic of threshold detection first introduced in Chapter 3. Here, much more attention is given to details of coherent and noncoherent integration and alternative ways of using the available data. Neyman-Pearson detection and the Swerling models are introduced, leading to optimum detectors for radar signals. Albersheim's and Shnidman's equations are presented as convenient computational aids. Chapter 16 continues the discussion by introducing constant false alarm rate (CFAR) threshold detection, a practical requirement in real interference environments. The properties, performance, and shortcomings of the basic cell-averaging CFAR are discussed in depth, and then many of the common "robust" and "adaptive" CFAR variants are introduced and compared. Chapter 17 covers two major forms of Doppler processing for clutter reduction: moving target indication (MTI), and pulse-Doppler processing. The discussion of MTI includes blind speeds, staggered pulse repetition frequencies, and airborne MTI. The sections on pulse-Doppler processing introduce the important topics of blind zones and ambiguity resolution. This chapter also includes a brief discussion of the pulse-pair processing method widely used in weather radar.

In the second half of Part 4, the focus turns to postdetection position measurements and tracking as well as high-resolution techniques. Chapter 18 addresses position measurements in range, angle, and Doppler. Basic concepts of precision and accuracy lead to the introduction of the Cramèr-Rao lower bound on precision. Several estimators of range, Doppler shift, and angle are then introduced, and their performance is evaluated. This chapter leads naturally into an introduction to tracking algorithms in Chapter 19. After a discussion of basic parameter estimation and some of the data association and resolution problems that complicate radar tracking, a number of tracking algorithms are introduced, from the basic  $\alpha-\beta$  tracker to the Kalman filter. Chapters 20 and 21 introduce the techniques needed to achieve high-resolution radar imaging. Chapter 20 describes pulse compression for high-range resolution. The matched filter is investigated in more depth and is then applied to the most common wideband waveforms, including linear frequency modulation or "chirp" and phase-coded waveforms ranging from Barker codes to a variety of polyphase codes. Methods of range sidelobe control are described, and the ambiguity function is introduced as a means of designing and understanding waveform properties. Finally, Chapter 21 provides an overview of synthetic aperture radar (SAR) imaging. SAR data collection is described, and general, widely applicable resolution and sampling equations are derived. While the range of SAR image formation algorithms is too extensive and too advanced for an introductory textbook, descriptions are given of the two extremes: Doppler beam sharpening, one of the simplest imaging algorithms; and backprojection, the current "gold standard" for advanced imaging. The chapter closes with a discussion of the unique phenomenology of SAR imaging, including layover, shadows, and speckle. Collectively, the extensive coverage of signal processing in Part 4 of *POMR* provides an excellent springboard to study of more advanced topics such as advanced SAR, space-time adaptive processing, and multiple-input multiple-output radar.

An appendix reviews two basic electrical engineering topics that are important for understanding radar but not deemed necessary for inclusion within the chapters: Maxwell's equations and the use of decibels in describing radar values.

## Features and Resources

*POMR* has been designed to ease the task of learning or teaching. Some of the features available to all readers include the following:

- Every chapter written by experts having “hands-on” experience in the design and development of radar systems.
- Every chapter reviewed by independent radar experts and edited by technical and publishing experts for content accuracy, level consistency, and readable style.
- Consistent notation and terminology employed throughout.
- Numerous illustrations integrated throughout, all newly drawn, clearly labeled, and carefully captioned.
- Table of common symbols and notation provided for quick reference.
- Table of acronyms, so plentiful in radar, presented alphabetically.
- Extensive, professionally prepared index facilitates reference use.
- At least 12 problems included in every chapter—over 250 total—to check and advance the student's understanding and capability. Answers to the odd-numbered problems are provided.

Several aids are available to adopting course instructors, with more being developed. The following aids can be obtained through request to SciTech at **[pomr@scitechpub.com](mailto:pomr@scitechpub.com)**:

- All problem answers and detailed solutions.
- All illustrations in the text in Microsoft PowerPoint sets or in high-resolution JPEG image formats for construction of custom viewgraphs.
- Copies of all equations in Microsoft Equation Editor format.

Several additional aids—tutorial simulations in MATLAB<sup>®2</sup> worked examples, additional problems for homework or exams—are expected to be available, and more are being developed and contributed by the radar community.

Publication of this first edition of *POMR* is just the first step in the development of a comprehensive set of resources for introducing radar systems and technology to a new generation of radar engineers. A website has been established to provide to readers these supporting materials, a complete and up-to-date list of reported errata, and an evolving set of new supplements. Visit the website periodically to check for the latest supplements and announcements:

**<http://www.scitechpub.com/pomr>**

---

<sup>2</sup>MATLAB is a registered trademark of The MathWorks, Inc. For MATLAB product information and cool user code contributions, go to <http://www.mathworks.com>, write The MathWorks, Inc., 3 Apple Hill Dr., Natick, MA 01760-2098 or call (508) 647-7101.

## Companion Publications

Several remarkable publications are planned to complement, augment, and extend the material in *POMR: Basic Principles*:

*Principles of Modern Radar: Advanced Techniques and Applications* edited by William L. Melvin and James A. Scheer (2011)

Building on *POMR: Basic Principles*, this sequel provides extensive coverage of both advanced techniques in radar and a wide variety of specific modern applications that integrate the fundamental technologies into complete systems. Examples of advanced techniques include advanced waveforms, stripmap and spotlight synthetic aperture imaging, space-time adaptive processing, multiple-input, multiple-output radar, polarimetry, target protection, and electronic protection. Applications discussed include airborne pulse-Doppler radar, space-based radar, weather radar, air traffic control, and passive and bistatic systems. Together, the two *POMR* volumes will provide integrated and comprehensive coverage of modern radar, from basic concepts to advanced systems, all in a coherent and consistent style and notation.

*Pocket Radar Guide: Key Radar Facts, Equations, and Data* by G. Richard Curry (2010)

A quick reference in shirt pocket size to the very most important and commonly used facts, figures, and tables in real-world radar engineering practice.

## Acknowledgments

*Principles of Modern Radar* could not have come into being without the dedicated efforts of many people. Each of our authors dedicated much personal time to contributing his or her individual chapters and then again to working with the entire *POMR* team to integrate the pieces into a whole that is greater than just the sum of those parts.

The authors were greatly aided by the reviewers and master reviewers. The complete list of reviewers is given in the “Publisher’s Acknowledgments” section and so won’t be repeated here, but every one of them had a direct hand in improving the final product in coverage, style, and correctness. Without their ability and willingness to critique the book based on their expert knowledge and their own experience with other introductory radar textbooks, we could not have achieved the level of consistency and coherency across such broad coverage and multiple authors. The authors and editors are greatly indebted to them for their efforts.

The entire *POMR* project might not have succeeded without the vision, support, and encouragement of SciTech Publishing and its president, Dudley Kay. SciTech is a wonderful asset to the radar community, and we hope this new book will add to that strength. Editorial assistant Katie Janelle managed the massive review process so important to *POMR*’s completion and quality. Production of a book is a complex endeavor requiring the efforts of many accomplished and dedicated staff. Robert Lawless is the production manager for *POMR*, responsible for managing the workflow and bringing together all the many pieces into the final product. Kristi Bennett, our copy editor, deserves great credit for bringing clarity, precision, and consistency to the writing styles of 15 authors. Freelancer Kathy Gagne conceived the eye-catching cover design. Brent Beckley has done an excellent job in marketing and promoting *POMR* so that it will reach and serve, we

hope, a large audience. All of the SciTech team has been professional and, at the same time, a pleasure to work with every step of the way.

## Errors and Suggestions

We have tried to bring the radar community a carefully constructed and truly valuable new introductory textbook and professional reference in *POMR*, but we recognize that there are always some residual errors and inconsistencies. In addition, experience in using *POMR* and new developments in the rapidly evolving field of radar will inevitably bring to light a need to clarify or expand some topics and introduce new ones.

The extensive review process used to develop *POMR* raised and resolved many, many such issues. Those that remain are the responsibility of the editors. We welcome the assistance of *POMR* readers in identifying errata and in making recommendations for improvements in future printings and editions. All identified errata will be posted in a timely fashion on the *POMR* SciTech web site (<http://www.scitechpub.com/pomr>), accessible to all users.

One of our hopes for *POMR* is that it will be adopted for use in university, professional education, and in-house training classes. There is nothing like teaching the material to newcomers to the field to quickly identify areas where the book could be improved. We invite all instructors using *POMR* to help us design the next edition by letting us know of your experience in using it and how it can be improved in the future.

**Mark A. Richards**

Georgia Institute of Technology  
Atlanta, GA  
mark.richards@ece.gatech.edu

**James A. Scheer**

Georgia Institute of Technology  
Atlanta, GA  
jim.scheer@gtri.gatech.edu

**William A. Holm**

Georgia Institute of Technology  
Atlanta, GA  
bill.holm@gatech.edu

# Publisher Acknowledgments

## Master Reviewers

Above and beyond the peer reviews focused on technical content, we recognized the need to bring consistency of level, notation, and writing style to an edited book composed of numerous expert contributions if we were to attain our goal of an outstanding textbook. From the initial rounds of reviews and follow-up conversations, SciTech determined which reviewers best understood our concerns, and we invited deeper involvement from them. The reviewers listed herein were called on to help resolve controversial and contradictory reviewer suggestions, to respond to editor and contributor problems, and, most of all, to work closely with SciTech as representatives of the radar community. The dedication of these “Master Reviewers” therefore merits our special recognition and appreciation.

**Dr. John Milan (radar consultant):** John brings more than 36 years of experience in radar systems at ITT, Gilfillan, and many years on the IEEE Aerospace and Electronic Systems Society Radar Systems Panel. He reviewed every chapter of the book for the sake of internal consistency and became the volunteer “master of figure captions,” assessing every one for descriptive completeness and clarity. As impressive to us as the volume of review work undertaken, equally remarkable was John’s response time to every request or question.

**Mr. Byron Edde (radar/electronic warfare consultant and short course instructor, textbook author):** Drawing on 40 years of experience designing and improving radar and electronic warfare systems, before reviewing materials Byron composed a hierarchal list of “What makes a textbook great?” As a successful textbook and radar study guide author who teaches courses to Navy personnel, Byron understood exactly what the *POMR* twin goals were and why they would be challenging to attain. He thus helped “set the bar” and provided broad stroke feedback on maintaining consistent depth and balance of theory, math, and practical reference to current technology. He is author of *Radar: Principles, Technology, Applications* and *The IEEE Radar Study Guide*.

**Mr. G. Richard Curry (radar consultant and radar book author):** Dick offered perceptive technical improvement comments across numerous chapters and was one of those capable of, and interested in, comparing reviewer comments objectively to help suggest the best solution. He is the author of *Radar System Performance Modeling*.

**Mr. Paul G. Hannen (SAIC senior engineer, professor at Wright State University, and book author):** Paul was most persistent and helpful about the first three chapters that “set the scene.” He provided literally hundreds of suggested edits and worked directly with volume editor and chapter author Jim Scheer. If you perceive an especially meticulous handling of background radar facts in Part 1, give credit to Paul. He is coauthor of *Radar Principles for the Non-specialist* (3d ed.).

**Dr. Randy J. Jost (senior scientist at USU Space Dynamics Lab, book author, Department of Defense consultant):** Suggesting edits to various chapters for optimum organization, particularly Chapter 4, “Propagation Effects and Mechanisms,” and contributing substantial content to Chapter 10, “Radar Transmitters,” and always giving sound suggestions for improvements throughout, Randy proved once again why he is such an important author, reviewer, and advisor to SciTech. Randy is coauthor of *Fundamentals of Electromagnetics with MATLAB* (2d ed.).

**Dr. David G. Long (professor and research director of remote sensing at Brigham Young University):** David’s help was invaluable in critiquing the sophisticated radar signal and data processing chapters and his contributions of content to Chapter 18, “Radar Measurements.” David worked directly with volume editor and multiple chapter author Mark Richards to hone the chapters in Part 4.

**Dr. Marshall Greenspan (senior systems consulting engineer, Northrop Grumman Corporation [NGC]):** Marshall was not only a willing and able technical reviewer, particularly within signal processing chapters, but was also extremely helpful in suggestions and procurement of contemporary photographs via his contacts with the NGC public relations departments.

**Dr. Simon Watts (deputy scientific director, Thales UK and book author):** After providing excellent technical comments on several chapters, Simon was called on to assist with final edits to the organization, completeness, and notational consistency to his particular area of expertise, radar clutter, in Chapter 6. He is coauthor of the book *Sea Clutter: Scattering, the K Distribution and Radar Performance*.

## Technical Reviewers

SciTech Publishing gratefully acknowledges the contributions of the following technical reviewers, who selected chapters of interest and read each carefully and completely, often in multiple iterations and often with substantive suggestions of remarkable thought and depth. Taken in aggregate, the value of their reviews was beyond measure and quite possibly unprecedented for a radar book:

Dr. Clive Alabaster, *lecturer, Cranfield University, GBR*  
Chris Baker, *dean and director, ANU College of Engineering and Computer Science, Canberra, AUS*

Dr. Ronald Aloysius, *fellow engineer, Northrop Grumman Corporation*  
Edward Barile, *senior principal engineer, Raytheon Corporation*

Dan Bernabei, *engineer scientist, Department of Defense*

Lee Blanton, *radar systems engineer, General Atomics Aeronautical Systems, Inc.*

Neal Brune, *vice president of countermeasures research and development, Esterline Defense Technologies*

Gerry Cain, *DSP Creations Ltd.*

Kernan Chaisson, *U.S. Air Force retired, Washington editor, Forecast International*  
I.-Ting Chiang, *applicant consultant, Lorentz Solution Inc.*

Dr. Jean-Yves Chouinard, *professor, Université Laval, Quebec, CAN*

Lawrence Cohen, *electronics engineer, radar division, Naval Research Laboratory*

Carlton Davis, *senior advisory engineer, Northrop Grumman Corporation*  
 Dr. Muhammad Dawood, *assistant professor, New Mexico State University*  
 Patrick Dever, P.E., *fellow engineer, Northrop Grumman Corporation*  
 Robert Egri, *Cobham DES*  
 Dr. John J. Ermer, *engineering fellow, Raytheon Space and Airborne Systems*  
 Dr. Mark Frank, *principal engineer, Rohde & Schwarz Inc.*  
 Christophe Fumeaux, *associate professor, University of Adelaide, AUS*  
 Dr. Fulvio Gini, *Professor, University of Pisa, ITA*  
 James D. Gitre, *manager, Motorola*  
 Nathan A. Goodman, *associate professor, University of Arizona*  
 Dr. Martie Goulding, *senior radar systems engineer, MacDonald Dettwiler & Associates, CAN*  
 John M. Green, *senior lecturer, Naval Postgraduate School*  
 Dr. Hugh Griffiths, *chair of radiofrequency sensors, University College London, GBR*  
 Dr. Walter Gustavo Fano, *associate professor, Universidad Nacional de la Patagonia San Juan Bosco*  
 Dr. Stephen Harman, *radar systems technical manager, QinetiQ, UK*  
 Dr. Joseph Hucks, *electrical engineer, Harris Corporation*  
 Thomas Jeffrey, *senior engineering fellow, Raytheon Integrated Defense Systems*  
 Dr. Alan R. Keith, *Boeing Defense, Space and Security*  
 Stephane Kemkemian, *radar senior expert, Thales Airborne Systems, FRA*  
 Dr. Anatolii Kononov, *Senior Researcher—Dept. of Radio and Space Science, Chalmers University of Technology, SWE*  
 Dr. Theodoros G. Kostis, *research scientist, University of the Aegean, GR*  
 Dr. Richard Lane, *research scientist, QinetiQ*  
 François Le Chevalier, *scientific director, Thales Air Systems, FRA*  
 Tony Leotta, *radar consultant, ADL Associates*  
 Richard Lethin, *president, Reservoir Labs*  
 David Mackes, *senior engineer, Northrop Grumman Corporation*  
 Kevin McClaning, *senior radiofrequency designer, Johns Hopkins University*  
 Anders Nelander, *Swedish Defense Research Agency, SWE*  
 Natalia K. Nikolova, *professor, McMaster University, CAN*  
 Dr. Myriam Nouvel, *radar engineer, Radar and Warfare Technical Directorate, Thales Airborne Systems, FRA*  
 Dr. Chris Oliver, *CBE, technical director, InfoSAR, GBR*  
 Karl Erik Olsen, *senior scientist, Norwegian Defence Research Establishment, NOR*  
 Dr. Pinaki S. Ray, *research associate, The University of Adelaide, AUS*  
 Dr. Brian D. Rigling, *associate professor, Wright State University*  
 Firooz Sadjadi, *senior staff research scientist, Lockheed Martin Cooperation*  
 Dr. Earl Sager, *radar physics group chief scientist, System Planning Corporation*  
 Dr. Paul E. Schmid, *president, Engineering Systems, Inc.*  
 John Shipley, *senior scientist, Harris Corporation*  
 Dr. John Spurlin, P.E., *professor, Norfolk State University*  
 Dr. Roger Sullivan, *radar consultant*  
 Chin Yeng Tan, *research assistant, The University of Nottingham—Malaysia*  
 John Wendler, *Harris Corporation*  
 Dr. Andreas Wiesmann, *GAMMA Remote Sensing AG—Switzerland, CHE*  
 Richard Wiley, *Research Associates of Syracuse*  
 Ben Winstead, *principal development engineer, Honeywell International, Inc.*

# Editors and Contributors

## Volume Editors



**Dr. Mark A. Richards**

*Volume editor-in-chief and multiple chapter author*

Mark Richards is a faculty member in Electrical and Computer Engineering at the Georgia Institute of Technology, teaching and conducting research in the areas of digital signal processing, radar signal processing, and high performance embedded computing. He was previously Chief of the Radar Systems Division in the Sensors and Electromagnetic Applications Laboratory of the Georgia Tech Research Institute (GTRI). He is the author of *Fundamentals of Radar Signal Processing* (McGraw-Hill, 2005), as well as co-editor or contributor to four other books. He received his Ph.D. from Georgia Tech in 1982.



**Mr. James A. Scheer**

*Associate volume editor and multiple chapter author*

Jim Scheer has 40 years of hands-on experience in the design, development, and analysis of radar systems. He currently consults and works part time for GTRI and teaches radar-related short courses. He began his career with the General Electric Company (now Lockheed Martin Corporation), working on the F-111 attack radar system. In 1975 he moved to GTRI, where he worked on radar system applied research until his retirement in 2004. Mr. Scheer is an IEEE Life Fellow and holds a BSEE degree from Clarkson University and the MSEE degree from Syracuse University.



**Dr. William A. Holm**

*Associate volume editor and multiple chapter co-author*

Bill Holm is the associate vice provost for distance learning & professional education at Georgia Tech, program director for the defense technology professional education program, and is a principal research scientist at GTRI. His research in radar technology, signal processing techniques, and related subjects has resulted in over 75 technical papers, research papers, and book chapters. His 30+ years of instruction experience include the “Principles of Modern Radar” and “Basic Radar Concepts” short courses and teaching in the School of Physics. Dr. Holm holds a Ph.D. degree in physics from Georgia Tech.

## Chapter Contributors

**Mr. Christopher Bailey**

*Chapter 9 – Radar Antennas*

Chris Bailey is a GTRI research engineer with experience in phased-array antenna design, analysis, and modeling, and phased-array radar-system engineering. His recent research efforts include digital beamforming, overlapped subarrays architectures, and low-power/low-cost arrays. Bailey has written numerous reports on phased array technology and regularly teaches phased array courses with the Georgia Tech Defense Technology Professional Education Program. He holds a M.S.E.E. from Johns Hopkins University.

**Dr. William Dale Blair**

*Chapter 18 – Radar Measurements and Chapter 19 – Radar Tracking Algorithms*

Dale Blair is the academic administrator of the Radar Tracking GTRI Defense course. He is a senior research engineer at the GTRI Sensors and Electromagnetic Applications Laboratory (SEAL), and has been involved in the research and development and testing of target tracking algorithms and radar signal processing for more than 14 years, and is currently involved in phased array radar and multisensor tracking.

**Mr. Joseph A. Bruder, PE**

*Chapter 11 – Radar Receivers*

Joe Bruder retired from GTRI after 25 years but is actively working part-time there and Stiefvater Consultants. He has extensive experience in radar sensor technology, including radar system design, analysis and evaluation, test planning, testing and test measurements. At the USAF Rome Laboratory his research areas were space-based radar, bistatic radar, foliage penetration, and bird hazard detection. He is an IEEE Fellow, a member of the IEEE/AESS Radar Systems Panel and is the standards representative for the Panel.

**Mr. Nicholas (Nick) C. Currie**

*Chapter 5: Radar Clutter Characteristics*

Nick Currie served on the staff of GTRI for 30 years, performing measurements of the radar backscatter of the sea, rain, snow, vegetation, and sea ice, military and civilian land vehicles, small waterborne craft, missiles, and aircraft. He has consulted with DARPA and the National Institute of Justice on concealed weapon detection and through-the-wall surveillance, and with the USAF Rome Laboratory in the development of a cylindrical, bistatic RCS range. He is a Fellow of the IEEE for work in millimeter wave measurements. He has edited and coauthored four books in the field of radar measurements and clutter.

**Dr. Randy J. Jost**

*Chapter 10 – Radar Transmitters*

Randy Jost is a Senior Scientist at the Utah State University Space Dynamics Laboratory. He also holds adjunct positions in both the Electrical and Computer Engineering Department and the Physics Department. His areas of research expertise include Computational Electromagnetics, Radar, Remote Sensing, Electromagnetic Compatibility, Wireless Communication, Electronic Materials, Electromagnetic Measurements and Metrology & Characterization of Antenna, Radar and Optical Measurement Systems. Dr. Jost is an active member and officer in the IEEE Electromagnetic Compatibility Society and the Antenna Measurement Techniques Association (AMTA).



**Dr. Byron M. Keel**

*Chapter 16 – CFAR Processors and Chapter 20 – Pulse Compression Fundamentals*

Byron Keel is a Principal Research Engineer and Head of the Signal Processing Branch within the Radar Systems Division of GTRI. He has over 20 years of experience and active research in radar waveform design, signal processing, and systems analysis. He regularly teaches in GTRI sponsored short courses including “Principles of Modern Radar” and is course director and principal lecturer in “Radar Waveforms.”



**Dr. David G. Long**

*Chapter 18 – Radar Measurements*

David Long is a Professor in the Electrical and Computer Engineering Department at Brigham Young University (BYU) and is Director of the BYU Center for Remote Sensing. He has over 20 years of experience in the design of remote sensing radar systems, signal processing, and systems analysis. He is a Fellow of the IEEE.



**Mr. Jay Saffold**

*Chapter 4 – Propagation Effects and Mechanisms*

Jay Saffold is the Chief Scientist for RNI and has over 20 years engineering experience in both military and industry research in RF tags, virtual reality, digital databases, soldier tracking systems, millimeter wavelength (MMW) radar, multimode (MMW and optical) sensor fusion, fire-control radar, electronic warfare, survivability, signal processing, and strategic defense architecture. He lectures annually for GTRI on remote sensing and signal processing. He has authored or co-authored over 104 technical papers and reports. He holds a BSEE degree from Auburn University.



**Dr. Paul E. Schmid**

*Chapter 10 – Radar Transmitters*

Paul Schmid is president/owner of Engineering Systems, Inc. a Virginia consulting firm. He has fifty years industry and government experience in electromagnetic propagation, aerospace electronics, radio frequency systems, optical systems, and antenna theory that includes significant contributions to the Navy’s AEGIS phased array radar, NASA’s Apollo Program, and over fifty technical papers. He is a Life Senior Member of the IEEE.



**Dr. John Shaeffer**

*Chapter 6 – Target Reflectivity*

John Shaeffer has taught short courses on Radar Cross Section for over twenty years and is coauthor of *Radar Cross Section, 2nd Edition* (SciTech Publishing), the leading book on the subject. He has held senior engineering positions at McDonnell Douglas, GTRI, Lockheed Martin, and NASA, and was co-founder of Marietta Scientific and founder of Matrix Compression Technologies, LLC. He earned his PhD in Physics from Saint Louis University (1971).



**Dr. Gregory A. Showman**

*Chapter 21 – Introduction to Radar Imaging*

Greg Showman is a Senior Research Engineer at GTRI, acts as the Director of the Adaptive Sensor Technology Project Office within GTRI, and has over 20 years of experience in radar modeling, performance analysis, and signal processing algorithm development.

**Mr. Tracy Wallace***Chapter 10 – Radar Transmitters*

Tracy Wallace is Division Chief for the Air and Missile Defense Division of GTRI's Sensors and Electromagnetic Applications Laboratory. He supports solid-state, active-aperture radar development with focus on the frontend electronics, power systems, and system performance assessment. He has also designed and built high power tube-based transmitters for instrumentation radars. He teaches in numerous radar-related short courses: Principles of Modern Radar, Phased Array Radar Systems, Space-Based Radar, Transmit/Receive Modules for Phased Array Radar, and Coherent Radar Performance Estimation.

# List of Acronyms

The following acronyms are used throughout this text. Some acronyms, *e.g.* SIR, have more than one meaning; the appropriate meaning is generally clear from the context.

<b>Acronym</b>	<b>Definition</b>	<b>Acronym</b>	<b>Definition</b>
1-D	One Dimensional	CS	Censored
2-D	Two Dimensional	CUT	Cell Under Test
3-D	Three Dimensional	CW	Continuous Wave
A	Ampere	DAC	Digital-to-Analog Converter
AAW	Anti-Air Warfare	DARPA	Defense Advanced Research Projects Agency
AC	Alternating Current	dB	Decibel
ACF	Autocorrelation Function	dbc	Decibels relative to the Carrier
ADC	Analog-to-Digital Converter, Analog-to-Digital Conversion	DBS	Doppler Beam Sharpening
A-DPCA	Adaptive Displaced Phase Center Antenna	DC	Direct Current
AESA	Active Electronically Scanned Array	DCT	Discrete Cosine Transform
AF	Array Factor	DDS	Direct Digital Synthesis, Direct Digital Synthesizer
AGC	Automatic Gain Control	DFT	Discrete Fourier Transform
AGL	Above Ground Level	DOA	Direction of Arrival
AL	Altitude Line	DOF	Degrees of Freedom
AM	Amplitude Modulation	DPCA	Displaced Phase Center Antenna
AMTI	Airborne Moving Target Indication	DRO	Dielectric Resonant Oscillator
AOA	Angle of Arrival	DSP	Digital Signal Processing
API	Application Programming Interface	DSX	Direct Synthesizer
AR	Autoregressive	DTFT	Discrete Time Fourier Transform
ARMA	Autoregressive Moving Average	EA	Electronic Attack
ASIC	Application-Specific Integrated Circuit	ECM	Electronic Countermeasures
BIT	Built-In Test	EIO	Extended Interaction (Klystron) Oscillator
bps	Bits per second	EKF	Extended Kalman Filter
BPF	Bandpass Filter	EM	Electromagnetic
BMD	Ballistic Missile Defense	EMI	Electromagnetic Interference
BRL	Ballistics Research Laboratory (U.S. Army)	ENOB	Effective Number of Bits
CA	Cell Averaging	EP	Electronic Protection
CA-CFAR	Cell Averaging Constant False Alarm Rate	ES	Electronic Support
CBE	Cell Broadband Engine	ESA	Electronically Scanned Array
CDF	Cumulative Distribution Function	EW	Electronic Warfare
CDL	Common Data Link	$f/D$	Focal length to Diameter ratio
CFA	Crossed Field Amplifier	FAR	False Alarm Rate
CFAR	Constant False Alarm Rate	FCR	Fire Control Radar
CFLOPS	Complex Floating Point Operations Per Second	FDS	Fractional Doppler Shift
CMOS	Complementary Metal Oxide Semiconductor	FET	Field Effect Transistor
CNR	Clutter-to-Noise Ratio	FFT	Fast Fourier Transform
COHO	Coherent Oscillator	FIR	Finite Impulse Response
COTS	Commercial Off-the-Shelf	FLOPs	Floating Point Operations
CPI	Coherent Processing Interval	FLOPS	Floating Point Operations Per Second
CRLB	Cramèr-Rao Lower Bound	FM	Frequency Modulation
CRT	Chinese Remainder Theorem	FMCW	Frequency-Modulated Continuous Wave

<b>Acronym</b>	<b>Definition</b>	<b>Acronym</b>	<b>Definition</b>
FOPEN	Foliage Penetration	LOS	Line of Sight
FOV	Field Of View	LPD	Low Power Density
FPGA	Field Programmable Gate Array	LRT	Likelihood Ratio Test
ft	Foot, feet	LSB	Least Significant Bit, Lower Sideband
FWHM	Full Width at Half Maximum	LSI	Linear Shift-Invariant
GaAs	Gallium Arsenide	LUT	Look-Up Table
GaN	Gallium Nitride	LVDS	Low Voltage Differential Signaling
Gbps	Giga bits per second	m	Meter
gcd	Greatest Common Divisor	Mbps	Megabits per second
GCMLD	Generalized Censored Mean Level Detector	MB/s	MegaBytes per Second
GFLOPS	GigaFLOPS	MCM	Multichip Module
GHz	Gigahertz	MCRLB	Modified Cramèr-Rao Lower Bound
GMTI	Ground Moving Target Indication	MDD	Minimum Detectable Doppler
GOCA-CFAR	Greatest-Of Cell Averaging Constant False Alarm Rate	MDS	Minimum Detectable Signal
GOPS	GigaOperations Per Second	MDV	Minimum Detectable Velocity
GPEN	Ground Penetration	MEM	Micro-Electromechanical
GPR	Ground Penetrating Radar	MESFET	Metal Semiconductor Field Effect Transistor
GPU	Graphical Processing Unit	MFA	Multiple-Frame Assignment
GTRI	Georgia Tech Research Institute	MHT	Multiple-Hypothesis Tracking
HCE	Heterogeneous Clutter Estimation	MHz	Megahertz
HPC	High Performance Computing	MIPS	Millions of Instructions per Second
HPD	High Power Density	MIT	Massachusetts Institute of Technology
HPEC	High Performance Embedded Computing	MIT/LL	Massachusetts Institute of Technology Lincoln Laboratory
HRR	High Range Resolution	MLC	Mainlobe Clutter
Hz	Hertz (cycles per second)	MLS	Maximum Length Sequence
I	In-phase channel or signal	MMIC	Monolithic Microwave Integrated Circuit
IC	Integrated Circuit	MMSE	Minimum Mean Square Error
ICBM	Intercontinental Ballistic Missile	MMW	Millimeter Wave
ID	Identification	MoM	Method of Moments
IEEE	Institute of Electrical and Electronic Engineers	MOPA	Master Oscillator Power Amplifier
IID	Independent and Identically Distributed	MOTR	Multiple-Object Tracking Radar
IF	Intermediate Frequency	MPI	Message Passing Interface
IFF	Identification Friend or Foe	MPM	Microwave Power Module
IFM	Instantaneous Frequency Measurement	MPS	Minimum Peak Sidelobe
IFSAR	Interferometric Synthetic Aperture Radar	MTD	Moving Target Detector
IIR	Infinite Impulse Response	MTI	Moving Target Indication
IMPATT	Impact Ionization Avalanche Transit Time	MTT	Multi-Target Tracking
InP	Indium Phosphide	mW	Milliwatt
IPP	InterPulse Period	MW	Megawatt
I/Q	In-phase/Quadrature	NCA	Nearly Constant Acceleration
ISAR	Inverse Synthetic Aperture Radar	NCCS2	Non-Central Chi-Square of degree 2
ISR	Integrated Sidelobe Ratio	NCV	Nearly Constant Velocity
kHz	Kilohertz	NEES	Normalized Estimation Error Squared
kVA	KiloVolt-Ampere	NLFM	Nonlinear Frequency Modulation
kW	KiloWatt	NP	Neyman-Pearson
lcm	Least common multiple	NRA	No Return Area
LE	Leading Edge	NRE	Non-Recurring Engineering
LEO	Low Earth Orbit	NRL	Naval Research Laboratory
LFM	Linear Frequency Modulation	NRE	Non-Recurring Engineering
LHC	Left-Hand Circular	OLA	Overlap-Add
LNA	Low-Noise Amplifier	OS	Ordered Statistic
LO	Local Oscillator	OTH	Over the Horizon

<b>Acronym</b>	<b>Definition</b>	<b>Acronym</b>	<b>Definition</b>
PA	Power Amplifier, Power-Aperture	SIR	Signal-to-Interference Ratio
PAG	Power-Aperture-Gain	SIR-C	Shuttle Imaging Radar-C
PC	Personal Computer	SLAR	Side-Looking Airborne Radar
PDF	Probability Density Function	SLC	Sidelobe Clutter
PDR	Phase-Derived Range	SM	Standard Missile
PDR0	Phase-Locked Dielectric resonant Oscillator	SMT	Surface Mount Technology
PEC	Perfect Electric Conductor	SM2	Standard Missile 2
PFA	Polar Formatting Algorithm	SNR	Signal-to-Noise Ratio
PFN	Pulse-Forming Network	SOCA-CFAR	Smallest-Of Cell-Averaging Constant False Alarm Rate
PLL	Phase-Locked Loop	SPEC	Standard Performance Evaluation Corporation
PLO	Phase-Locked Oscillator	SPST	Single-Pole, Single-Throw
PPI	Plan Position Indicator	SQNR	Signal-to-Quantization Noise Ratio
ppm	Parts per million	sr	Steradian
PPP	Pulse Pair Processing	SSB	Single Sideband
PRF	Pulse Repetition Frequency	STALO	Stable Local Oscillator
PRI	Pulse Repetition Interval	STAP	Space-Time Adaptive Processing
PSD	Power Spectral Density	STC	Sensitivity Time Control
PSM	Polarization Scattering Matrix	SVD	Singular Value Decomposition
PSR	Point Spread Response	TB	Time-Bandwidth product
Q	Quadrature phase channel or signal, Quality factor	TDRSS	Tracking and Data Relay Satellite System
QPE	Quadratic Phase Error	TDU	Time Delay Unit
QRD	Q-R Decomposition	TE	Trailing Edge
RAM	Radar Absorbing Material	TFLOPS	TeraFLOPS
RASS	Radio-Acoustic Sounding System	THAAD	Theater High Altitude Air Defense
RBGM	Real Beam Ground Mapping	TI	Texas Instruments
RCS	Radar Cross Section	TMR	Target Motion Resolution
REX	Receiver/Exciter	TOPS	TeraOps Per Second
RF	Radiofrequency, Radar Frequency	T/R	Transmit/Receive
RFLOPS	Real Floating Point Operations Per Second	TRF	Tuned Radio Frequency
RHC	Right Hand Circular	TSS	Tangential Signal Sensitivity
RMA	Range Migration Algorithm	TRF	Tuned Radio Frequency
rms	Root Mean Square	TWS	Track While Scan
RPM	Revolutions per Minute	TWT	Traveling Wave Tube
ROC	Receiver Operating Curve, Receiver Operating Characteristic	TX	Transmit
RRE	Radar Range Equation	UAV	Unmanned Aerial Vehicle
rss	Root Sum of Squares	UDSF	Usable Doppler Space Fraction
RTL	Register Transfer Level	UHF	Ultra-High Frequency
rv	Random Variable	UMOP	Unintentional Modulation of Pulse
RX	Receive, Receiver	U.S.	United States
s	Second	USB	Upper Sideband
SAR	Synthetic Aperture Radar	V	Volt
SAW	Surface Acoustic Wave	VHDL	VHSIC Hardware Description Language
SBC	Single Board Computer	VHF	Very High Frequency
SBO	Shoe-Box Oscillator	VME	VersaModule Europe
SCR	Silicon-Controlled Rectifier	VSIPL	Vector, Signal, Image Processing Library
SFDR	Spurious-Free Dynamic Range	VSWR	Voltage Standing Wave Ratio
SiC	Silicon Carbide	VXS	VersaModule Europe Switched Serial
SiGe	Silicon-Germanium	W	Watt
SINR	Signal-to-Interference-plus-Noise Ratio		

# List of Common Symbols

The following symbol definitions are used in multiple chapters throughout this text. Each individual chapter introduces additional notation specific to that chapter. Some symbols; *e.g.*  $R$ ; have more than one usage; their meaning is generally clear from the context

Symbol	Definition	Symbol	Definition
$\alpha$	Attenuation coefficient	$B_d$	Doppler bandwidth in hertz
$\chi_1$	Single-sample Signal-to-Noise Ratio	$c$	Speed of electromagnetic wave propagation
$\chi_N$	$N$ -sample Signal-to-Noise Ratio	$D$	Antenna size; Divergence factor
$\delta$	Grazing angle; Discrete impulse function	$D_{SAR}$	Synthetic aperture size
$\delta_D$	Dirac (continuous-time) impulse function	$E\{\cdot\}$	Expected value operator
$\Delta$	Difference channel; Quantization Step Size	$E$	Energy
$\Delta CR$	Cross-range resolution	$E_x$	Energy in signal $x$
$\Delta f_d$	Doppler spectrum width	$\hat{f}$	Normalized frequency in cycles per sample
$\Delta R$	Range resolution	$f$	Frequency in hertz; focal length
$\epsilon_r$	Relative permittivity	$f_d$	Doppler Shift
$\Gamma$	Fresnel reflection coefficient	$f_s$	Sampling frequency in samples per second
$\eta$	Clutter volume reflectivity; Extinction efficiency	$F$	Noise factor; Noise figure; Propagation factor
$\eta_a$	Aperture efficiency	$FAR$	False alarm rate
$\lambda$	Wavelength	$G$	Antenna gain
$\Lambda$	Likelihood ratio	$G_t$	Transmit antenna gain
$\mu$	Permeability	$G_r$	Receive antenna gain
$\phi$	Elevation angle (from horizontal plane); General angle or phase	$(\cdot)^H$	(superscript $H$ ) Hermitian (conjugate) transpose
$\phi_3$	Elevation 3-dB one-way beamwidth	$h(t)$ or $h[n]$	Filter impulse response (continuous or discrete)
$\phi_R$	Elevation Rayleigh (peak-to-null) beamwidth	$H(\cdot)$	Filter frequency response
$\phi_{xx}$	Autocorrelation function	$H_0$	Null (target absent) hypothesis
$\theta$	Azimuth angle; General angle or phase	$H_1$	Target present hypothesis
$\theta_3$	Azimuth 3 dB one-way beamwidth	$I$	In-phase channel or signal
$\theta_B$	Brewster's angle	$\mathbf{I}$	Identity matrix
$\theta_C$	Critical angle	$I_0$	Modified Bessel function of the first kind
$\theta_{cone}$	Cone angle	$ISR$	Integrated sidelobe ratio
$\theta_R$	Azimuth Rayleigh (peak-to-null) beamwidth	$J(\cdot)$	Cramèr-Rao Lower bound
$\theta_{scan}$	Scan angle	$k$	Boltzmann's constant
$\sigma$	Radar cross section	$\hat{k}_s$	Normalized total wavenumber (spatial frequency) in radians per sample
$\sigma^0$	Clutter area reflectivity	$K$	Discrete Fourier transform (DFT) Size
$\sigma_n^2$	Noise variance	$k$	Total wavenumber (spatial frequency) in radians per meter
$\sigma_x^2$	Variance of random variable or process $x$	$k_x; k_y; k_z$	$x$ ; $y$ ; and $z$ components of wavenumber (spatial frequency) in radians per meter
$\sum_x$	Sum channel	$L$	General loss; Number of range bins; Number of fast-time samples
$\tau$	Pulse width (duration)	$L_a$	Atmospheric loss
$\hat{\omega}$	Normalized frequency in radians per sample	$L_s$	System loss
$\omega$	Frequency in radians per second	$M$	Number of pulses; Number of slow-time samples
$\omega_d$	Doppler frequency in radians per second		
$\Omega$	Solid angle in steradians; Impedance in ohms		
$A_e$	Effective aperture		
$b$	Number of Bits		
$B$	Bandwidth in hertz		

<b>Symbol</b>	<b>Definition</b>	<b>Symbol</b>	<b>Definition</b>
$n$	Index of refraction	$SINR$	Signal-to-interference-plus-noise ratio
$N$	Number of samples; Vector length	$SNR$	Signal-to-noise ratio
$N(u; v)$	Normal (Gaussian) distribution with mean $u$ and variance $v$	$SQNR$	Signal-to-quantization noise ratio
$N_0$	Noise power spectral density	$t$	Time
$O(\cdot)$	“On the Order of”	$(\cdot)^T$	(superscript $T$ ) Matrix or vector transpose
$p_x(x)$	Probability density function of $x$	$T$	Threshold value; Pulse Repetition Interval (Interpulse Period)
$p_{avg}$	Average power	$T_0$	Standard temperature; Period of radiofrequency (RF) sinusoid
$P_D$	Probability of detection	$T_{ad}$	Antenna dwell time
$P_{FA}$	Probability of false alarm	$T_d$	Dwell time
$P_r$	Received power	$T_s$	Sampling interval; System noise temperature
$PRF$	Pulse repetition frequency	$v$	Velocity
$PRI$	Pulse repetition interval	$v_r$	Radial velocity
$PSR$	Peak sidelobe to peak mainlobe ratio	$\text{var}(x)$	Variance of a random variable or process $x$
$P_t$	Transmitted power	$\mathbf{X}$	General vector variable
$Q$	Quadrature channel or signal; Power density	$\mathbf{X}$	General matrix variable
$Q_M$	Marcum’s $Q$ function	$\bar{x}$	Mean of a random variable or process $x$
$R$	Range; Rain rate	$x_I(t); x_I[t]$	In-phase signal (continuous or discrete)
$\mathbf{R}_I$	Interference covariance matrix	$x_Q(t); x_Q[t]$	Quadrature phase signal (continuous or discrete)
$R_{ua}$	Unambiguous range		
$S_{xx}$	Power spectrum of random process $x$		
$SIR$	Signal-to-interference ratio		

# Characteristics of Clutter

*Nicholas C. Currie*

## Chapter Outline

5.1	Introduction and Definitions .....	165
5.2	General Characteristics of Clutter .....	172
5.3	Clutter Modeling .....	202
5.4	Concluding Remarks .....	206
5.5	Further Reading .....	207
5.6	References .....	207
5.7	Problems .....	210

## 5.1 | INTRODUCTION AND DEFINITIONS

### 5.1.1 What Is Clutter?

Radar clutter is a radar return from an object or objects that is of no interest to the radar mission. For example, the mission of many radar systems is the detection and tracking of “targets” such as aircraft, ships, or ground vehicles. To these systems, clutter is considered to be an interfering return from a natural object such as precipitation, vegetation, soil and rocks, or the sea. However, to radars designed for remote sensing such as synthetic aperture radar (SAR) imagers, these objects may be the primary targets of interest. For this chapter, it will be assumed that targets of interest are man-made while natural target returns are unwanted (i.e., clutter).

### 5.1.2 Comparison of Clutter and Noise

Chapter 3 introduced detection in the presence of random noise, including noise properties and the effect on detection of targets. The returns from natural clutter can be strikingly similar to the effects of noise on detection yet also be quite different. So, how do clutter returns differ from noise effects? Figure 5-1 shows a high (fine) resolution (1 ft × 1 ft), two-dimensional (2-D) SAR image of a suburban terrain scene near Stockbridge, New York, collected from an airborne platform [1]. As can be seen from the figure, some areas appear uniform in nature (e.g., grassy lawns), while others appear quite nonuniform (e.g., trees and man-made structures). The high-resolution image shown in Figure 5-1 produces significantly different clutter properties from a lower-resolution radar, which averages out much of the structure shown in the figure. As an introductory text, this chapter will discuss the characteristics of lower-resolution (real-beam) systems.

**FIGURE 5-1** ■ Synthetic aperture radar image of suburban terrain. (From Novak and Owirka [1]. With permission.)

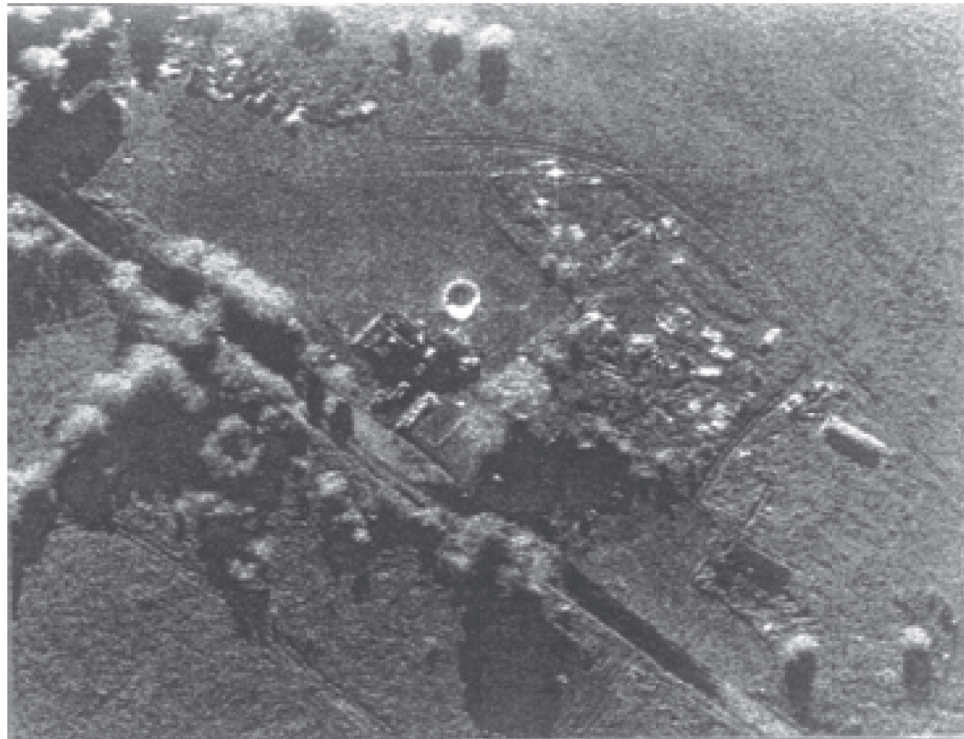


Table 5-1 summarizes the primary differences between clutter returns and receiver noise. Random noise, although varying with time, exhibits a specific set of characteristics:

- The probability density function (PDF) is Rayleigh for a linearly detected (voltage) signal, or exponential<sup>1</sup> for a square law detected (power) signal (see Chapter 3 for a description of the Rayleigh and exponential PDFs).
- The width of the autocorrelation function (ACF) is approximately the inverse of the receiver bandwidth.
- The power spectral density (PSD) function (power spectrum) width is approximately equal to the receiver bandwidth.

Clutter statistics can be similar to those of noise when the natural targets are composed of small, nearly equal-sized scatterers but can be quite different when the nature of the scatterers change or scatterers of differing types (e.g., a tree line) are present in the radar field of view. For this case, amplitude distributions having much longer “tails” than the Rayleigh distribution have been observed. Finally, although noise is independent of transmitted frequency, spatial position, and environmental parameters, clutter varies with all of these parameters, making clutter characterization very complex.

---

<sup>1</sup>The exponential PDF is sometimes called a *Rayleigh power PDF*. Confusingly, this is sometimes shortened to just Rayleigh PDF, even though the mathematical form intended is the exponential PDF. The Rayleigh PDF describes the amplitude (magnitude) of the noise signal; the magnitude squared (power) is described by an exponential PDF.

**TABLE 5-1** ■ Clutter Signals versus Noise

Noise Signal	Clutter Signal
Amplitude independent of radar return signal level	Amplitude proportional to radar return signal level
Wide bandwidth (limited by receiver noise bandwidth)	Narrow bandwidth (created by scatterer motion)
Statistically independent between pulses	May be highly correlated between pulses
Amplitude variation described by Rayleigh statistics	Amplitude variation may vary from none to extremely wide (log normal or Weibull statistics)
Average value is constant and independent of spatial position	Time average will differ between spatial samples as the clutter types change
Independent of transmitted frequency	Varies with changing frequency
Independent of environmental parameters	Can vary with changing environmental conditions
No spatial component	Varies with beam position and resolution

Source: Adapted from Long [2]. (© 2006 IEEE. Used with permission.)

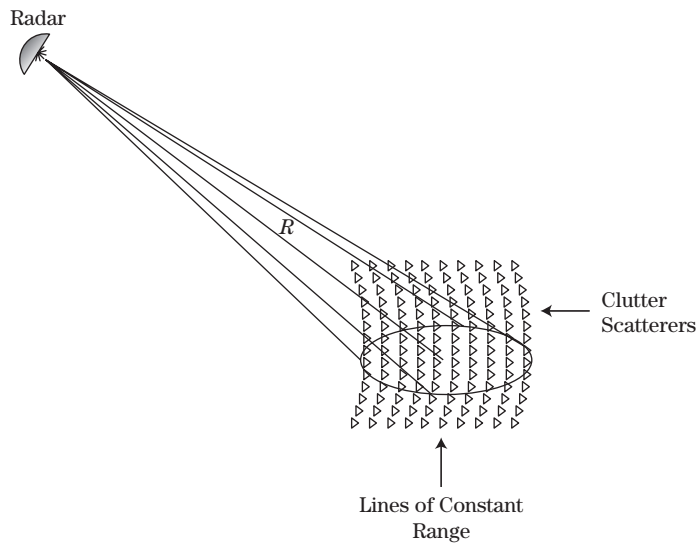
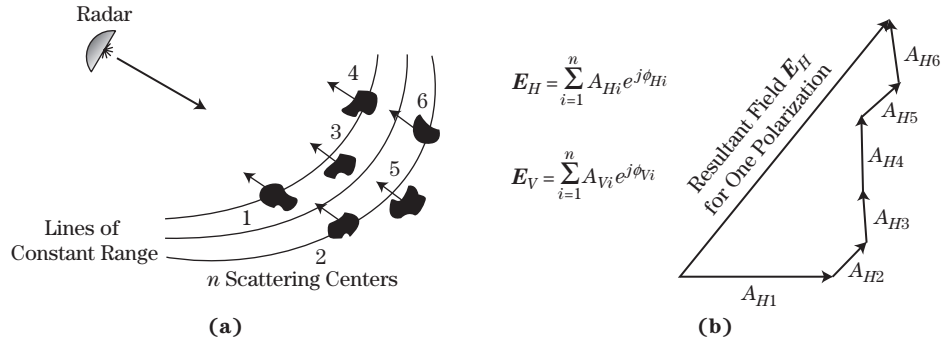
**FIGURE 5-2** ■ Radar scan over clutter scatterers illustrating lines of constant range.

Figure 5-2 shows a typical situation where the radar beam illuminates a number of scatterers, each having a different reflectivity,  $\sigma_i$ , and distance,  $d_i$ , from the radar. Lines of constant range to the radar form ellipses on a level surface. The electric field amplitude (horizontal or vertical polarization component) measured at the radar due to the echo from the  $i$ -th scatterer will be proportional to the square root of the received power given by the radar range equation

$$|E_i| = \left[ \frac{P_t G^2 \lambda^2 \sigma_i}{(4\pi)^3 L_s d_i^4} \right]^{1/2} = k \frac{\sqrt{\sigma_i}}{d_i^2} \quad (5.1)$$

where  $P_t$  is the transmitted power,  $G$  is the antenna gain,  $\lambda$  is the wavelength, and  $L_s$  is the system loss (including hardware and atmospheric losses) as discussed in Chapter 2. The constant,  $k$ , absorbs all the factors that are the same for each scatterer. The phase of

**FIGURE 5-3** ■  
 Vector summation of scatterers at different positions and ranges.  
 (a) Geometry of multiple scatterers.  
 (b) Vector summation forms resultant E-field amplitude.



the received electric field, relative to the phase of the transmitted wave, is determined by the scatterer reflection phase,  $\theta_i$ , and the two-way propagation distance:

$$\arg \{E_i\} = \theta_i - \frac{4\pi}{\lambda} d_i = \theta_i + \phi_i \quad (5.2)$$

Scatterers located at the same range will generate echoes that return with the same time delay and phase at the radar, assuming that each scatterer has the same reflection phase (i.e.,  $\theta_i = \theta$ ) for some constant,  $\theta$ . However, scatterers with slightly different ranges but falling within the same beam or range bin interval will have different echo phases. As shown in Figure 5-3a, the total return  $E$ -field amplitude at the radar is therefore proportional to the vector summation of the electric field amplitude and phase of each group of scatterers contributing to a single radar measurement. This resultant  $E$ -field is given by

$$\begin{aligned} E &= \sum_i E_i = \sum_i k \frac{\sqrt{\sigma_i}}{d_i^2} \exp \left[ j \left( \frac{4\pi}{\lambda} d_i + \theta \right) \right] \\ &\approx \frac{k}{d^2} \sum_i \sqrt{\sigma_i} \exp \left[ j \left( \frac{4\pi}{\lambda} d_i + \theta \right) \right] \\ &\equiv \frac{k'}{d^2} \sqrt{\sigma} \exp [j\phi] \end{aligned} \quad (5.3)$$

where  $\sigma$  is the equivalent radar cross section (RCS) of the total clutter return, and  $\phi$  is the equivalent phase. This process is illustrated in Figure 5-3b. The complex quantity  $\sqrt{\sigma} \exp [j\phi]$  is called the *backscatter coefficient* of the clutter.

As the radar beam scans across the scatterers in the scene, the range to the particular scatterers in the beam changes so that the resulting equivalent RCS changes. This variation in return has come to be known as “speckle”: the “noise-like” returns resulting from the random summation of individual scatterer echoes. The reduction of this characteristic, “despeckling,” is very important in SAR processing. As the beam scans farther, new scatterers enter the beam, while other scatterers leave the beam. For a mechanically scanned system, the changes are smooth, while for an electronic scan system the changes occur abruptly as the beam is step-scanned. As long as the scatterers illuminated at any given time are similar in amplitude and phase, the return will exhibit noise-like statistics with constant parameters. However, if the beam scans across a set of scatterers that are physically different the character of the return can change. An example is scanning from a grassy field to a line of trees, which would likely result in an increase in the echo strength and thus the equivalent RCS. Also, the presence of one or two large scatterers among the smaller scatterers can cause the return to exhibit very nonnoise-like statistics.

Since the returns from clutter vary by type, polarization, environmental, and geometric conditions, it is very difficult to model clutter mathematically. Attempts to do so are briefly discussed in Section 5.3. More practically, many experiments have been conducted to measure clutter returns as functions of the various dependent parameters. Practical clutter modeling usually involves a combination of empirical and theoretical results.

### 5.1.3 Basic Definitions

#### 5.1.3.1 Scattering Coefficients

To use published data on clutter, methods must be defined to normalize the returns so that data can be applied to many different radars and applications. One form of the radar equation can be written as

$$P_r = \frac{P_t G^2 \lambda^2 \sigma}{(4\pi)^3 L_s R^4} \quad (5.4)$$

where the variables are the same as in equation (5.1). This form of the radar equation is suitable for point targets (i.e., targets much smaller than the resolution of the radar) but is not convenient for distributed targets such as clutter, where many scatterers contribute at once to the total echo. Thus, equation (5.4) must be modified to account for the area or volume defined by the beamwidths and range resolution of the radar.

For surface clutter it is convenient to define the radar cross section per unit area, or *surface reflectivity*,

$$\sigma^0 \equiv \frac{\sigma}{A} \quad (5.5)$$

where  $\sigma$  is the total RCS of the contributing clutter, and  $A$  is the area of the contributing clutter defined by the radar beam intersection with the surface. The units of  $\sigma^0$  are meters<sup>2</sup>/meters<sup>2</sup> so that  $\sigma^0$  is unitless. It is often expressed in the literature in decibels, denoted dBsm.

For volume clutter, the radar cross section per unit volume, or *volume reflectivity*, is defined as

$$\eta = \frac{\sigma}{V} \quad (5.6)$$

where  $V$  is the volume defined by the radar beam and range resolution cell. The units of  $\eta$  are meters<sup>2</sup>/meters<sup>3</sup>, or meter<sup>-1</sup>. It is expressed in the literature in decibels per meter.

Given  $\sigma^0$ , the area  $A$  to be used in computing clutter RCS using equation (5.5) for surface clutter is determined by the beamwidths and the range resolution of the radar. Two situations arise: (1) the case where the range resolution is large compared with the projection of the vertical beam width onto the surface; and (2) the case where the range resolution is smaller than the projection extent. Both were considered in Section 2.13. In the *beam-limited* case, the result for the beam area on the ground was

$$A = \pi R^2 \tan\left(\frac{\theta_3}{2}\right) \tan\left(\frac{\phi_3}{2}\right) \csc \delta \quad (5.7)$$

where  $\phi_3$  and  $\theta_3$  are the azimuth and elevation beamwidths of the antenna, respectively, and  $\delta$  is the *grazing angle* of the antenna boresight with the clutter surface. For beamwidths less than about 10 degrees the small angle approximation  $\tan(x) \approx x$  is valid, and

equation (5.7) becomes

$$A = \frac{\pi R^2}{4} \theta_3 \phi_3 \csc \delta \quad (5.8)$$

Note that since the clutter area grows as  $R^2$  due to beam spreading, so will the clutter RCS,  $\sigma$ . When used in equation (5.4), the resulting received power due to a constant clutter reflectivity will be proportional to  $R^{-2}$  instead of the  $R^{-4}$  proportionality seen for point targets. Thus, beam-limited surface clutter power does not decline with range as rapidly as does point target power.

In the *pulse-limited* case, the area defined by the beam and pulse width on the ground is given by

$$A = \left(\frac{c\tau}{2}\right) 2R \tan\left(\frac{\theta_3}{2}\right) \csc \delta = c\tau R \tan\left(\frac{\theta_3}{2}\right) \csc \delta \quad (5.9)$$

and, again, if the beam width is less than  $10^\circ$ , a small angle approximation gives

$$A = \left(\frac{c\tau R \theta_3}{2}\right) \csc \delta \quad (5.10)$$

Note that in this case the clutter area is proportional to  $R$  instead of  $R^2$ . Consequently, the pulse-limited echo power from constant-reflectivity surface clutter declines as  $R^{-3}$ . If the radar uses pulse compression techniques (see Chapter 20) to obtain fine-range resolution, then the radar range resolution in meters should replace the factor  $c\tau/2$  in equations (5.9) and (5.10).

The grazing angle at which the clutter cell area transitions from the beam-limited case to the pulse-limited case can be found by setting the pulse- and beam-limited areas equal to one another and is given by

$$\tan \delta = \frac{2R \tan(\phi_3/2)}{c\tau/2} \quad (5.11)$$

or, for small antenna beamwidths,

$$\tan \delta = \frac{2R\phi_3}{c\tau} \quad (5.12)$$

When the value of  $\tan \delta$  exceeds the value in equations (5.11) or (5.12), the beam-limited case applies. Conversely, when  $\tan \delta$  is less than that value, the pulse-limited case applies.

Note that the beamwidths used in the previous equations are assumed to be the 3 dB two-way beamwidths. Actual radar beams are not rectangular, so some errors can occur in beam area and clutter power estimation based on the actual beam shape and sidelobes. These errors can be significant for airborne pulse-Doppler processors.

The previous discussion can be applied to area clutter (e.g., ground, sea). For computing the equivalent RCS of atmospheric clutter using equation (5.6), the reflectivity,  $\eta$ , and the resolution cell volume,  $V$ , defined by the radar beam and the pulse width are needed. The formula for  $V$  was given in Chapter 2. Since air search radars are almost always narrow beam, the small angle approximation formula is usually adequate. This is given by

$$V = \pi \left(\frac{R\theta_3}{2}\right) \left(\frac{R\phi_3}{2}\right) \left(\frac{c\tau}{2}\right) = \left(\frac{\pi R^2 \theta_3 \phi_3}{4}\right) \left(\frac{c\tau}{2}\right) \quad (5.13)$$

Again, the actual range resolution should be used in place of the  $(c\tau/2)$  term in pulse compression radars.

### 5.1.3.2 Clutter Polarization Scattering Matrix

The scattering properties of clutter are dependent on the transmitted and received polarization. This effect is quantified by the use of a 2-by-2 matrix known as the *polarization scattering matrix* (PSM),  $\mathbf{S}$  [3]. Equation (5.14) gives a form of the matrix expressed in terms of vertical and horizontal polarization:

$$\mathbf{S} = \begin{bmatrix} \sqrt{\sigma_{HH}} e^{j\phi_{HH}} & \sqrt{\sigma_{HV}} e^{j\phi_{HV}} \\ \sqrt{\sigma_{VH}} e^{j\phi_{VH}} & \sqrt{\sigma_{VV}} e^{j\phi_{VV}} \end{bmatrix} \quad (5.14)$$

The first subscript represents the received polarization, while the second represents the transmitted polarization. For example, the lower left term in the matrix describes the vertically polarized received voltage signal component in response to a horizontally polarized transmitted signal. In fact, a matrix can be developed in terms of any two orthogonal polarizations, including circular and elliptical polarizations.

The terms in the complex matrix  $\mathbf{S}$  represent the backscattering coefficients of the clutter for four polarization cases: (1) transmit and receive horizontal polarization; (2) transmit horizontal and receive vertical polarization; (3) transmit vertical and receive horizontal polarization; and (4) transmit and receive vertical polarization. For a specific frequency and geometry of the radar and a specific set of environmental parameters, the polarization scattering matrix contains all of the available information about the clutter return at the time of the measurement.

Unfortunately, a radar that can transmit and receive all four polarizations is both complex and expensive. Fortunately, for the case of a monostatic radar the *reciprocity theorem* [3] requires that the two “cross polarized” terms are equal, that is,  $\sigma_{VH} = \sigma_{HV}$  and  $\phi_{VH} = \phi_{HV}$ . Thus, only three complex polarization values must be measured to determine the full scattering matrix.

Much work has been done to try to exploit the information inherent in the scattering matrix to identify targets in the presence of clutter. Holm [4] and others have attempted to use the scattering matrix to separate targets from clutter as well as to identify classes or types of targets on the theory that the PSMs of man-made targets and natural clutter will be significantly different. He determined that, to be effective, high-range and azimuthal resolution is required so that individual range-azimuth cells contain only target returns or only clutter returns. If cells contain a mixture of both target and clutter returns, the results are much less useful even if the clutter returns are much lower in amplitude than the targets.

In the past, attempts to use partial polarization matrix information to discriminate between targets and clutter have been tried with mixed results [3,5]. Such discriminants have included the following:

- Parallel/cross polarization ratio:  $\sqrt{\sigma_{HH}}/\sqrt{\sigma_{VH}}$ .
- Vertical/horizontal polarization ratio:  $\sqrt{\sigma_{VV}}/\sqrt{\sigma_{HH}}$ .
- Polarimetric phase:  $\phi_{HH} - \phi_{VV} \equiv \phi_{H-V}$ .

Polarimetric phase is usually expressed as quadrature components  $\cos(\phi_{H-V})$  and  $\sin(\phi_{H-V})$ . These discriminants have the advantage of requiring only the polarimetric amplitude or phase instead of the entire PSM and can improve target detectability in clutter under some conditions.

## 5.2 | GENERAL CHARACTERISTICS OF CLUTTER

### 5.2.1 Overview

Because clutter is one of the major limitations in target detection for practical radar, clutter measurements have been performed since the advent of radar use in World War II. The development of digital recording techniques has greatly improved the quality (and quantity) of data in the last 20 years. Because clutter exhibits noise-like fluctuations in echo strength, clutter is characterized in terms of statistical parameters describing the variability of  $\sigma^0$  and  $\eta$ , including the following:

- Mean or median values.
- Standard deviations or variances.
- Probability density functions.
- Spectral bandwidths for temporal variability.
- Autocorrelation functions or power spectral density functions for temporal and spatial variations.

These measured values almost always include propagation factor effects (see Chapter 4). Usually, for clear air measurements of surface clutter at moderate to high angles the propagation factor effects are negligible. However, for measurements of atmospheric precipitation or for low grazing angles for surface clutter, attenuation due to multipath can be significant. These effects can be minimized by using calibration targets located near the clutter region being measured but can never be totally eliminated. For this reason, data from precipitation or surface clutter at large ranges tend to have more variability than measurements of surface clutter at steeper grazing angles. Since an operational radar will experience these same effects under the same conditions, this situation is not necessarily bad.

### 5.2.2 Surface Clutter

#### 5.2.2.1 General Dependencies

Given that the radar-received clutter power in a particular application affects the detection performance and influences radar design, a simple and accurate way is needed to estimate clutter levels for a variety of scenarios. The goal is to develop models that include in a mathematical form all the known parameter dependencies of the backscattering coefficient that have been identified through experimental measurements. Fundamentally, clutter model development starts with theoretical calculations of reflectivity and comparison with the interpretation of experimental observations, which leads to an understanding of the underlying scattering mechanisms. Some of the observed dependencies are as follows:

- *Grazing angle*: Grazing angle,  $\delta$ , is the angle at which the illumination energy strikes a clutter surface.
- *Vertical variation of the clutter scatterers*: Rough surfaces have a larger  $\sigma^0$  than smooth ones for low grazing angles; at very high grazing angles (near  $90^\circ$ ), smooth surfaces have a higher  $\sigma^0$  than rough ones.
- *Wavelength*:  $\sigma^0$  is a function of vertical texture expressed in wavelengths.

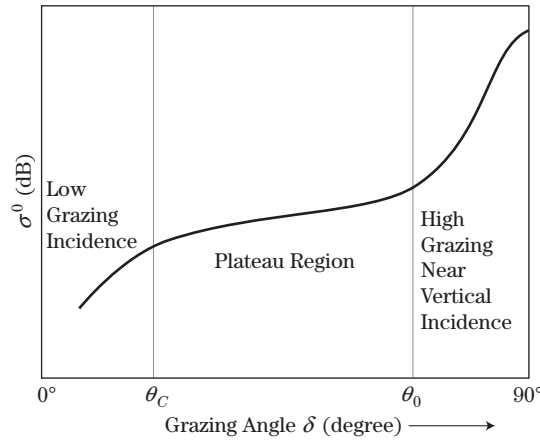


**FIGURE 5-4** ■ General dependence of  $\sigma^0$  on grazing angle. (Adapted from [6]. With permission.)

Depression angle is closely related to grazing angle. It is the angle below the radar's local horizontal at which the illumination energy is transmitted from the radar. For a flat horizontal clutter surface the depression and grazing angles are identical. Grazing angle is the most relevant for describing scattering, but clutter reflectivity data are often reported as a function of depression angle in the literature because the grazing angle may not be known precisely. In this chapter, the two are generally assumed to be the same unless otherwise stated, and the discussion is framed in terms of grazing angle. Depression angle is used when referring to previous published results given in terms of depression angle.

Rough surface theory and experimental measurements have determined that the back-scattering for both land and sea surfaces—as a function of grazing angle—exhibit a common general dependence on grazing angle as shown in Figure 5-4. From this figure, three distinct regions of clutter behavior can be identified: (1) a low grazing angle region; (2) a plateau region; and (3) a high grazing angle region. The boundaries of these three regions, defined by  $\theta_C$  and  $\theta_0$ , change with frequency, surface condition, and polarization [6].

The *low grazing angle region* extends from zero to a *critical angle*,  $\theta_C$ , determined by the root mean square (rms) height of surface irregularities in wavelengths. This critical angle is the grazing angle below which a surface seems “smooth” by Rayleigh’s definition and above which it is “rough.” Based on Rayleigh’s definition, a surface is smooth if

$$\sigma_h \sin \delta < \frac{\lambda}{8} \quad (5.15)$$

where  $\sigma_h$  is the rms height of the surface irregularities,  $\delta$  is the grazing angle, and  $\lambda$  is the radar wavelength. Thus, the critical angle is given by

$$\sin \delta_C = \frac{\lambda}{8\sigma_h} \quad (5.16)$$

In the *plateau region* the incident wave encounters the surface irregularities in such a way that the dependence of  $\sigma^0$  on grazing angle is much less than at lower angles. Chapter 7 provides an introduction to the “rough surface” theory applicable to this regime.

For a constant  $\sigma^0$  and beam-limited geometry, it is expected that the return power for surface clutter would vary as  $R^{-4} \times R^2 = R^{-2}$  since the power from a point target varies as  $R^{-4}$  while the area of surface clutter increases as  $R^2$ . However, measurements have indicated that clutter power often varies as  $R^{-3}$ . For this to be the case,  $\sigma^0$  must vary as

$R^{-1}$ . The grazing angle satisfies the equation  $\sin \delta = h/R$ , where  $h$  is the radar altitude and  $R$  is the slant range. If the height of the radar is constant, then  $\sin \delta$  is proportional to  $1/R$ . This fact led to the definition of the so-called *constant gamma model* for clutter reflectivity, given by

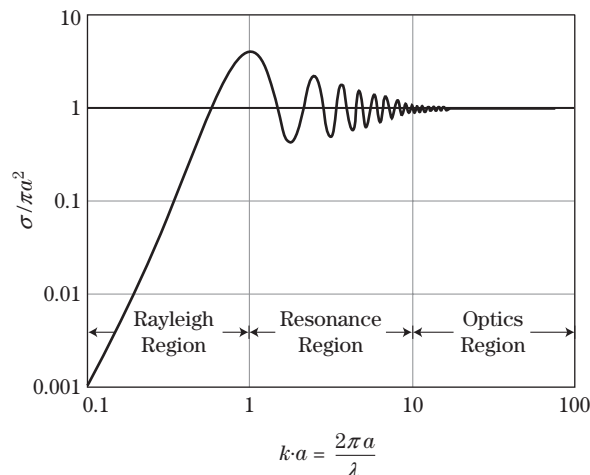
$$\sigma^0 = \gamma \sin \delta = \frac{\gamma}{R} \quad (5.17)$$

Here  $\gamma$  is a constant depending on terrain type, surface roughness (sea state and terrain type for sea and land, respectively), and frequency. If equation (5.17) applies, then clutter reflectivity will be proportional to  $R^{-1}$ , and the  $R^{-3}$  clutter power dependence would be expected. Note that the constant gamma model is applicable only in the plateau angular region.

In the *high grazing angle region* the scattering becomes more directional and rapidly increases to a maximum value based on the reflectivity and smoothness of the clutter, in a manner somewhat analogous to the behavior of the main lobe of a rough flat plate at near perpendicular incidence (see Chapter 6).

Figure 5-5 gives the RCS of a conducting sphere of diameter  $a$  normalized to its projected area as a function of the circumference normalized to the wavelength. As can be seen from the figure, the relative RCS increases with frequency,  $1/\lambda$ , until  $\lambda$  equals twice the circumference, whereupon the RCS varies rapidly until  $\lambda$  is about  $1/5$  the circumference, at which point the RCS equals the projected cross sectional area of the sphere and is independent of frequency. Thus, for large wavelengths (low frequencies), the return from a sphere would be expected to increase with increasing frequency until the point known as the *resonance region*, where the RCS fluctuates rapidly with frequency. Cylinders exhibit similar frequency dependence relative to the ratio of circumference to wavelength. Since most clutter scatterers can be considered to be approximately either spherical or cylindrical in shape, clutter RCS should be expected to increase with decreasing wavelength up to a wavelength in the millimeter wave region for most scatterers. At high frequencies facets or ripples create resonance effects that overcome this effect. As will be seen in the data, this effect does exist, although variations among different types of clutter return can often be much greater than frequency effects.

**FIGURE 5-5** ■ Dependence of the RCS of a sphere on wavelength.



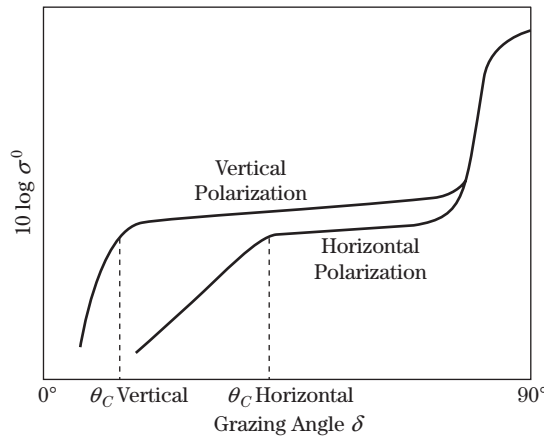


**FIGURE 5-6** ■ Theoretical polarization dependence of a relatively smooth surface. (From Long [6]. With permission.)

Figure 5-6 gives the theoretical polarization dependence of  $\sigma^0$  (generally verified by experiment) as a function of grazing angle for a moderately smooth surface, which tends to occur at lower frequencies. The critical angle,  $\theta_C$ , occurs at different grazing angles for the two polarizations due to multipath effects so that at lower angles the difference between clutter reflectivity at vertical and horizontal polarizations can be quite large. However, for higher angles and frequencies, the horizontal polarization reflectivity is usually only a few dB lower than the vertical polarization reflectivity. Although these polarization trends on average are valid, for specific clutter patches the occasional presence of natural diplanes can result in widely varying polarization returns.

### 5.2.2.2 Temporal and Spatial Dependencies

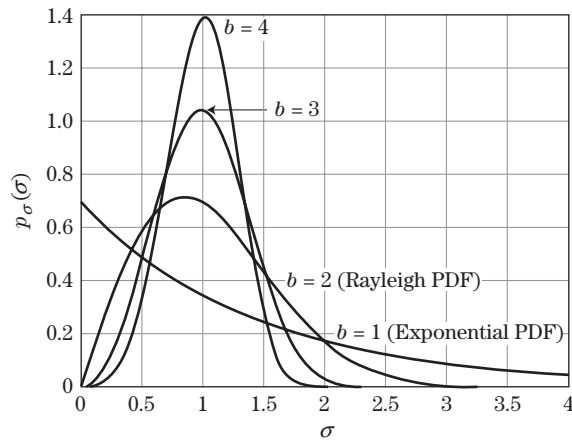
Temporal and spatial variations occur due to either the motion of scatterers within the radar cell (usually due to wind) or the nature of scatterers changing as the radar cell moves in range or azimuth. Such statistical variation is described in terms of probability distributions with simple mathematical equations to facilitate modeling. Coherent receiver noise has a complex normal (Gaussian) amplitude distribution before detection and a Rayleigh distribution after detection, assuming a linear (voltage) detector, or an exponential distribution if a square law (power) detector is used. Clutter amplitudes can also appear Gaussian or Rayleigh distributed for the low-resolution case where there are a large number of scatterers within the radar cell. However, as the resolution improves, the radar cell may contain only a few clutter scatterers, resulting in a non-Gaussian or Rayleigh distribution. Also, shadowing at low grazing angles can result in hiding large scatterers some of the time. The resulting distributions are said to have long “tails” because the probability of observing large values of the clutter amplitude is greater than with Rayleigh statistics.

A commonly used family of distributions for describing clutter power is the Weibull, which is illustrated in Figure 5-7. One form of the equation for the general Weibull distribution is [6]

$$p_{\sigma}(\sigma) = \begin{cases} \frac{b\sigma^{b-1}}{\alpha} \exp\left(-\frac{\sigma^b}{\alpha}\right), & \sigma \geq 0 \\ 0, & \sigma < 0 \end{cases} \quad (5.18)$$

where  $\alpha = \sigma_m^b / \ln 2$ , and  $\sigma_m$  is the median of the distribution. The parameter  $a = 1/b$  is called the *width* parameter;  $b$  itself is called the *shape* parameter. The parameter  $\alpha^{1/b}$  is

**FIGURE 5-7** ■ Weibull distributions for  $\sigma_m = 1$  and several values of  $b$ .



called the *scale* parameter. For a given  $\sigma_m$  or  $\alpha$ , the higher the value of  $a$  and thus the lower the value of  $b$  and the longer the high value “tails” of the distribution. Figure 5-7 illustrates this for  $\sigma_m = 1$ . When  $a = 1$  (and thus  $b = 1$ ), the Weibull distribution reduces to the exponential PDF, while for  $a = 1/2$  ( $b = 2$ ) it reduces to the Rayleigh PDF.

Because the Weibull is, in general, a two-parameter ( $b$  and  $\sigma_m$ ) distribution, it can be adjusted to fit both the mean and variance of experimental data. Experimenters express the variation of clutter by choosing values of  $b$  and  $\sigma_m$  to best fit a Weibull distribution to their data.

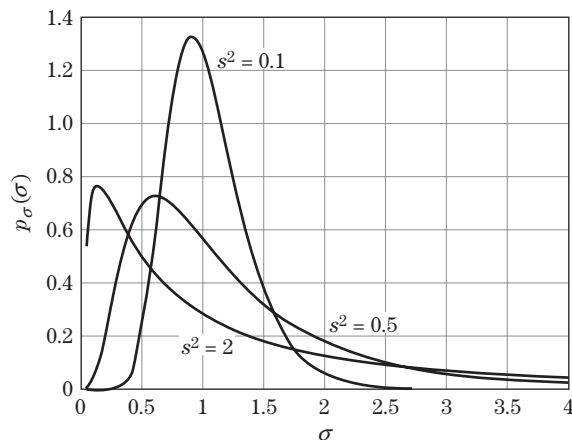
Other experimenters prefer to use the log-normal distribution, another two-parameter function. The log-normal distribution is simply a distribution in which the logarithm of the return is normally distributed. It is given by [6]

$$p_{\sigma}(\sigma) = \frac{1}{\sigma s \sqrt{2\pi}} \exp\left(-\frac{(\ln \sigma - \bar{\sigma})^2}{2s^2}\right) \quad (5.19)$$

where  $\bar{\sigma}$  is the mean RCS, and  $s^2$  is the variance of  $\sigma$ .

This distribution is often used when modeling radars using a logarithmic receiver. The logarithmic receiver increases dynamic range by compressing large values of returns relative to smaller returns. An advantage of the log-normal distribution is that it models even higher “tails” than the Weibull, so it may provide a better fit to severe clutter data. Figure 5-8 gives several samples of the log-normal family, all with  $\sigma_m = 1$  as in Figure 5-7.

**FIGURE 5-8** ■ Log-normal distributions for  $\sigma_m = 1$  and several values of  $s^2$ .



When compared with Figure 5-7, it is obvious that log-normal-distributed data will exhibit a larger percentage of high values than Weibull-distributed data with the same median.

Some authors simply express the variation of clutter data in terms of the mean (or median) and the variance (or standard deviation, the square root of variance) without specifying an associated PDF. This approach is adequate for comparing the general strength and variability of different types of clutter for various conditions but does not provide enough information for analysis of radar detection performance.

### 5.2.2.3 Average Value Data

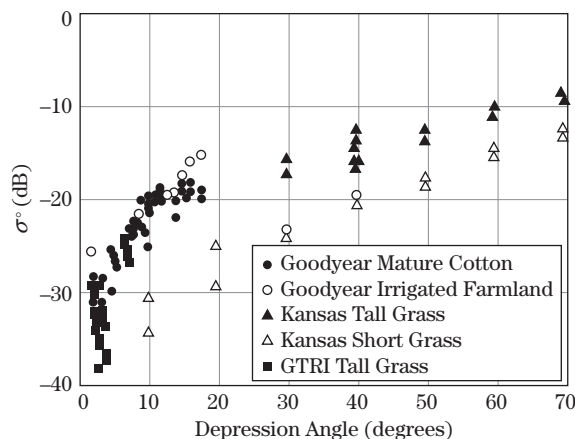
An extensive body of definitive experiments has been performed in the last 40 years to characterize radar clutter. Some of the key studies are as follows:

- Rain backscatter measurements from 10 to 100 GHz performed jointly by the U.S. Army Ballistic Research Laboratory (BRL) and the Georgia Tech Research Institute (GTRI) in the mid 1970s [7,8].
- Measurement of frozen precipitation by the U.S. Army Harry Diamond Laboratory millimeter waves in the late 1980s [9].
- University of Kansas measurements on terrain at high angles in the 1980s [10].
- Measurement of land clutter at low grazing angles by the Massachusetts Institute of Technology Lincoln Laboratories (MIT/LL) in the 1980s and 1990s [11].
- Naval Research Laboratory (NRL) four frequency sea clutter measurements at high grazing angles [12].
- Georgia Tech measurements of sea clutter at low grazing angles [13,14].
- The “SNOWMAN” MMW measurements performed jointly by the U.S. Army MICOM and GTRI on snow-covered ground [15].

Countless other measurement programs have been conducted in the United States and Europe. This section will attempt to summarize data from these and many other experimental programs, but the interested reader is urged to also review the references at the end of the chapter.

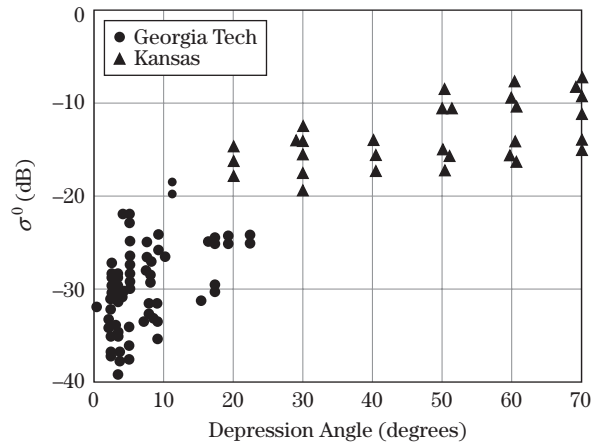
### Land Reflectivity

**Dependence on Grazing Angle** Figure 5-9 shows the backscatter reflectivity of crops and short grass at X-band compiled from three data sources. The data are reported as a function



**FIGURE 5-9** ■  $\sigma^0$  data for grass and crops from several sources at X-band. (Data from [16–18]. With permission.)

**FIGURE 5-10** ■  $\sigma^0$  data for trees from two sources for X-band. (Data from [16,18]. With permission.)

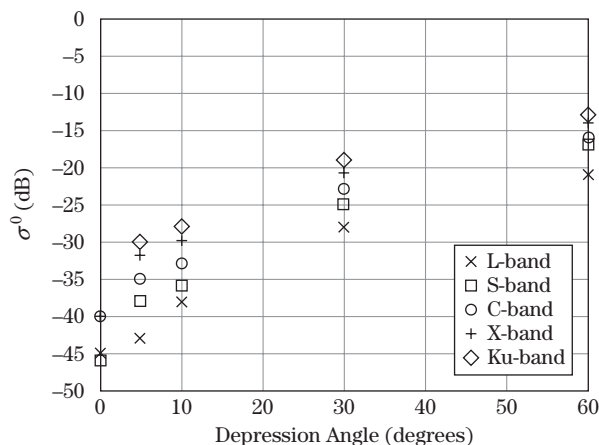


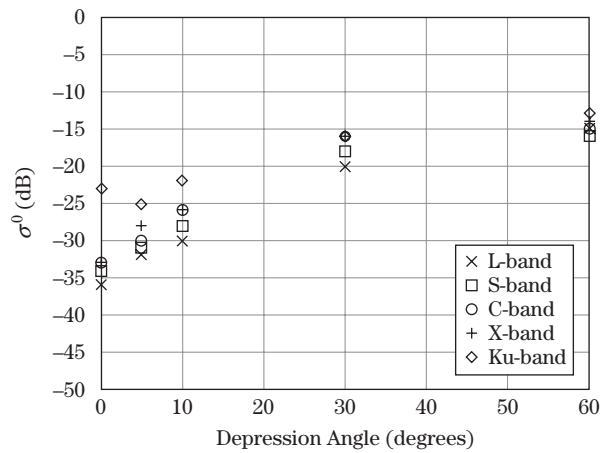
of depression angle [16–18]. The data consist of time averages of individual spatial samples and exhibit the expected characteristic dependence on grazing angle shown in Figure 5-6, being relatively independent of angle above 10 degrees while rapidly decreasing in value at angles below 10 degrees. The greater spread in the data at very low depression angles is most likely due to shadowing effects.

Figure 5-10 presents backscatter reflectivity data from trees over the same angular regime as Figure 5-8. Again, the data represent time averages of spatial samples. A similar dependence is exhibited for the angular dependence as for grass and crops; however, the values for  $\sigma^0$  are several dB higher, and the spatial variation is greater.

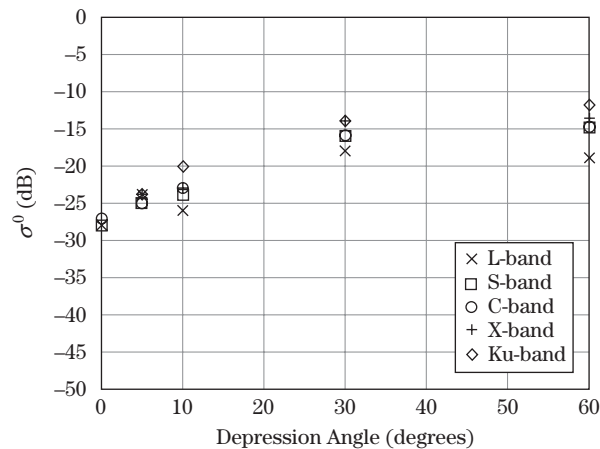
**Dependence on Frequency Band** Figures 5-11 through 5-14 present plots of averaged reflectivity data for five frequency bands compiled by Nathanson [15]. The data consist of  $\sigma^0$  values at 0–1.5°, 3°, 10°, 30°, and 60°. Figure 5-11 gives data for relatively flat desert for L-band through X-band as a function of grazing angle. The spread in the data over the frequency range is approximately 10 dB, and the spread over 0 to 60° depression angle is more than 30 dB. Data from other sources including bare hills at L-band have yielded extremely high values for the reflectivity ( $\sigma^0 > 0$  dB with corresponding RCS values of +40 dBsm) when viewing the sides of the hills at essentially 0° depression angle [16].

**FIGURE 5-11** ■ Averaged reflectivity data for desert terrain as a function of frequency. (Adapted from Nathanson [15]. With permission.)





**FIGURE 5-12** ■ Averaged reflectivity data for rural farmland as a function of frequency. (Adapted from Nathanson [15]. With permission.)



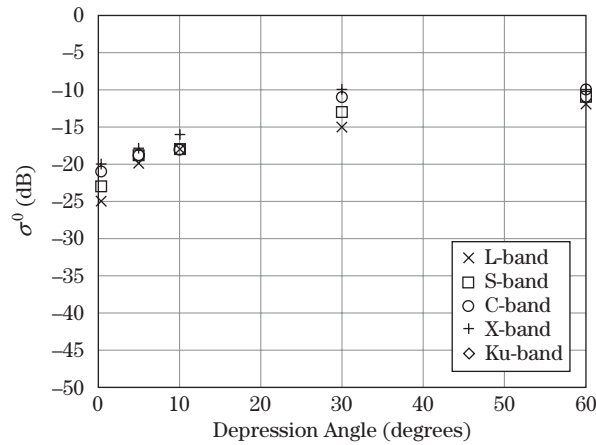
**FIGURE 5-13** ■ Plot of averaged reflectivity data for heavy vegetation/jungle as a function of frequency. (Adapted from Nathanson [15]. Used with permission.)

Figure 5-12 shows averaged data for rural farmland. The spread in the data with frequency is lower than for the desert terrain, being approximately 6 dB. Also, the variation with depression angle is somewhat less, being approximately 25 dB. Figure 5-13 gives averaged data for heavy vegetation and jungle. The spread in the data with frequency is again approximately 6 dB with a similar angular variation as Figure 5-12.

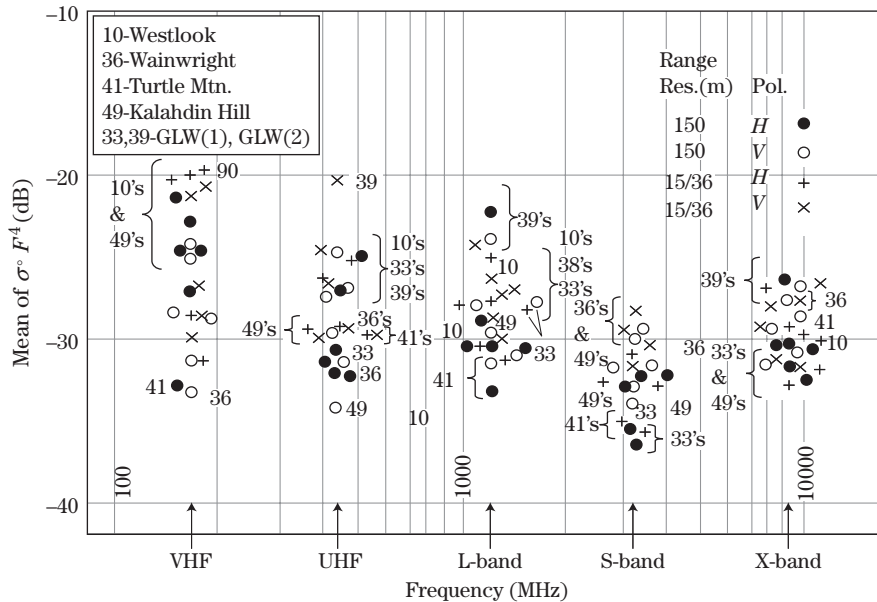
Figure 5-14 gives averaged data for urban environments. The spread in the data with frequency band is lower than the previous plots, but the data are high in value as might be expected since presumably many man-made targets are included. Also, the dependence on depression angle is less than for the previous figures.

Very low angle clutter returns are of particular concern as such returns can significantly affect the detection of low flying objects such as missiles. The MIT Lincoln Laboratory performed extensive measurements in the 1980s to characterize low angle clutter over many terrain types [11]. Figure 5-15 gives  $\sigma^0$  data collected by the MIT/LL for very low depression angles (0.4 to 1°) and for several frequency bands from UHF to X-band, including both vertical and horizontal polarizations. As can be seen from the figure,  $\sigma^0$  appears to be at a maximum in the UHF band, decreasing at the higher frequencies, presumably due to absorption of the energy. Also, little difference is seen between

**FIGURE 5-14** ■ Plot of averaged reflectivity data for urban terrains as a function of frequency. (Adapted from Nathanson [15]. With permission.)



**FIGURE 5-15** ■  $\sigma^0$  data for several forest/low-relief terrains at low ( $0.4\text{--}1^\circ$ ) depressions angles as a function of frequency. (From Billingsley [11]. With permission)



horizontal and vertical polarizations. Figure 5-16 gives data on mountain terrains for several frequency bands. As can be seen, the reflectivity decreases rapidly with increasing frequency, presumably caused by vegetation attenuating the returns from bare rock and ground at the higher frequencies. Note that  $\sigma^0$  values of nearly 0 dB are reported at the lowest-frequency bands. Such values can often overwhelm radar MTI processors, leading to false alarms.

**Sea Reflectivity** The sea surface is composed of salty water with a reflection coefficient of almost  $-1$  at microwave frequencies for small grazing angles. Thus, a smooth sea appears like an infinite flat conductive plate that scatters all of the energy impacting the surface in a forward direction so no backscatter occurs. As the wave height starts to increase, the sea begins to appear like a rough surface, and as the wave height continues to grow, organized

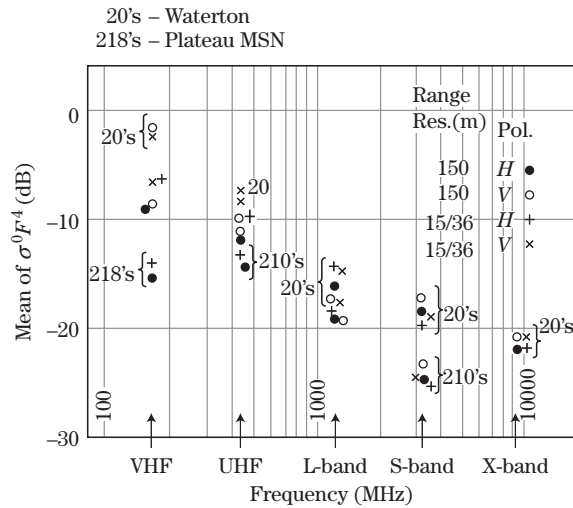


**FIGURE 5-16** ■  $\sigma^0$  data for two mountain terrains at low ( $1.2^\circ$ ) depression angles as a function of frequency. (From Billingsley [11]. With permission.)

**TABLE 5-2** ■ Parameters Affecting Sea Return

PARAMETER	COMMENTS
Wave height	Strong proportional dependence
Wind speed	Dependence increases with increasing frequency
Wind/wave look direction	Significant difference between up-wave and down-wave
Polarization	Dependence decreases with increasing frequency
Grazing angle	Strong dependence at low angles, weaker dependence in the plateau region
Frequency band	Proportional to frequency in the microwave region

wavefronts occur that provide a strong directional dependence to the scattering. Table 5-2 gives the primary physical parameters that can affect sea return.

As can be seen from Table 5-2, wave height is one of the major physical parameters affecting sea return. Unfortunately, wave height is often difficult to measure during experiments. In addition, wave height is irregular. The wave height is considered to be the “significant wave height,” which is an estimate of the average peak-to-trough height of the largest one-third of the observed waves.

Since it is easier to estimate a range of wave heights than a specific wave height, sea return data are often give in terms of *sea state*. The Douglas sea number [6] is a specific, widely used scale of sea states, correlated wind speeds, and subjective descriptions in which each defined sea state represents a range of wave heights as given in Table 5-3.<sup>2</sup> Note that sea states are defined only for a fully developed sea, that is, a sea over which a constant wind has been blowing long enough to build waves to their maximum height and the distance over which the wind has been blowing (called the *fetch*) is far enough to build waves to their maximum value.

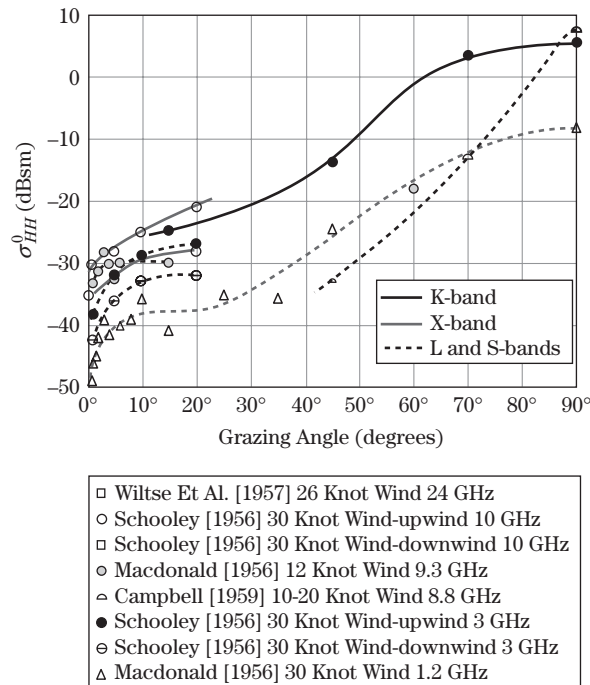
<sup>2</sup>Other sea scales exist, such as the Beaufort scale and the World Meteorological Organization (WMO) scale. The WMO scale generally adopts the Douglas sea-scale definitions.

**TABLE 5-3** ■ Douglas Sea State versus Wave Height and Wind Speed for a Fully Developed Sea

Sea State	Significant Wave Height (ft)	Wind Speed (Kts)
0	0 to 0.5	0 to 2
1	0.5 to 1	2 to 7
2	1 to 3	7 to 12
3	3 to 5	12 to 16
4	5 to 8	16 to 20
5	8 to 12	20 to 25
6	12 to 20	25 to 32
7	20 to 40	32 to 45
8	40+	45+

Source: Adapted from Long [6] (with permission).

**FIGURE 5-17** ■ Sea return as a function of grazing angle for four radar bands. (From Long [6]. With permission.)



**Angular and Frequency Dependencies** Figure 5-17 gives horizontally polarized sea return data from several original sources for four radar bands as a function of grazing angle, wind speeds corresponding to high sea states, and upwind versus downwind directions. The data illustrate strong angular, frequency, and look direction dependence. Note that very high values of  $\sigma^0$  (above 0 dB) are seen at nadir. This suggests that sea clutter could be a significant limitation when searching for a small, slow-moving target on the sea surface. In addition to high backscatter, shadowing and sea Doppler accentuate the detection problem.

Figure 5-18 presents a plot of averaged data for sea clutter from Nathanson [15] for five radar bands as a function of depression angle for sea state 1. For this low sea state,  $\sigma^0$  is relatively small, particularly for low depression angles. Note that there is much more

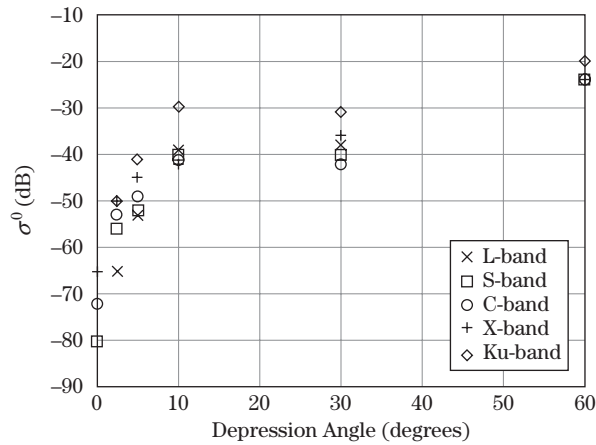


**FIGURE 5-18** ■ Averaged sea return as a function of depression angle and radar band, sea state 1, VV polarization. (Adapted from Nathanson [15]. With permission.)

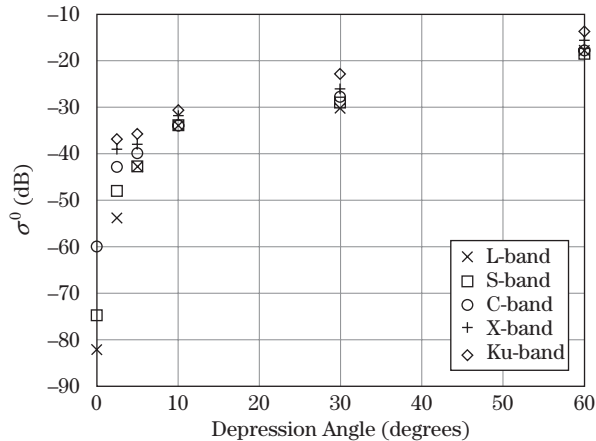


**FIGURE 5-19** ■ Averaged sea return as a function of depression angle and radar band, sea state 3, VV polarization. (Adapted from Nathanson [15]. With permission.)

variation with frequency at the lower depression angles. Figure 5-19 gives averaged sea return data for sea state 3. These data are almost 10 dB higher than for sea state 1. The frequency dependencies appear to be similar to those for Figure 5-18.

Figure 5-20 compares values of  $\sigma^0$  for vertical and horizontal polarized returns from sea clutter at L- and X-bands. As was discussed previously, there is a much greater difference between the vertical and horizontal values of  $\sigma^0$  at L-band than there is at X-band.

One important parameter for sea return is the range fall-off of sea clutter echo power. As range increases, the grazing angle  $\delta$  at which the sea surface is viewed decreases. When  $\delta$  falls below the critical angle,  $\theta_C$ , the surface becomes “smooth” by the Rayleigh criterion of equation (5.15). Figure 5-21 gives the measured sea data as a function of range dependence for two regions: above and below the critical angle; and low and high wave heights [19]. Note that the range for the critical angle moves in (higher depression angle), and the wave height (and thus, the rms surface roughness) increases as predicted by equation (5.16). These data show that, below the critical angle, the  $R^{-3}$  range dependence of pulse-limited sea clutter return transitions to approximately an  $R^{-7}$  dependence so that the clutter return rapidly becomes insignificant. In addition, the critical angle often appears near the first multipath null angle, further enhancing the clutter roll-off with range. (See Chapter 4 for a discussion of multipath.)

**FIGURE 5-20** ■ Sea return as a function of depression angle for VV and HH polarizations, land X-bands, sea state 3. (Adapted from Nathanson [15]. With permission.)

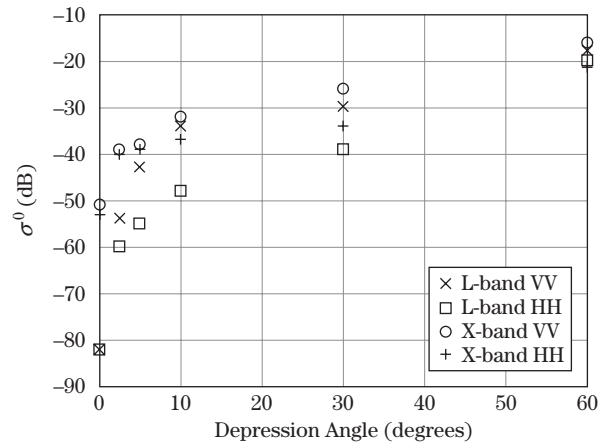
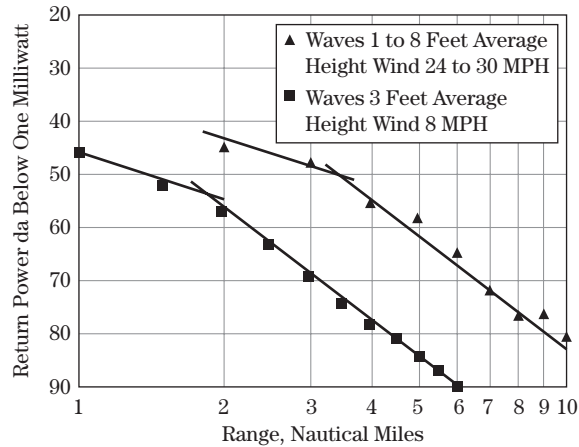


**FIGURE 5-21** ■ Range dependence of sea return for two wave conditions, X-band, HH polarization. (From Dyer and Currie [19]. With permission.)



**Ducting** Because the sea surface has a strong reflection coefficient and water vapor is always present near the surface, conditions can occur such that a high water concentration and thus a reflective layer occur over some region above the water. When this happens, the high water concentration layer and the sea surface act like a two-dimensional waveguide, trapping the radiofrequency (RF) energy and extending the range of sea return detection. The reflection coefficient of the sea determines the duct shape and transmission efficiency. Figure 5-22 shows two sets of sea return data as a function of grazing angle taken with the same radar, the only difference being the lapse of several hours in time. The morning data show much less dependence on angle than the afternoon data. Apparently, ducting conditions were present in the morning but were absent in the afternoon. These data were collected in February in Wildwood, New Jersey, showing that ducting can occur in cold as well as tropical conditions.

Figure 5-23 gives a summary of range dependence measurements above and below the critical angle performed in Boca Raton, Florida, over a period of several years at X-band. Range dependencies quite different from the expected  $R^{-3}$  for a pulse-limited radar occurred a significant portion of the time, indicating both ducting conditions and possibly variations in the multipath field from time to time.

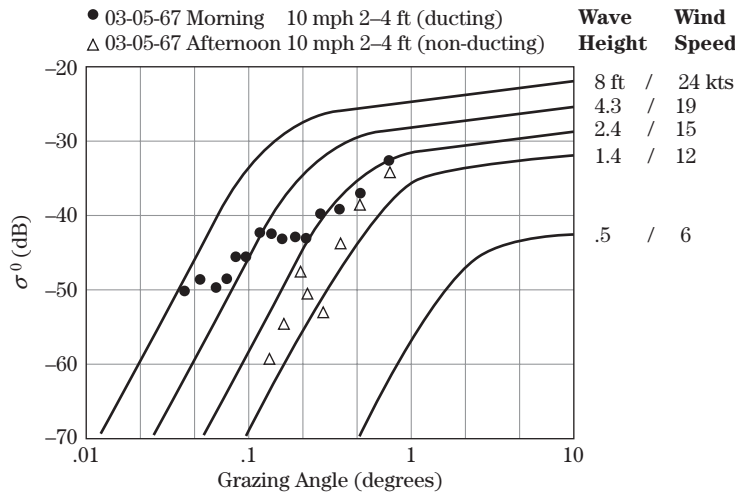


**FIGURE 5-22** ■ Comparison of sea return achieved under ducting and nonducting conditions, X-band, HH polarization. (From Dyer and Currie [19]. With permission.)

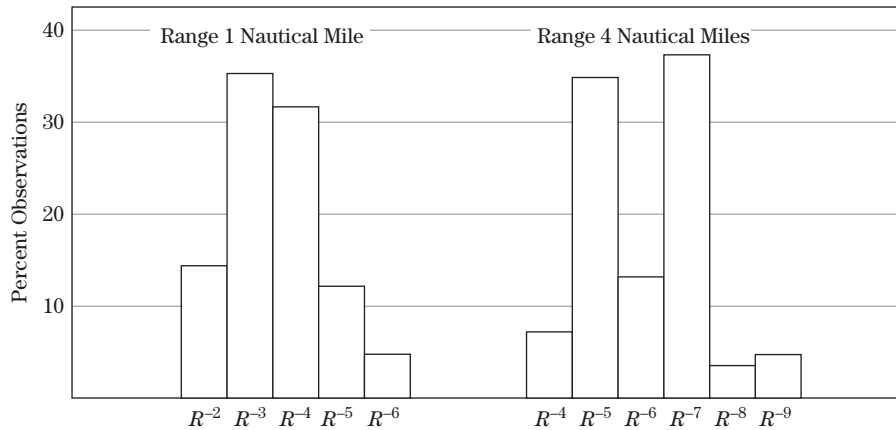


**FIGURE 5-23** ■ Measured range dependencies above and below the critical grazing angle as a percentage of total measurements. (From Dyer and Currie [19]. With permission.)

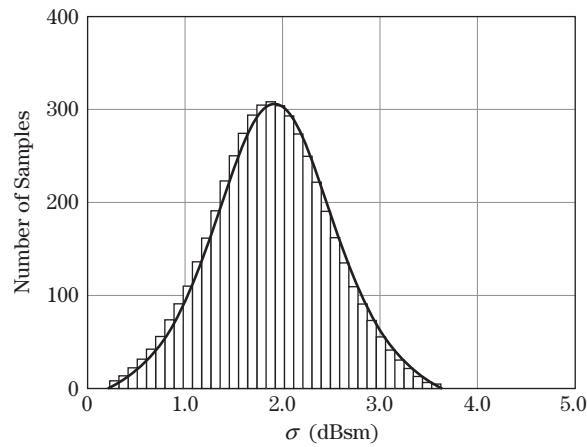
### 5.2.2.4 Clutter Variability Properties

In the previous section average values for surface clutter were discussed, but the variability of clutter reflectivity with time and or space is as least as important, if not more so. These topics are addressed in this section.

#### Land Clutter Variations

**Temporal Variations** Land clutter generally contains some vegetation. Consequently, land clutter returns will vary with time due to wind-blown motion of leaves, needles, branches, and stalks. Since such motion makes detection more difficult, it must be described and allowances made for it when calculating the probability of detection for a target in clutter. The probability density function,  $p_{\sigma}(\sigma)$ , and the cumulative distribution function (CDF),  $P_{\sigma}(\sigma)$ , are used to describe the variation in RCS or power. Figure 5-24 illustrates an estimated unnormalized probability density function obtained as the histogram of the measured data, which is just a plot of the number of independent clutter samples that fall within a series of narrow power intervals. If the histogram is normalized by dividing the sample counts by the total number of samples times the width of an amplitude bin, an estimate of the PDF is obtained.

**FIGURE 5-24** ■ A histogram provides an estimate of an unnormalized probability density function.



The CDF is the integral of the PDF,

$$P_{\sigma}(\sigma) = \int_{-\infty}^{\sigma} P_{\sigma}(v) dv \quad (5.20)$$

Values of the CDF increase monotonically from zero to one. If the area under the normalized histogram from the lowest value to some value  $\sigma$  is calculated, an estimate of the CDF is obtained. Cumulative distributions are quite useful because some key parameters are easily read from a plot of the CDF. For instance, the median value is the 50% point ( $P_{\sigma}(\sigma) = 0.5$ ) on the curve. Rivers [20] observed that for log-normal and Weibull distributions with parameters appropriate for modeling measured sea clutter, the mean value of the power,  $\bar{\sigma}$ , can be estimated from the value corresponding to the 90% point on the CDF,  $\sigma_{0.9}$ , to be 3.5 dB below the 90% point by the relation

$$\bar{\sigma} = (\sigma_{0.9} - 3.5 \text{ dB}) \pm 0.5 \text{ dB} \quad (5.21)$$

Newer land clutter data observed by Billingsley [11] is spikier than that used by Rivers, suggesting that the  $\pm 0.5$  dB tolerance in equation (5.21) should be wider [6]. As another example of the usefulness of CDFs, the standard deviation in dB of a log-normal distribution is  $\sigma_{0.84} - \sigma_{0.16}$ .

Figure 5-25 gives a measured CDF for wind-blown trees at X-band. The dotted line approximates the CDF corresponding to an exponential PDF in this plot format. The data in Figure 5-25 appear approximately exponential in their general shape, but their distribution is seen to be wider than exponential. For example, the 90% mark on the CDF occurs at about  $-39$  dB for the exponential distribution, but not until the larger value of  $-30$  dB for the X-band tree data. Variable clutter complicates detection in two ways. First, since the return is changing with time, part of the time the reflectivity will be larger than the average value. Second, the rate of fluctuation can limit the effectiveness of Doppler processing.

Table 5-4 gives the standard deviations (square root of the variance) measured for wind-blown vegetation as a function of frequency and polarization. The standard deviation for an exponential distribution, converted to a decibel scale, is approximately 5.7 dB [6]. Thus, at 9 GHz the distributions appear narrower than exponential, but at 95 GHz and higher they are wider than exponential.

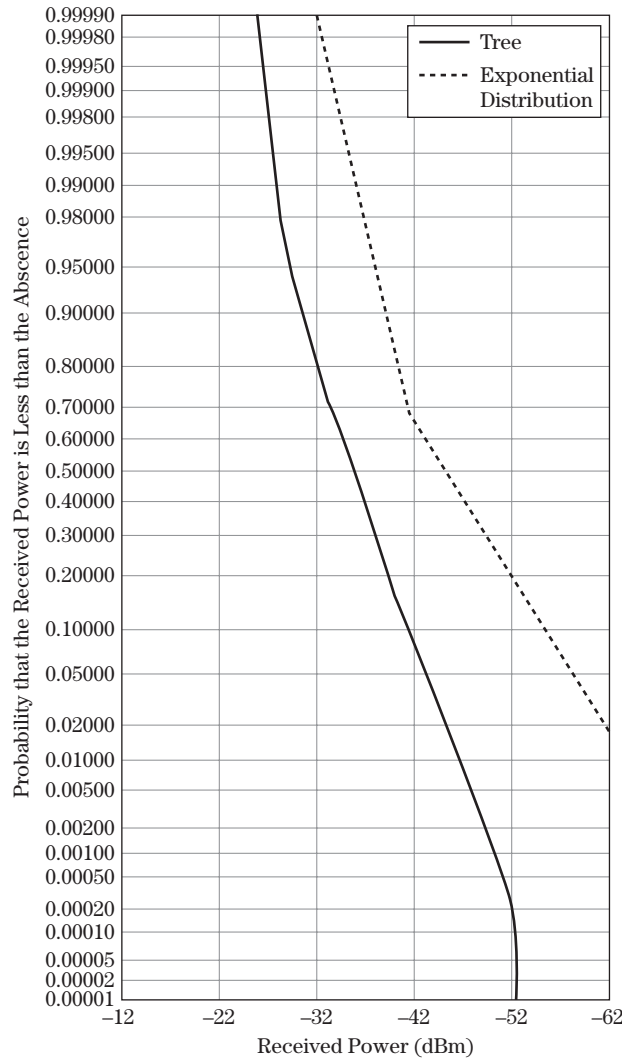


**FIGURE 5-25** ■ Cumulative probability distribution for deciduous trees at X-band, 4.1° depression angle. (From Currie et al. [21]. With permission.)

**Decorrelation Time** An important metric of clutter temporal properties is the decorrelation time. The decorrelation time,  $\tau_0$ , is defined as the time lag required for the autocorrelation function of a set of clutter samples to decay to some defined fraction, usually 0.5 or  $1/e = 0.367$  of its peak value at zero lag. The autocorrelation function  $\phi_{cc}(\tau)$  of the time-varying clutter return,  $c(t)$ , measures how similar successive data samples are to a first sample as the delay time between samples increases. The power spectral density function is the Fourier transform of  $\phi_{cc}(\tau)$ ,

$$S_{cc}(f) = \int_{-\infty}^{+\infty} \phi_{cc}(\tau) e^{-j2\pi f\tau} d\tau \quad (5.22)$$

where  $\tau$  is the autocorrelation lag time.

If the clutter power spectrum is “white” (constant) over the receiver bandwidth  $B$ , then the decorrelation time equals  $1/B$ . This is the same as the case for random noise.

**TABLE 5-4** ■ Measured Standard Deviations of Temporal Variations for Trees

Frequency Clutter Type	Polarization	Average Value of Standard Deviation (dB)			
		9.5 GHz	16.5 GHz	35 GHz	95 GHz
Deciduous trees, summer	Vertical	3.9	—	4.7	—
	Horizontal	4.0	—	4.0	5.4
	Average	4.0	—	4.3	5.4
Deciduous trees, fall	Vertical	3.9	4.2	4.4	6.4
	Horizontal	3.9	4.3	4.3	5.3
	Average	3.9	4.2	4.3	5.0
Pine trees	Vertical	3.5	3.7	3.7	6.8
	Horizontal	3.3	3.8	4.2	6.3
	Average	3.4	3.7	3.9	6.5
Mixed trees, summer	Vertical	3.3	—	4.0	—
	Horizontal	4.6	—	4.2	—
	Average	4.4	—	4.1	—
Mixed trees, fall	Vertical	4.1	4.1	4.7	6.3
	Horizontal	4.5	4.3	4.6	5.0
	Average	4.4	4.2	4.6	5.4
Field, tall grass	Vertical	1.5	—	1.7	2.0
	Horizontal	1.0	1.2	1.3	—
	Average	1.3	1.2	1.4	2.0
Rocky area	Vertical	1.1	2.2	1.8	1.6
	Horizontal	1.2	1.7	1.7	1.7
	Average	1.1	1.9	1.8	1.7
10-in. corner reflector located in grassy field		1.0	1.0	1.2	1.2

Source: From Currie et al. [21] (with permission).

Because the receiver bandwidth also determines the Nyquist rate of its output, the received signal output will normally be sampled at a rate of about  $1/B$  samples per second (see Chapter 14). Since the samples are spaced by the decorrelation time, the sampled data will appear uncorrelated with a white power spectrum. If the clutter instead has a decorrelation time greater than  $1/B$  seconds, then the sampled clutter data will not appear white and will have some degree of correlation from one sample to the next.

The decorrelation time is important for detection analysis because it determines the number of uncorrelated samples,  $N_i$ , available for integration for signal-to-clutter improvement according to

$$N_i = \begin{cases} \frac{N_t PRI}{\tau_0}, & PRI \leq \tau_0 \\ N_t, & PRI \geq \tau_0 \end{cases} \quad (5.23)$$

where  $N_t$  is the total number of clutter samples and  $PRI$  is the time between samples. As will be seen in Chapter 15, coherent or noncoherent integration of radar data can improve the detectability of targets in the presence of interference, provided that the interference samples are uncorrelated so they can be made to “average out” while the target signal is reinforced. Thus, if the total sample collection time  $N_t PRI$  is shorter than the decorrelation time, no uncorrelated clutter samples are obtained, and no improvement in target detectability is gained by integration of successive samples.

If the clutter does decorrelate during the collection time, then some improvement in target detectability is possible by integrating multiple samples. In coherent integration, the complex (in-phase [I] and quadrature [Q]) data are integrated (added) to cause the target component of the samples to add in phase, whereas the uncorrelated clutter and noise components do not add in phase. In this case, the signal-to-clutter ratio (SCR) and signal-to-noise ratio (SNR) (and thus signal-to-interference ratio [SIR]) are increased, significantly improving target detectability. In noncoherent integration, the magnitude or magnitude squared of the complex receiver output data is taken and then integrated. Discarding the phase information eliminates the possibility of a gain in SCR. Nonetheless, an improvement in target detectability is still achieved, though less than in the coherent integration case. Chapter 15 discusses the effects of coherent and noncoherent integration on target detection in white interference in greater detail.

Figure 5-26 presents the autocorrelation functions for windblown trees in conditions described as a “windy day,” while Table 5-5 gives the 50% ( $\tau_{1/2}$ ) and  $1/e$  ( $\tau_{1/e}$ ) decorrelation times in seconds. As can be seen, essentially no integration improvement could be achieved at the lower frequency bands, and only limited improvement could be achieved at X-band.

Figure 5-27 gives measured decorrelation times for higher frequencies (10 GHz through 95 GHz) as a function of wind speed. As can be seen, at the higher frequencies much shorter decorrelation times are observed, an advantage for obtaining better noncoherent integration efficiency.

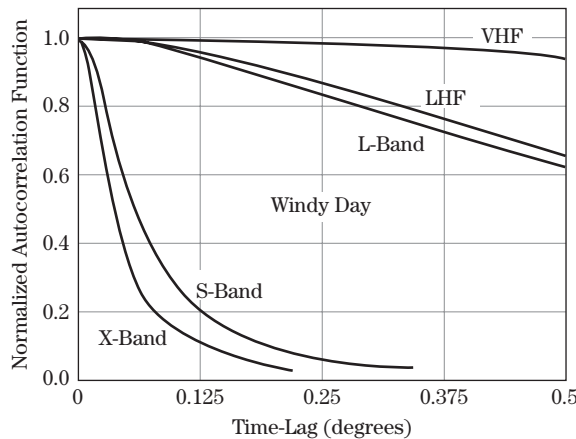


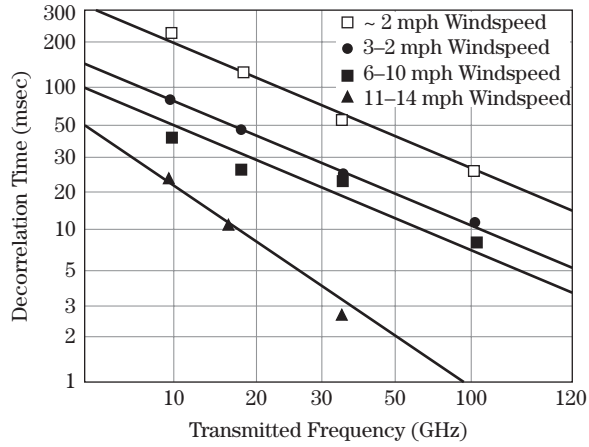
**FIGURE 5-26** ■ Autocorrelation functions of the returns from windblown trees for several frequency bands on a windy day. (From Billingsley [11]. With permission.)

**TABLE 5-5** ■ Measured Decorrelation Times at Five Frequency Bands

Frequency Band	Correlation Time(s)	
	$\tau_{1/2}$	$\tau_{1/e}$
VHF	4.01*	5.04*
UHF	0.69	0.94
L-Band	0.67	0.95
S-Band	0.062	0.081
X-Band	0.033	0.049

Note: \* = extrapolated estimate  
 Source: From Billingsley [11] (with permission).

**FIGURE 5-27** ■ Decorrelation time for windblown trees as a function of wind speed. (From Currie et al. [21]. With permission.)

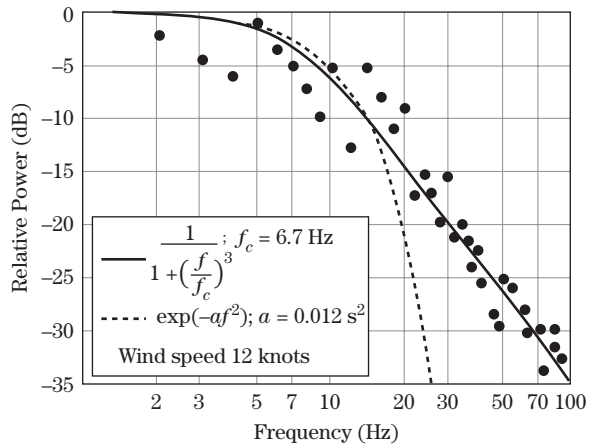


**Clutter Frequency Spectra** A second way to look at temporal variations in clutter returns is in terms of clutter power spectra. Power spectra tell us how rapidly a return is varying. This is of interest since many radars use Doppler processing to improve target detection in heavy clutter. Clutter spectra are of interest for two situations: (1) very slow-moving targets such as ground vehicles or boats; and 2) high-speed targets that may be affected by aliasing (“foldover”) of the clutter spectra around the pulse repetition frequency (PRF). (See Chapter 8 for a discussion of Doppler foldover.)

Theoretical formulations of clutter spectra yield Gaussian-shaped spectra, yet a number of actual clutter measurements have yielded power law-shaped spectra. These differences are of concern since power law spectral shapes roll off more gradually with frequency than Gaussian spectra. This problem was first identified by Fishbein et al. [22] when attempting to develop models for the spectral data on trees at X-band shown in Figure 5-28 [22]. They found that a Gaussian curve fit rolled off much too rapidly. A much better fit was obtained with a power law curve of the form

$$S_{cc}(f) = \sigma_{DC} \left( \frac{1}{1 + \left(\frac{f}{f_c}\right)^n} \right) \tag{5.24}$$

**FIGURE 5-28** ■ Spectral data from trees at X-band with Gaussian and power function curve fits. (From Fishbein et al. [22]. With permission.)



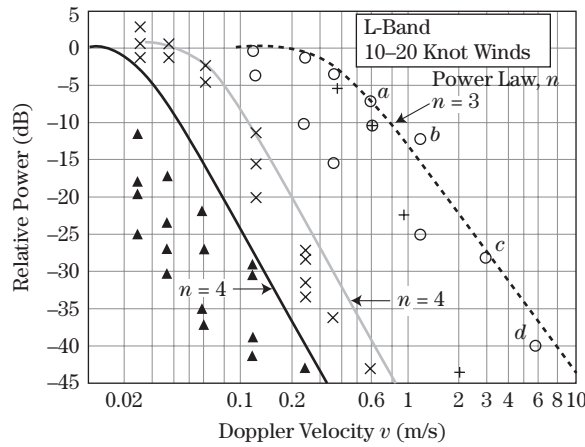


**FIGURE 5-29** ■ L-band spectral data with various power law curve fits. (From Simpkins et al. [23]. With permission.)

Measurements	Models
Mountains	▲
Partially Wooded Hills	×
Heavily Wooded Valleys (Lowlands)	○
a, b, c, d: Extrema	—
+ : Widest Lincoln Measurement	- - -

where  $\sigma_{DC}$  is the DC clutter power return,  $f_c$  is the 3 dB cutoff frequency for the power spectrum, and  $n$  is an integer selected to best fit the data. Fishbein et al. found that a value of  $n = 3$  fit the data best. Other experimenters have also measured power law dependencies. Figure 5-29 presents power spectral data at L-band for woods and wooded hills measured by the U.S. Air Force’s Rome Air Development Center (RADC) [23]. For these data, the best power law fits were obtained with  $n = 3$  or 4.

Table 5-6 presents the cutoff and power law exponents determined for wind-blown tree data at 10 GHz though 95 GHz for both logarithmic and linear receiver transfer functions. The exponent seems to lessen with increasing frequency, implying a slower roll-off, while the logarithmic receiver provides a steeper roll-off than the linear case.

To date, theorists have not been able to determine a theoretical basis for power law frequency dependence, yet experimenters continue to observe them in measured data. One possibility is that Doppler spectra can be significantly affected by radar system imperfections such as nonlinearities, dynamic range limits, and oscillator phase noise. Recently, Billingsley [11] measured tree data with a high-quality coherent instrumentation radar having high linearity over a wide dynamic range, stabilized oscillators, and low-sidelobe narrow Doppler filters. He obtained clutter power spectra that were well modeled by a

**TABLE 5-6** ■ Corner Frequencies and Power Exponents for Tree Return Spectra

Power Function Parameter	Frequency			
	9.5 GHz	16 GHz	35 GHz	95 GHz
$n$ (linear)	3	3	2.5	2
$n$ (log)	4	3	3	3
$f_c$ (Hz), 6–15 mph wind speed	9	16	21	35

Source: From Currie et al. [21] (with permission).

two-sided exponential roll-off. This spectrum has a rate of decay that falls between the Gaussian and power law models.

These observations suggest that equipment imperfections may be a significant contributor to the slower decay of data that are well modeled by power law spectra. However, many fielded systems will suffer these limitations, so a practical approach to performance assessments could use both Gaussian and power law clutter power spectrum models to establish upper and lower bounds on performance in the presence of clutter.

**Spatial Variations** As discussed earlier, when the radar scans across the surface, the number and types of scatterers within the radar beam change, resulting in a changing return. These variations are described using the same tools as for temporal variations (i.e., amplitude distributions and spatial correlation functions).

Spatial amplitude distributions can be much wider than temporal distributions, particularly at lower grazing angles where shadowing and multipath come into play. Most experimenters resort to Weibull distributions to describe the variations. A key finding of experimenters is that at higher grazing angles, spatial distributions tend to appear exponential (Weibull width parameter  $a \approx 1$ ) while at low grazing angles the width parameter increases greatly. The calculated spatial distributions by Booth [24] for cultivated land at X-band in Figure 5-30 illustrate this effect. They are approximately exponential-distributed (width parameter  $a \approx 1$ ) at a grazing angle of  $5^\circ$  but become much wider at lower angles.

**FIGURE 5-30** ■ Spatial distributions of cultivated land as function of grazing angle X-band. (From Booth [24]. With permission.)

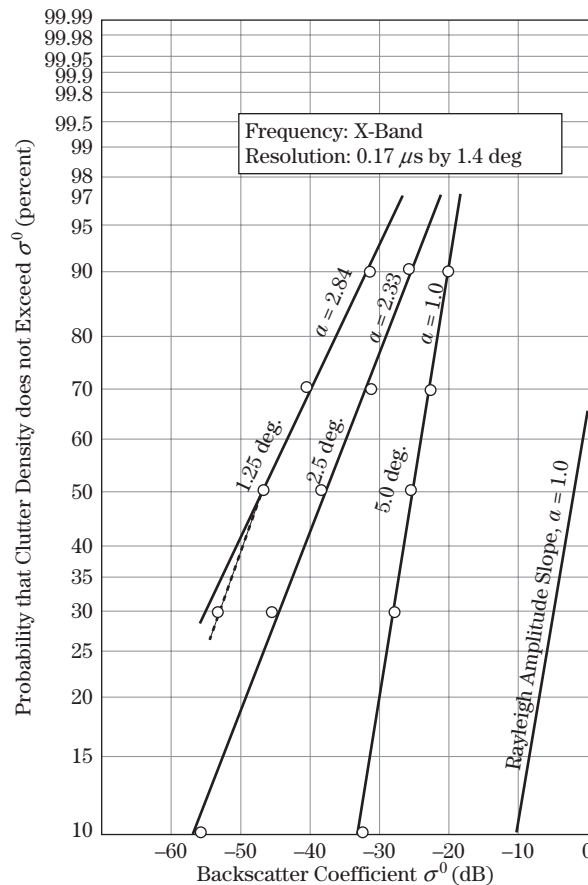


**TABLE 5-7** ■ Spatial Statistical Attributes for X-Band Ground Clutter

Terrain Type	Depression Angle (deg)	Weibull Parameters			Ensemble Mean Clutter Strength $\sigma^0$ (dB)	Percent of Samples above Radar Noise Floor	Number of Patches
		$a$	$\sigma_m$ (dB)	$\sigma_w^0$ (dB)			
Rural/	0.00–0.25	4.8	–60	–33	–32.0	36	413
Low-Relief	0.25–0.50	4.1	–53	–32	–30.7	46	448
	0.50–0.75	3.7	–50	–32	–29.9	55	223
	0.75–1.00	3.4	–46	–31	–28.5	62	128
	1.00–1.25	3.2	–44	–30	–28.5	66	92
	1.25–1.50	2.8	–40	–29	–27.0	69	48
	1.50–4.00	2.2	–34	–27	–25.6	75	75
Rural/	0–1	2.7	–39	–28	–26.7	58	176
High-Relief	1–2	2.4	–35	–26	–25.9	61	107
	2–3	2.2	–32	–25	–24.1	70	44
	3–4	1.9	–29	–23	–23.3	66	31
	4–5	1.7	–26	–21	–22.2	74	16
	5–6	1.4	–25	–21	–21.5	78	9
	6–8	1.3	–22	–19	–19.1	86	8
Urban	0.00–0.25	5.6	–54	–20	–18.7	57	25
	0.25–0.70	4.3	–42	–19	–17.0	69	31
	0.70–4.00	3.3	–37	–22	–24.0	73	53

$\sigma_m$  = median reflectivity

$\sigma_w^0$  = mean reflectivity

$F$  = propagation factor (see Chapter 4)

Source: Adapted from Billingsley [11] (with permission).

The effect of grazing angle on the PDF is further illustrated by Table 5-7, which gives spatial statistics for rural and urban settings as a function of grazing angle for very low angles. For rural settings, and angles above 5 degrees, the Weibull width parameter  $a$  indicates an approximately exponential power PDF ( $a \approx 1$ ), while the PDF becomes much wider for lower angles. As might be expected, the urban setting exhibits larger width parameters and thus distributions wider than exponential even at 4°. Thus, in general, exponential power statistics are expected in the plateau regions for all but urban clutter, but much wider distributions are seen for low grazing angles. For urban settings, wide distributions may be observed even in the plateau region because of the height of man-made structures that cause shadowing even at higher grazing angles.

**Sea Clutter Variation** The return from the sea varies in time due to the effects of the wind on sea waves. These effects are of several types: waves created by the wind blowing for a period of time over a given “fetch” of water, ripples that appear on the surface due directly to the wind, white caps created when the tops of waves break over the front of the waves, and airborne spray that results from ripples and white caps.

Initially, amplitude (voltage) statistics from a fixed range-azimuth cell were assumed to be Rayleigh. This model fit measured data for low-resolution radars well. However, as finer-resolution radars came into use over time, non-Rayleigh statistics were encountered. The current view is that wind-produced ripples on the sea surface produce noise-like variations in sea return or “speckle” that are approximately Rayleigh distributed in amplitude but that the large-scale moving structure of the sea swells changes the local slope of the

rippled surface, imposing a time-varying change in the mean of the Rayleigh PDF in a give spatial cell. The resulting amplitude statistics of the return are non-Rayleigh, implying a non-Gaussian model of the complex I/Q data.

In general, the amplitude statistics are observed to become “spikier” with decreasing grazing angle and decreasing radar footprint area, possibly due to a decreasing average or median clutter value while the strength of the sea clutter spikes remains relatively constant. Also, horizontal polarization tends to present spikier clutter than does vertical polarization, particularly at low grazing angles. Sea clutter statistics also vary with the radar-wind/wave look direction.

Experimenters have used Weibull, log-normal, and K distributions to model sea statistics. In particular, Ward et al. [25] and Ward [26] performed extensive modeling of sea return using the K distribution, a two-parameter distribution that can be related to the Weibull and the log-normal. It is given by [6]

$$p_{\xi}(\xi) = \begin{cases} \frac{2b}{\Gamma(v)} \left(\frac{b\xi}{2}\right)^v K_{v-1}(b\xi), & \xi > 0 \\ 0, & \xi < 0 \end{cases} \quad (5.25)$$

where

$\xi = \sqrt{\sigma}$  is the clutter amplitude.

$v$  is the “shape factor.”

$b$  is a scale factor.

$\Gamma(\cdot)$  is the gamma function.

$K_n$  is the modified Bessel function of the third kind and order  $n$ .

Ward showed that this distribution describes the statistics of the product of two random variables, one described by a Rayleigh PDF and the other by a chi or gamma PDF [26]. Thus, the Rayleigh component can be used to model the speckle portion of the sea return, while the chi component can be used to model the time-varying mean of the local Rayleigh PDF due to large-scale sea structure, as discussed previously. The K distribution is believed to provide a better fit to sea clutter data, particularly for high resolution radars. See [25–27] for more information.

### **Temporal Variations**

*Correlation Properties* Work on calculating autocorrelation functions for sea returns has demonstrated that there are three mechanisms involved: (1) return from sea spray and white caps; (2) specular returns (spikes) from wavefronts; and (3) Bragg scattering [28]. The return from sea spray and Bragg scattering decorrelates very rapidly, while the specular return from the wavefront is highly correlated in time. Figure 5-31 illustrates this effect. The figure shows the autocorrelation function for sea return at  $K_u$ -band on two time scales. The upper scale indicates that almost 600 ms are required for the return to decorrelate to 50% of the ACF peak. The lower scale shows that the return drops from a normalized correlation of 1 to 0.85 in approximately one ms. The initial 15% decorrelation is due to the rapidly moving sea spray, while the longer 50% decorrelation time is due to the much slower motion of the wavefronts. Attempts have been made to use frequency agility to decorrelate sea return, but only the decorrelation due to sea spray and speckle is affected. Thus, sea waves tend to be highly correlated over many milliseconds, so that only scan-to-scan integration will be effective in increasing target detectability.

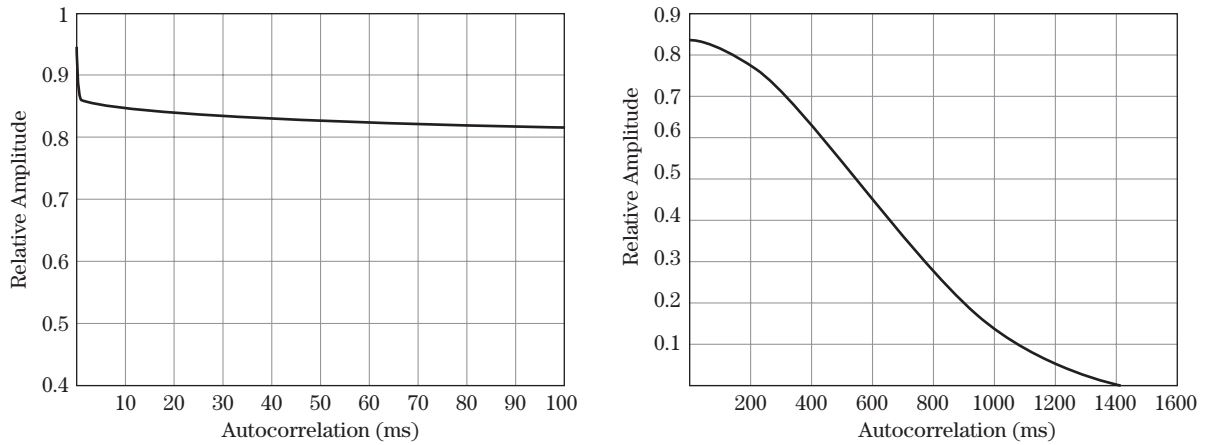


**FIGURE 5-31** ■ Autocorrelation function of sea return at  $K_u$ -band,  $3.9^\circ$  depression angle, and downwind/down-wave look direction. (From Ward et al. [25]. With permission.)

*Spectral Properties* The spectrum for sea clutter differs from that of land since sea waves can move physically toward or away from the radar. Thus, sea clutter can have a nonzero average Doppler frequency, unlike land clutter where moving scatterers are anchored in place. The Doppler frequency at which the motion of scatterers at a radial velocity,  $v$ , appears is given by the equation

$$f_d = \frac{2v}{\lambda} \quad (5.26)$$

Consequently, the width,  $\Delta f_d$ , of the Doppler spectrum is related to the width,  $\Delta v$ , of the velocity spectrum according to

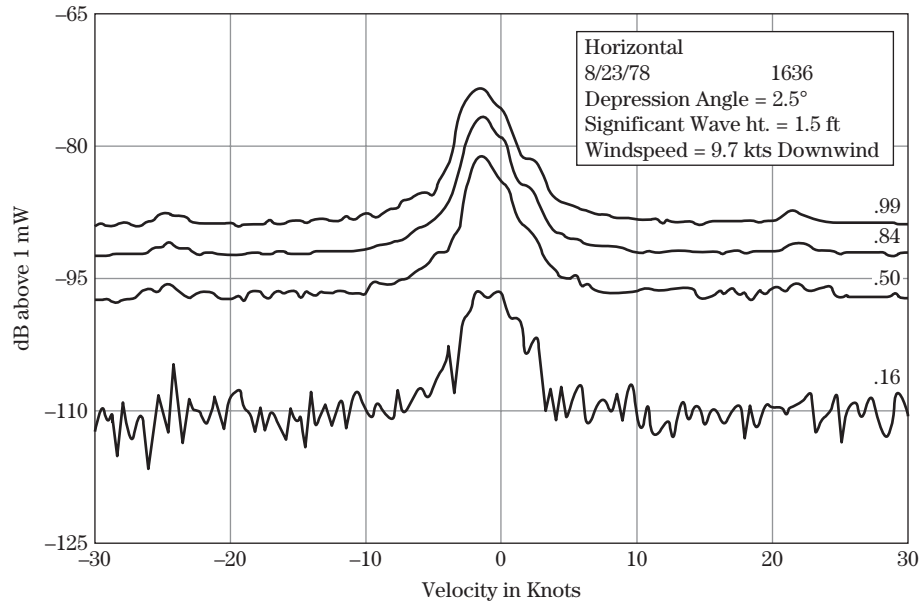
$$\Delta v = \frac{\lambda}{2} \Delta f_d \quad (5.27)$$

Figure 5-32 gives an example of the coherent spectrum at L-band, indicating the spectrum width for various amplitude levels [29]. At higher frequencies the center frequency and spectral width would be expected to scale proportional to the transmitted frequency in accordance with equations (5.26) and (5.27). While the spectra in this figure are approximately symmetric and Gaussian in shape, sea clutter spectra, especially at fine resolution and low grazing angle, are often distinctly asymmetric; see [28] for a number of examples.

*Sea Spikes* *Sea spikes* are strong returns from highly localized points or regions on the sea surface. The region generating the spike is usually, but not always, much smaller than the resolution cell area. Spikes are a problem for radar detection because they can exceed the signal level of small targets and can last for many seconds. Explanations of the causes for such returns are disputed by various researchers and have included returns from white caps, to sea spray, to returns from particular facets located on the wavefronts. Most likely all are responsible. Some general properties of sea spikes from the radar point of view reported by Werle [30] are as follows:

- Spikes occur significantly more often for horizontal than for vertical polarization.
- Spike intensity is usually greater for horizontal than for vertical polarization.
- HH/VV polarization ratios of greater than 10 dB were observed.

**FIGURE 5-32** ■  
Percentile of  
Doppler spectra at  
L-band. (From  
Plummer et al. [29].  
With permission.)



- Spikes at both HH and VV occurred much less often than for HH alone.
- Rarely was a VV spike seen without a concurrent HH spike.

Walker [28] states that the HH/VV intensity difference holds for the specular and Bragg scattering components but that the white cap component has roughly equal HH and VV backscatter. Given these properties, use of a dual-polarized radar and analysis of measured HH/VV polarization ratios may be one technique for recognizing and removing spikes from clutter data.

**Spatial Variations** Sea clutter returns are due to moving scatterers: the wind-driven spray and the gross and fine shape of the moving waves. Consequently the temporal and spatial variations of sea clutter are correlated. The only major difference between the two is due to wind-wave look direction. Generally, upwind/up-wave provides the highest radar return while downwind/down-wave provides the lowest return. This occurs because waves lean away from the wind so that the more vertical wavefronts are exposed in the upwind/up-wave direction, while the sloping backs are exposed in the downwind/down-wave direction.

### 5.2.3 Atmospheric Clutter

Atmospheric clutter primarily consists of hydrometeors, of which rain is the primary case of interest. Other atmospheric phenomena such as *angels* (clear air returns of unknown origin) can be of concern but will not be covered here. Frozen precipitation is also of interest, but primarily at millimeter wave frequencies because of the lower reflectivity of ice compared with water in the microwave bands. Experiments to determine average reflectivity as well as the spectral properties of rain are discussed in the following sections.

#### 5.2.3.1 Average Value Data

**Rain Reflectivity Average Values** Raindrops can be modeled as dielectric spheres of differing sizes that are contained within the radar resolution cell. The radar return from the rain is, thus, the sum of the reflectivity of all the drops. As a result, the drop-size distribution is critical to the resultant reflectivity. The variability between most rain clutter

**TABLE 5-8** ■ Average Rain Reflectivity versus Frequency Band

$Z$ , dBz	Radar band: Type	$\eta$ , dB m <sup>-1</sup>						
		Transmit frequency, GHz						
		S 3.0	C 5.6	X 9.3	K <sub>u</sub> 15.0	K <sub>a</sub> 35	W 95	mm 140
-12	Heavy stratus clouds				-100	-85	-69	-62
14	Drizzle, 0.25 mm/h	-102	-91	-81	-71	-58	-45*	-50*
23	Light rain, 1 mm/h	-92	-81.5	-72	-62	-49	-43*	-39*
32	Moderate rain, 4 mm/h	-83	-72	-62	-53	-41	-38*	-38*
41	Heavy rain, 16 mm/h	-73	-62	-53	-45	-33	-35*	-37*

\* Approximate

Source: From Nathanson [15] (with permission).

models is due to differences in the drop-size distribution selected. Referring to Figure 5-5, recall that the reflectivity of a sphere is a strong function of the ratio of the circumference to the wavelength in the Rayleigh scattering region, so that rain reflectivity depends strongly on the percentage of large drops and will increase with increasing frequency until the resonance region is encountered.

Of course, every rainstorm has a different drop-size distribution, and distributions often change in differing parts of the same storm. Thus, a great deal of variation in the return with both time and space can be expected. Consequently, when discussing average values for reflectivity, it should be understood that considerable variation will be encountered in a realistic situation.

Table 5-8 gives average rain backscatter from several sources for S-band through W-band for several rain situations. As can be seen, the backscatter coefficient increases with increasing frequency (at least up to 35 GHz) and increasing rain rate. Observers of rainstorms have noted that rain drop size increases with increasing rain rate, which accounts for the direct dependence of reflectivity on rain rate. Attenuation has been eliminated from the rain data, so the apparent backscatter can be less for heavy rain rates.<sup>3</sup>

Table 5-8 includes a column listing an alternative scale for rain reflectivity denoted with the symbol  $Z$ . This scale, common in meteorological applications, is also called volume reflectivity. It relates radar reflectivity to the distribution of drop sizes, which is more useful for estimating rain rates. It is usually expressed in decibel units and denoted dBz. The relationship between  $\eta$  and  $Z$  is [31]

$$\eta = \frac{\pi^5 |K|^2}{\lambda^4} Z \quad (5.28)$$

where  $K$  is the complex index of refraction and  $Z$  is in units of m<sup>6</sup>/m<sup>3</sup> = m<sup>3</sup>. While  $K$  depends on temperature and wavelength, for most weather conditions  $|K|^2 \approx 0.93$  for liquid scatterers (e.g., rain, fog) and 0.197 for frozen scatterers (e.g., snow, hail).

For use in meteorology,  $Z$  is converted to units of mm<sup>6</sup>/m<sup>3</sup> (which requires multiplication of  $Z$  in m<sup>3</sup> by 10<sup>18</sup>) and then to a decibel scale denoted dBz. Thus,

$$Z \text{ (dBz)} = 10 \log_{10}(10^{18} Z) = 10 \log_{10}(Z) + 180 \quad (5.29)$$

The calculations of equations (5.28) and (5.29) were used to obtain the dBz values in Table 5-8.

<sup>3</sup>Of course, the target echo signal strength is reduced by rain attenuation as well.

**FIGURE 5-33** ■  
Least squares fit to  
rain data at four  
frequency bands.  
(From Currie [32].  
With permission.)

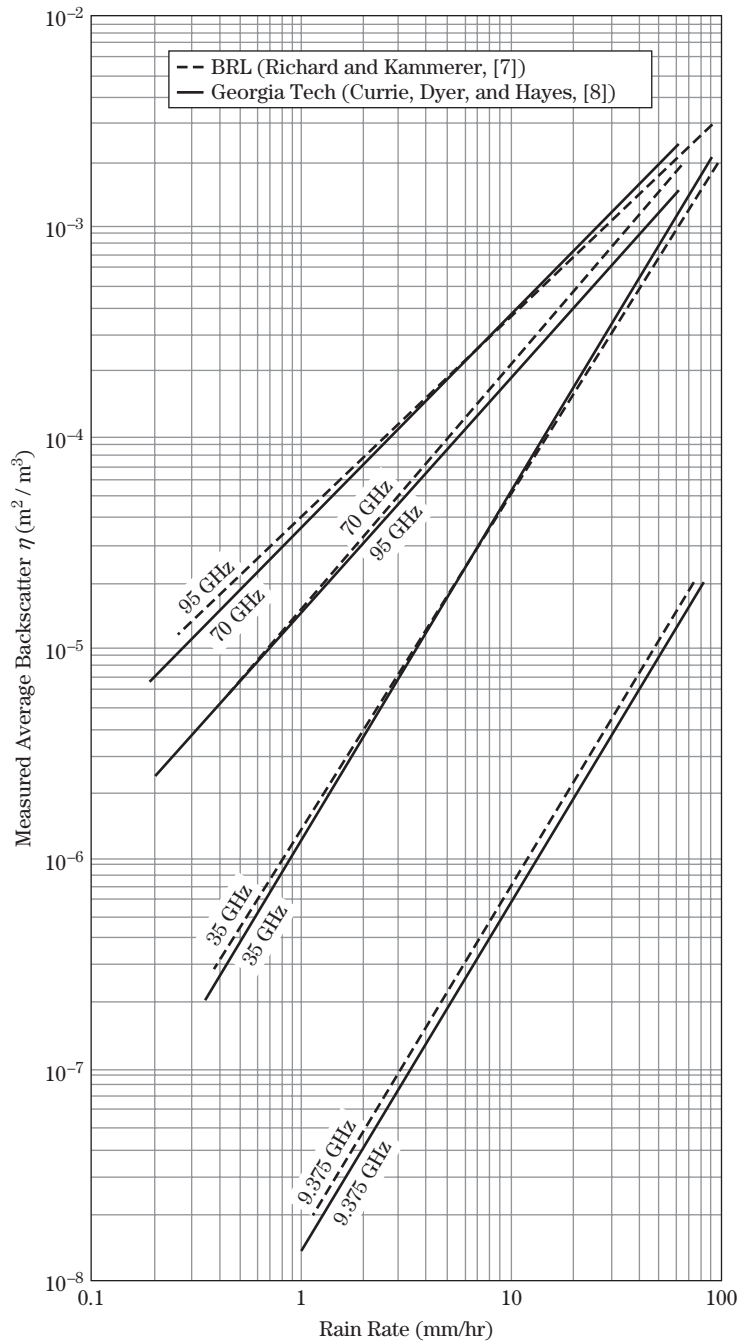
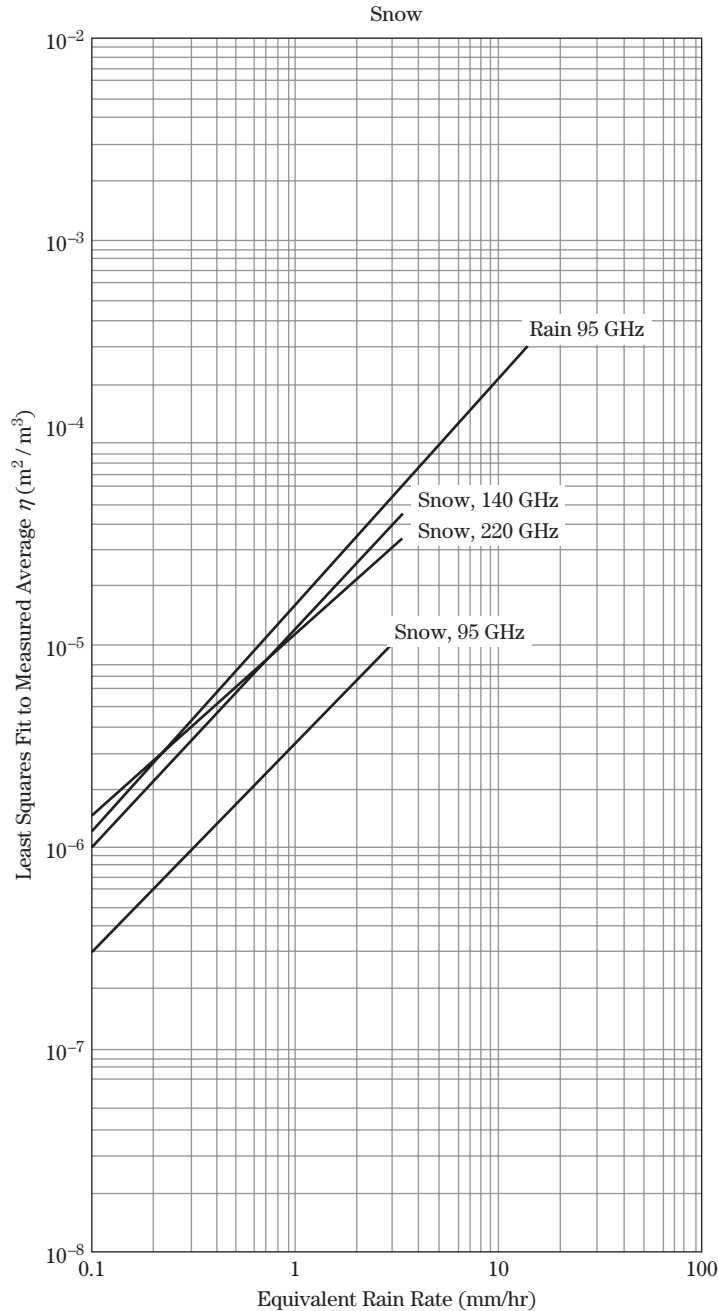


Figure 5-33 gives least square fit curves to rain data obtained from thunderstorms in a joint experiment between the U.S. Army BRL and GTRI in Orlando, Florida, in the 1970s [32]. Thunderstorms are known for producing large drops, so the wide variation in reflectivity with rain rate is not surprising. One interesting factor is the flattening of the curves at 70 and 95 GHz. This may indicate that the ratio of drop circumference to wavelength is approaching the resonance or optical regions, resulting in a lessened

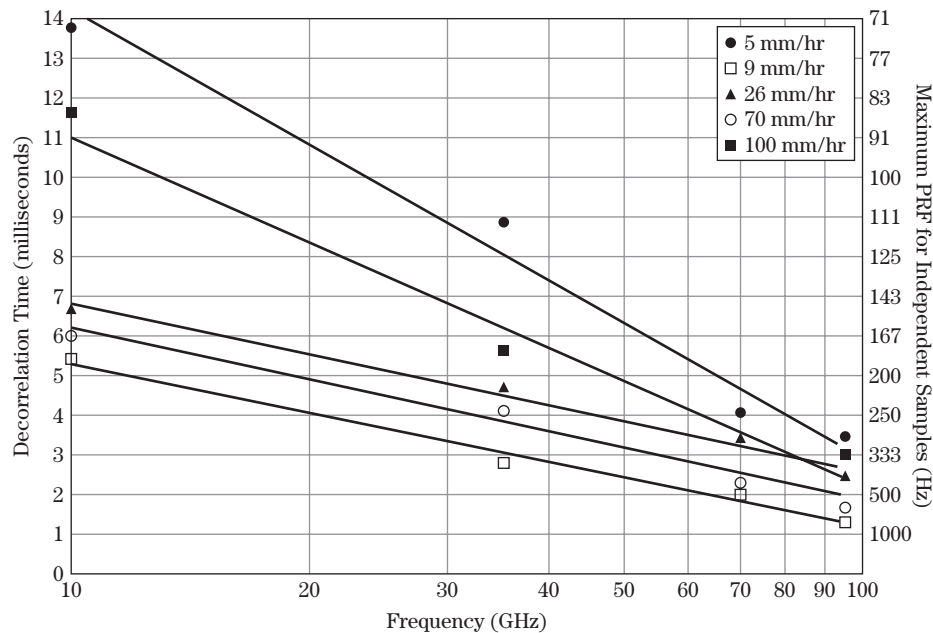
dependence on drop size. BRL and GTRI each separately analyzed the data, getting slightly different results as shown. However, the overall spread in the data dwarfs these small differences.

**Frozen Precipitation** As indicated earlier, the reflectivity of frozen precipitation such as snow is generally ignored at microwave frequencies. However, at higher frequencies snow reflectivity can be significant. Figure 5-34 presents data on snow reflectivity at 95,



**FIGURE 5-34** ■ Least squares fit to snow data at two frequency bands compared with rain data. (From Currie et al. [34]. With permission.)

**FIGURE 5-35** ■ Decorrelation time for rain backscatter as a function of frequency. (From Currie et al. [8]. With permission.)



140, and 220 GHz measured by Nemanich et al. [33,34] at the U.S. Army Harry Diamond Laboratory compared with the Georgia Tech 95 GHz rain data from Figure 5-33. The snow data are plotted versus equivalent rain rate based on snow water content. While the snow return is much lower at 95 GHz than the rain return, the snow returns at higher frequencies are comparable to the rain return for 95 GHz.

### 5.2.3.2 Temporal Spectra

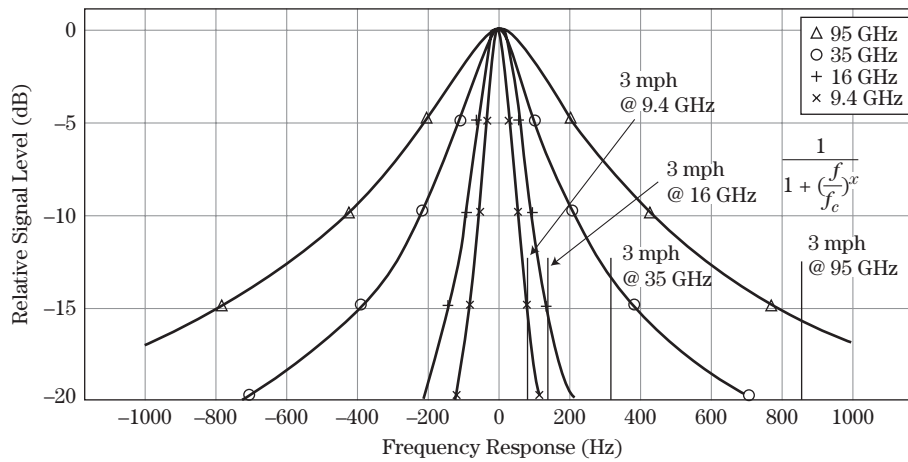
Figure 5-35 presents data on the decorrelation time for rain return at 10 through 95 GHz. The maximum PRF for independent samples, calculated as the inverse of the decorrelation time as discussed in Section 5.2.2.4, is given on the right side. Note that for 5 mm/hr rain rate and 10 GHz, the maximum PRF for independent samples is only 71 Hz. At higher rain rates and higher frequencies, the maximum PRF increases significantly.

Figure 5-36 shows the spectral response at 10 through 95 GHz measured during the experiment displayed in Figure 5-33 [35]. Also shown is the Doppler shift for a slow-moving target at 3 mph. The spectral curves were matched to power law functions of the form of equation (5.24) in a manner similar to the data for trees discussed earlier. The figure shows that the rain return frequency spectra would be approximately 15 dB down from the peak (constant power level) at the Doppler frequency for a 3 mph target. This implies that the SCR could be improved by up to 15 dB through the use of careful Doppler processing.

Other important factors related to rain clutter are the spatial extent of a storm (both horizontal and vertical) and its Doppler characteristics, which are affected by prevailing winds, rain rates, and atmospheric turbulence. Attenuation due to rain is extremely important and was discussed in Chapter 4.

### 5.2.4 Millimeter Wave Clutter

The only difference between millimeter waves and microwaves is the wavelength. However, because of the change in the reflectivity properties of spheres and cylinders as the



**FIGURE 5-36** ■ Rain spectral response for four frequencies compared with a 3 mph moving target. (From Hayes [35]. With permission.)

circumference-to-wavelength ratio approaches unity, significant differences in reflectivity can be observed at higher frequencies. The dependence of rain reflectivity on rain rate at 70 and 95 GHz in Figure 5-33 is one example.

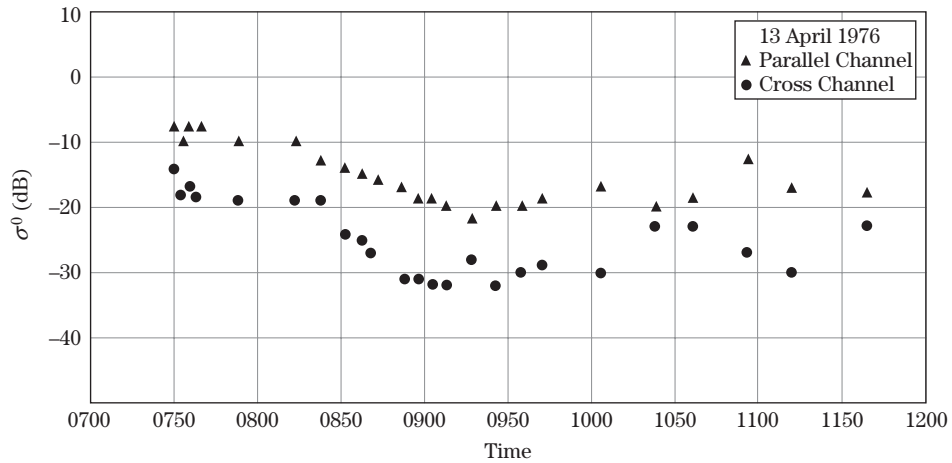
Table 5-9 compares the circumference-to-wavelength ratios of different natural and man-made objects at 35 through 300 GHz. As the ratio approaches 1 or larger unusual reflectivity effects will be observed. From the table it can be seen that this can occur for many types of common scatterers.

As an example of unusual effects at millimeter waves, Figure 5-37 shows the radar reflectivity of snow-covered ground at 35 GHz as a function of time of day. The air temperature was below freezing at the start of the measurement but rose above freezing between 8 a.m. and 8:15 a.m. As can be seen, the reflectivity of the snow dropped about 10 dB in 45 minutes. The temperature continued to hover around freezing, and the reflectivity varied depending on whether the temperature fell below or rose above freezing. This phenomenon has been observed at lower frequencies, but the effect was much smaller. The current theory is that when snow melts and refreezes, large resonant crystals form that reflect RF energy back to the radar, whereas, when melting occurs, surface water prevents

**TABLE 5-9** ■ Comparison of the Circumference in Wavelengths of Different Natural and Man-made Items

Scatterer	Diameter (mm)	Ratio of Diameter to Wavelength ( $a/\lambda$ )			
		35 GHz	95 GHz	140 GHz	300 GHz
Raindrops	0.2–6	0.02–0.7	0.6–2	0.09–2.8	0.2–6
Sea Spray	0.2–10	0.02–1.15	0.6–3.3	0.09–4.7	0.2–6
Pine Needles	0.5–1.5	0.057–0.171	0.167–0.5	0.23–0.7	0.5–1.5
Screw Heads	1.5–25	0.17–2.9	0.5–8.3	0.7–11.7	1.5–25
Rivets	10	1.15	3.3	4.7	10
Grass Blades	2–8	0.23–0.92	0.7–2.7	0.93–3.7	2–8
Deciduous Leaves	6–20	0.7–2.31	2.0–6.7	2.8–9.4	6–20
Branches	5–76	0.7–8.78	2.0–25	2.8–35.5	6–76
Snow Crystals	5–50	0.58–5.77	1.7–16	2.3–23.3	5–50
Hail	1–10	0.12–1.15	0.3–3.3	0.47–4.7	1–10

**FIGURE 5-37** ■  
Snow-covered  
ground reflectivity at  
35 GHz as a function  
of time of day. (From  
Currie et al. [36].  
With permission.)



penetration into the snow layers to forward scatter more of the energy. The key point of this discussion is that the radar designer must be aware of possible unusual scattering effects as the frequency increases into the millimeter wave region.

## 5.3 | CLUTTER MODELING

### 5.3.1 General Approaches for Estimating Detection Performance in Clutter

Although a great deal of effort has been expended in developing theoretical models for clutter, most of these models have severe limitations because of the complexity of the real world. As a result, most radar designers either develop their own empirical models from clutter data or use models from the literature to estimate radar performance in clutter. For readers interested in pursuing theoretical modeling, several references are presented at the end of this chapter. The remainder of this section presents some empirical models that have been proven to be of use over the years.

### 5.3.2 Clutter Models

#### 5.3.2.1 Surface Clutter

In the late 1970's GTRI developed an open literature empirical model for the reflectivity  $\sigma^0$  of varying types of land clutter for grazing angles in the low angle and plateau regions [36]. In the 1980s this model was extended to higher frequencies, and additional data were used to refine the model [37]. The model takes into account wavelength, rms surface roughness, and grazing angle and has the form

$$\sigma^0 = A(\delta + C)^B \exp \left[ \frac{-D}{1 + \frac{0.1\sigma_h}{\lambda}} \right] \quad (5.30)$$

**TABLE 5-10** ■ Coefficients for GTRI Empirical Model

Constant	Frequency	Soil/ Sand	Grass	Tall Grass Crops	Trees	Urban	Wet Snow	Dry Snow
A	3	0.0045	0.0071	0.0071	0.00054	0.362	—	—
	5	0.0096	0.015	0.015	0.0012	0.779	—	—
	10	0.25	0.023	0.006	0.002	2.0	0.0246	0.195
	15	0.05	0.079	0.079	0.019	2.0	—	—
	35	—	0.125	0.301	0.036	—	0.195	2.45
	95	—	—	—	3.6	—	1.138	3.6
B	3	0.83	1.5	1.5	0.64	1.8	—	—
	5	0.83	1.5	1.5	0.64	1.8	—	—
	10	0.83	1.5	1.5	0.64	1.8	1.7	1.7
	15	0.83	1.5	1.5	0.64	1.8	—	—
	35	—	1.5	1.5	0.64	—	1.7	1.7
	95	—	1.5	1.5	0.64	—	0.83	0.83
C	3	0.0013	0.012	0.012	0.002	0.015	—	—
	5	0.0013	0.012	0.012	0.002	0.015	—	—
	10	0.0013	0.012	0.012	0.002	0.015	0.0016	0.0016
	15	0.0013	0.012	0.012	0.002	0.015	—	—
	35	—	0.012	0.012	0.012	—	0.008	0.0016
	95	—	0.012	0.012	0.012	—	0.008	0.0016
D	3	2.3	0.0	0.0	0.0	0.0	—	—
	5	2.3	0.0	0.0	0.0	0.0	—	—
	10	2.3	0.0	0.0	0.0	0.0	0.0	0.0
	15	2.3	0.0	0.0	0.0	0.0	—	—
	35	—	0.0	0.0	0.0	—	0.0	0.0
	95	—	0.0	0.0	0.0	—	0.0	0.0

Source: From Currie [32] (with permission).

where  $\delta$  is the grazing angle in radians,  $\sigma_h$  is the rms surface roughness, and  $A$ ,  $B$ ,  $C$ , and  $D$  are empirically derived constants.

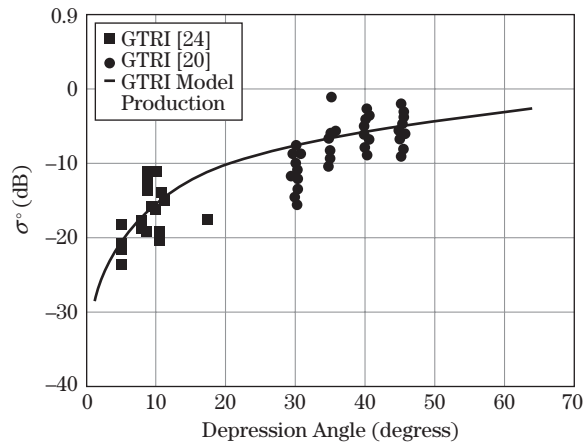
Table 5-10 gives the values for  $A$ ,  $B$ ,  $C$ , and  $D$  for frequencies of 3 through 95 GHz for several types of clutter. Figure 5-38 shows the model output for trees at X-band plotted against some GTRI data on tree reflectivity. Note that the model prediction appears a little high when compared to the data since the model attempts to predict an average of both temporal and spatial variations. This model has not been updated to reflect the low angle data reported by Billingsley [11].

Although several empirical models have been developed for sea return, the GTRI model has been one of the more popular ones used, particularly for low angles. The model is based on many years of radar data collection at a test site near Boca Raton, Florida. The model predicts average sea clutter values as a function of polarization, wavelength, grazing angle, radar boresight-wind direction, average wave height, and wind speed. Table 5-11 summarizes the equations for the model.

The definitions of variables are as follows:

- $\lambda$  is the radar wavelength.
- $\delta$  is the grazing angle.

**FIGURE 5-38** ■ Comparison of GTRI model output with data for deciduous trees at X-band. (From Currie [32]. With permission.)



- $\phi$  is the angle between radar boresight and wind direction.
- $h_{av}$  is the average wave height.
- $A_i$  is the “interference factor,” which takes into account rms surface roughness and multipath.
- $A_u$  is the upwind/downwind factor.
- $A_w$  is the wind speed factor.

Figure 5-39 gives a sample output of the model. Shown is the value of  $\sigma^0$  as a function of bore sight-upwind direction for three frequencies. (The model assumes that the wind and waves are proceeding in the same direction.) Note that after the original 1 to 10 GHz sea clutter model was developed, a second model was developed for 10 to 100 GHz [38].

**TABLE 5-11** ■ GTRI Sea Clutter Model Equations

$$\sigma_{HH}^0 = 10 \log[3.9 \times 10^{-6} \lambda \delta^{0.4} A_i A_u A_w]$$

For 1 to 3 GHz

$$\sigma_{VV}^0 = \sigma_{HH}^0 - 1.73 \ln(h_{av} + 0.015) + 3.76 \ln(\lambda) + 2.46 \ln(\delta + 0.0001) + 222$$

For 3 to 10 GHz

$$\sigma_{VV}^0 = \sigma_{HH}^0 - 1.05 \ln(h_{av} + 0.015) + 1.09 \ln(\lambda) + 1.27 \ln(\delta + 0.0001) + 9.70$$

$$\sigma_\phi = (14.4\lambda + 5.5)\delta h_{av}/\lambda$$

$$A_i = \sigma_\phi^4 (1 + \sigma_\phi^4)$$

$$A_u = \exp[0.2 \cos \phi (1 - 2.8\delta)(\lambda + 0.015)^{-0.4}]$$

$$q_w = 1.1/(\lambda + 0.015)^{-0.4}$$

$$V_w = 8.67 h_{av}^{0.4}$$

$$A_w = [1.94 V_w / (1 + V_w / 15.4)]^{q_w}$$

Note: Values for  $h_{av}$  and  $\lambda$  are given in meters,  $\delta$  and  $\phi$  are in radians.

Source: From Horst et al. [39] (with permission).

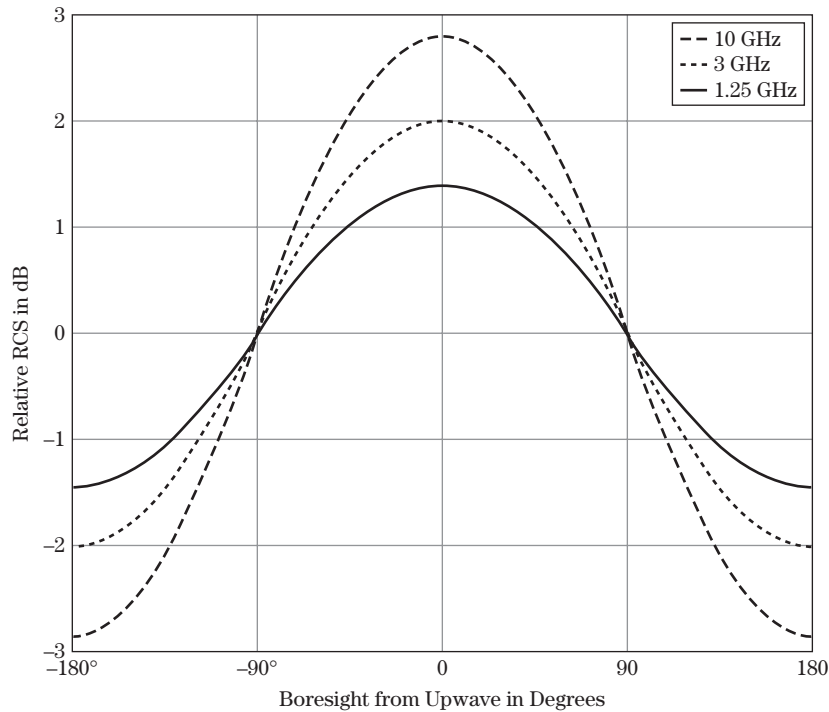


**FIGURE 5-39** ■ GTRI sea clutter model output for three frequencies at 1° grazing angle. (From Long [6]. With permission.)

Unfortunately, the experimenters used a different X-band data set from that used for the original model development so that the results of the two models do not agree at 10 GHz. Some users that need to model sea return over the entire frequency range average the results from the two models at 10 GHz.

### 5.3.2.2 Atmospheric Clutter Models

The equations for the least squares fit to rain data presented in Figure 5-33 are presented in Table 5-12. The equations have the form

$$\eta = AR^B \text{ m}^{-1} \quad (5.31)$$

where  $\eta$  is the radar cross section per unit volume, and  $A$  and  $B$  are constants given in Table 5-12. Note that significant variability in the data occurred around the calculated least squares fits.

**TABLE 5-12** ■ Model Coefficients for Rain

Frequency (GHz)	$A$	$B$
9.4	$1.3 \times 10^{-8}$	1.6
35	$1.2 \times 10^{-6}$	1.6
70	$4.2 \times 10^{-5}$	1.1
95	$1.5 \times 10^{-5}$	1.0

Source: From Currie et al. [34] (with permission).

## 5.4 | CONCLUDING REMARKS

This chapter defined the required terminology for dealing with radar clutter; discussed the average, temporal, and spatial properties of clutter; and introduced some empirical models for clutter. In no way should this discussion be considered as comprehensive in nature. Dozens of books have been written on this topic from both theoretical and empirical points of view. Some of these books are listed in Section 5.4.2. The next section provides a summary of average clutter data taken from the sources discussed previously.

### 5.4.1 Reflectivity Summary

Table 5-13 gives some average values for land clutter as a function of aspect angle that are plotted in Figures 5-13 through 5-16, which were adapted from Nathanson [15]. Table 5-14 summarizes average values for sea clutter as a function of polarization and depression angle which were plotted in Figures 5-20 through 5-22, again adapted from Nathanson. These data reflect the general trends discussed previously but omit any dependence on wind direction, a weakness corrected by the GTRI model of Table 5-11.

Table 5-8 given previously summarizes average values for rain return as a function of frequency and rain rate, again, taken from Nathanson [15].

The temporal and spatial variations of land clutter were best represented by Weibull distributions. The width parameters (standard deviation or Weibull width parameter) for land clutter were given in Tables 5-4 and 5-7. Spectral bandwidth and roll-off characteristics for wind-blown trees were presented in Table 5-6. Rain spectral constants were presented in Figure 5-35.

**TABLE 5-13** ■ Summary of Averaged Land Reflectivity ( $\sigma^0$  in db)

Clutter Type	Frequency Band	Grazing Angle (Deg.)			
		1.5	10	30	60
Desert	L	-45	-38	-28	-21
	S	-46	-36	-25	-17
	C	-40	-33	-23	-16
	X	-40	-30	-21	-14
	K <sub>u</sub>	-40	-28	-19	-13
Farmland	L	-36	-30	-20	-15
	S	-34	-28	-18	-16
	C	-33	-26	-16	-15
	X	-33	-26	-16	-14
	K <sub>u</sub>	-23	-22	-16	-13
Woods	L	-28	-26	-18	-19
	S	-28	-24	-16	-15
	C	-27	-23	-16	-15
	X	-26	-23	-14	-14
	K <sub>u</sub>	-13	-20	-14	-12
Urban	L	-25	-18	-15	-12
	S	-23	-18	-13	-11
	C	-21	-18	-11	-10
	X	-20	-16	-10	-10
	K <sub>u</sub>				

**TABLE 5-14** ■ Summary of Averaged Sea Reflectivity ( $\sigma^0$  in db)

Sea State	Frequency Band	Polarization	Grazing Angle (Deg.)			
			0.1	10	30	60
1	L	VV		-39	-38	-22
	L	HH		-56	-46	-24
	S	VV	-80	-40	-40	-24
	S	HH	-80			-25
	C	VV	-72	-41	-42	-24
	C	HH	-75	-53	-48	-26
	X	VV	-65	-42	-36	-24
	X	HH	-71	-51	-44	-24
	K <sub>u</sub>	VV		-40	-31	-20
	K <sub>u</sub>	HH			-38	-20
3	L	VV	-82	-34	-30	-18
	L	HH	-82	-48	-39	-20
	S	VV	-75	-34	-29	-19
	S	HH	-68	-46	-38	-20
	C	VV	-60	-34	-28	-18
	C	HH	-69	-40	-37	-20
	X	VV	-51	-32	-26	-16
	X	HH	-53	-37	-34	-21
	K <sub>u</sub>	VV		-31	-23	-14
	K <sub>u</sub>	HH		-32	-28	-16

### 5.4.2 Clutter Effect on Detection

This chapter has summarized the clutter characteristics and provided clutter data and modeling for simulating clutter. Clutter limits detection of targets due to its competing signal, which interferes with the target signal. Methods for dealing with these problems using Doppler processing are discussed in Chapter 17.

## 5.5 | FURTHER READING

Perhaps the two best comprehensive references for understanding radar clutter are the texts by Long [6] and Ulaby and Dobson [10]. Both combine in-depth discussion of clutter phenomenology and modeling with extensive summaries of real-world clutter measurements. Ward et al. concentrate on sea clutter measurements and modeling with the K-distribution in [25].

More extensive theoretical analyses are given for sea clutter by Ward et al. in [25] and for various clutter sources in [40–43]. An in-depth analysis of land clutter data is given by Billingsley [11]. Other good reviews of land and sea clutter data can be found in [15,40–43].

Most of the preceding sources are concerned with radar clutter at microwave frequencies. Additional discussion of millimeter-wave clutter data is available in the publications by Currie and various colleagues [34,44,45].

## 5.6 | REFERENCES

- [1] Novak, L.M., and Owirka, G.J., “Radar Target Identification Using an Eigen-Image approach,” *1994 IEEE National Radar Conference*, Atlanta, GA, p. 130, March 29–31, 1994.

- [2] Long, M.W., "Radar Clutter," Tutorial presented at the *2006 IEEE Radar Conference*, Verona, NY, April 2006.
- [3] Mott, H., *Polarization in Antennas and Radar*, Wiley, New York, 1986.
- [4] Holm, W.A., "MMW Radar Signal Processing Techniques," Chapter 6 (pp. 279–310) in *Principles and Applications of Millimeter-Wave Radar*, Ed. N.C. Currie and C.E. Brown, Artech House, Norwood, MA, 1987.
- [5] Echard, J.D., et al., "Discrimination between Targets and Clutter by Radar," Final Technical Report on Contract DAAAG-29-780-C\_0044, Georgia Tech Research Institute, Atlanta, December 1981.
- [6] Long, M.W., *Radar Reflectivity of Land and Sea*, 3d ed., Artech House, Norwood, MA, 2001.
- [7] Richard, V.W., and Kammerer, J.E., "Rain Backscatter Measurements and Theory at Millimeter Wave Measurements," Report No. 1838, U.S. Army Ballistic Research Laboratory, Aberdeen Proving Ground, MD, October 1975.
- [8] Currie, N.C., Dyer, F.B., and Hayes, R.D., "Analysis of Radar Rain Return at Frequencies of 9.375, 35, 70, and 95 GHz," Technical Report No. 2 on Contract DAAA 25-76-C-0256, Georgia Tech Research Institute, Atlanta, February 1975.
- [9] Nemarich, J., Wellman, R.J., and Lacombe, J., "Backscatter and attenuation of Falling Snow and Rain at 96, 140, and 220 GHz," *IEEE Trans. Geoscience and Remote Sensing*, vol. 26, no. 3, pp. 330–342, May 1988.
- [10] Ulaby, F.T., and Dobson, M.C., *Handbook of Radar Scattering statistics for Terrain*, Artech House, Norwood, MA, 1989.
- [11] Billingsley, J.B., *Low-Angle Radar Land Clutter*, William Andrew Publishing, Norwich, NY, 2002.
- [12] Aley, J.C., Davis, W.T., and Mills, N.B., "Radar Sea Return in High Sea States," Naval Research Laboratory Report No. 7142, September 1970.
- [13] Long, M.W., et al., "Wavelength Dependence of Sea Echo," Final Report on Contract N62269-3019, Georgia Tech Research Institute, Atlanta, 1965.
- [14] Trebits, R.N., et al., "Millimeter Wave Radar Sea Return Study," Interim Technical Report on Contract N60921-77-C-A168, Georgia Tech Research institute, Atlanta, July 1978.
- [15] Nathanson, F.E., "Sea and Land Backscatter," Chapter 7 in *Radar Design Principles*, 2d ed., McGraw-Hill, Inc New York, 1991.
- [16] Currie, N.C., "Performance Tests on the AN/TPQ-31a Radar," Technical Report on Contract N00014-75-C-0228, Mod P00001, Georgia Tech Research Institute, Atlanta, 1975.
- [17] "Radar Return Study," Goodyear Aircraft Corp., Final Report on Contract NOAS-59-6186-CGERA 463, Phoenix, AZ, September 1959.
- [18] Stiles, W.H., Ulaby, F.T., and Wilson, E., "Backscatter Response of Roads and Roadside Surfaces," Sandia Report No. SAND78-7069, University of Kansas center for Research, Lawrence, March 1979.
- [19] Dyer, F.B., and Currie, N.C., "Some Comments on the Characteristics of Radar Sea Echo," 1974 IEEE APS International Symposium, Atlanta, GA, June 1974, pp. 323–326.
- [20] Rivers, W.K., "Low Angle Sea Return at 3mm Wavelength," Final Technical Report on Contract N62269-70-C-0489, Georgia Tech Research Institute, Atlanta, November 1970.
- [21] Currie, N.C., Dyer, F.B., and Hayes, R.D., "Radar Land Clutter Measurements at 9.375, 16, 35, and 95 GHz," Technical Report No. 3 on Contract DAA25-73-0256, Georgia Tech Research Institute, Atlanta, February 1975.

- [22] Fishbein, W., et al., “Clutter Attenuation Analysis,” Technical Report No. ECOM-2808, US Army ECOM, Ft, Monmouth, NJ, March 1967.
- [23] Simpkins, W.L., Vannicola, V.C., and Ryan, J.P., “Seek Igloo Radar Clutter Study,” Technical Report No. RADC-TR-77-338, RADC, Rome, NY, October 1977.
- [24] Booth, R.R., “The Weibull Distribution Applied to Ground Clutter Backscatter Coefficient,” Report No. RE-TR-69-15, US Army Missile command, Huntsville, AL, June 1969.
- [25] Ward, K.D., Tough, R.J.A., and Watts, S., *Sea Clutter: Scattering, the K Distribution and Radar Performance*, Institution of Engineering and Technology, London, 2006.
- [26] Ward, K.D., “Compound Representation of High Resolution Sea Clutter,” *Electron Lett.*, vol. 17, pp. 561–565, 1981.
- [27] Watts, S., “Radar Detection Prediction in K-Distributed Sea Clutter and Thermal Noise,” *IEEE Trans. AES*, vol. 23, pp. 40–45, 1987.
- [28] Walker, D., “Doppler Modelling of Radar Sea Clutter,” *IEE Proceedings—Radar, Sonar and Navigation*, vol. 148, no. 2, pp. 73–80, April 2001.
- [29] Plummer, D.K., et al., “Some Measured Statistics of Coherent Radar Sea Echo and Doppler at L-Band,” Final Technical Report on Contract NADc-78254-30, Georgia Tech Research Institute, Atlanta, December 1969.
- [30] Werle, B.O., “Sea Backscatter Spikes, and Wave Group Observations at Low Grazing Angles,” *Proceedings of the 1995 IEEE International Radar Conference*, Washington, DC, pp. 187–195, May 1995.
- [31] Richards, M.A., *Fundamentals of Radar Signal Processing*, McGraw-Hill, New York, 2005.
- [32] Currie, N.C., “MMW Clutter Characteristics,” Chapter 5 in *Principles and Applications of Millimeter-Wave Radar*, Ed. N.C. Currie and C.E. Brown, Artech House, Norwood, MA, 1987.
- [33] Nemarich, J., et al., “Comparative Near Millimeter Wave Propagation Properties of Snow and Rain,” *Proceedings of Snow Symposium III*, U.S. Army CRREL, Hanover, NH, August 1983.
- [34] Currie, N.C., Hayes, R.D., and Trebits, R.N., *Millimeter-Wave Radar Clutter*, Artech House, Norwood, MA, 1992.
- [35] Hayes, R.D., private communication, Atlanta, GA, 1980.
- [36] Currie, N.C., et al., “Radar Millimeter Wave Measurements: Part 1, Snow and Vegetation,” Report No. AFATL-TR-77-92, July 1977.
- [37] Currie, N.C., and Zehner, S.P., “MMW Land clutter Model,” *IEE Radar 82 International Symposium*, London, September 1982.
- [38] Horst, M.M., and Perry, B., “MMW Modeling Techniques,” Chapter 8 in *Principles and Application of Millimeter-Wave Radar*, Ed. N.C. Currie and C.E. Brown, Artech House, Norwood, MA, 1987.
- [39] Horst, M.M., Dyer, F.B., and Tuley, M.T., “Radar Sea Clutter Model,” Proceedings of the IEEE Conference on Antennas and Propagation, November 1978.
- [40] Skolnik, M.I., *Radar Handbook*, 2d ed., Chapters 12, “Ground Echo” and 13, “Sea Echo,” McGraw-Hill Publishing Company, New York, 1990.
- [41] Ulaby, F.T., Moore, R.K., and Fung, A.K., *Microwave Remote Sensing: Vol. II, Radar Remote Sensing and Surface Scattering and Emission Theory*, Addison-Wesley Publishing Company, Reading, MA, 1982.
- [42] Ulaby, F.T., and Elachi, C. (Eds.), *Radar Polarimetry for Geoscience Applications*, Artech House, Norwood, MA, 1990.

- [43] Bogush Jr., A.G., *Radar and the Atmosphere*, Artech House, Norwood, MA, 1989.
- [44] Currie, N.C., and Brown, C.E. (Eds.), “MMW Clutter Characteristics,” Chapter 5 in *Principles and Applications of Millimeter-Wave Radar*, Artech House, Norwood, MA, 1987.
- [45] Button, K.J., and Wiltse, J.C. (Eds.), “Millimeter Radar,” Chapter 2 in *Infrared and Millimeter Waves: vol. 4, Millimeter Systems*, Academic Press, New York, 1981.

## 5.7 | PROBLEMS

1. A radar has a pulse length of  $\tau = 10 \mu\text{s}$ , an azimuth beamwidth  $\theta_3 = 3^\circ$ , and an elevation beamwidth  $\phi_3 = 3^\circ$ . At what grazing angle  $\delta$  does the transition occur between the pulse-limited and beam-limited ground clutter cases when the nominal range to the ground is  $R = 10 \text{ km}$ ? Repeat for  $R = 50 \text{ km}$ .
2. For the same radar used in problem 1, what is the volume  $V$  in cubic meters of a volume clutter resolution cell at  $R = 10 \text{ km}$ ? Repeat for  $R = 50 \text{ km}$ .
3. A radar is attempting to detect a point target in the presence of ground clutter. The parameters of the radar and its environment are such that the SNR at a range of  $R_0 = 10 \text{ km}$  is 30 dB, while the SCR at the same range is 20 dB. The detection performance at this range is “clutter limited” because the clutter is the dominant interference. Assuming pulse-limited clutter interference, at what range will the SNR and SCR be equal? (At ranges longer than this, the detection performance for this target will be “noise limited.”)
4. Consider two radar targets with polarization scattering matrices  $\mathbf{S}_1$  and  $\mathbf{S}_2$  as follows:

$$\mathbf{S}_1 = \begin{bmatrix} 1 & 0 \\ 0 & 1 \end{bmatrix}, \quad \mathbf{S}_2 = \begin{bmatrix} 1 & j \\ -j & -1 \end{bmatrix}$$

where  $j = \sqrt{-1}$ . Compute the parallel/cross-polarization ratio and the vertical/horizontal polarization ratio for each target. Which ratio could be used to discriminate between the two targets?

5. Compute the critical grazing angle for an X-band (10 GHz) radar when the surface roughness  $\sigma_h$  is 1.0 cm, and again when  $\sigma_h = 10.0 \text{ cm}$ . Repeat for an L-band (1 GHz) radar and a K-band (35 GHz) radar.
6. Compute the diameter of a conducting sphere at the boundary between the Rayleigh and resonance regions at a radar frequency of 5 GHz (C-band). Repeat for the boundary between the resonance and optics regions.
7. Show that the Weibull distribution reduces to the exponential distribution when  $b = 1$ , and to the Rayleigh distribution when  $b = 2$ .
8. A radar collects  $N_i = 30$  samples of clutter data having a decorrelation time  $\tau_0$  of 1 ms. What is the number of uncorrelated samples  $N_i$  if the PRF is 1 kHz? Repeat for PRF = 5 kHz and 40 kHz.
9. Consider the GTRI model for land clutter reflectivity given by equation (5.30). Show that the model predicts that  $\sigma^0$  becomes independent of surface roughness when  $\sigma_h \ll 10\lambda$ .
10. Use equations (5.28) and (5.29) to confirm that a reflectivity  $\eta = -92 \text{ dB}$  corresponds to a meteorological reflectivity of 23 dBz at S-band (3 GHz) as shown in Table 5-8.

# Index

## A

- AAW. *See* Anti-air warfare (AAW)
- Absorption
  - atmospheric, 117, 121
  - bands, 125
- A7C Corsair aircraft, 236, 238
- Accuracy, in radar measurements. *See* Precision and accuracy, in radar measurements
- ACF. *See* Autocorrelation function (ACF)
- Active-aperture array, 353
- Active array architectures, 339–341
  - advantages of, 340–341
  - vs. passive array architectures, 340–341
- Active electronically scanned array (AESA), 339, 340, 371, 374, 375
- Active phased array, 350
- Adaptive DPCA (A-DPCA) processor, 644
- Adaptive Kalman filtering, 740–741
- ADC. *See* Analog-to-digital converter (ADC)
- A-DPCA. *See* Adaptive DPCA (A-DPCA) processor
- Aegis system, 48
- Aerosols, smoke and, 130
- AESA. *See* Active electronically scanned array (AESA)
- AF. *See* Array factor (AF)
- AGC. *See* Automated gain control (AGC)
- AGL. *See* Aircraft above ground level (AGL)
- AIM-7 missile, 44
- Airborne interceptor, 46
- Airborne moving target indication (AMTI), 465
- Aircraft above ground level (AGL), 53
- Air defense systems, 40
- Air Force E3A Sentry (AWACS), 46
- Airport surveillance radar, 49
- Albersheim's equation, 106, 575–578, 581–583
  - conditions for, 576
  - vs. Shnidman's equation, 581–583
- Algorithm metrics, of radar signal processor, 464
- Aliased sinc, 508
- Along-track position, 838
- Alpha-beta filters, 34, 718, 719, 731–732, 738
- Alpha-beta-gamma filter, 739–741
  - for scalar coordinate, 740
- Altera, 474
- Altimeters, 361
- AM. *See* Amplitude modulation (AM)
- Ambiguity functions, 800–801
  - for LFM waveform, 803
  - range-Doppler coupling, 803–805
  - spectral interpretation of, 806–807
  - V-LFM, 808
- Ambiguity surface, 801
  - ridged, 802
  - for simple pulse, 802
- Amdahl's Law, 483
- Amplifiers, for excitors, 451–452
- Amplitude, 29
  - threshold, 26
- Amplitude comparison monopulse radar system, 701–702
- Amplitude fluctuations, millimeter wave system and, 138
- Amplitude modulation (AM), 379
- AMTI. *See* Airborne moving target indication (AMTI)
- Analog Devices, Inc., 474
- Analog-to-digital converter (ADC), 4, 64, 392, 395, 409–414, 504, 590, 788, 795, 847
  - configuration, 410
  - radar signal processor and, 472–473
  - sample of, 411
- AN/FPS-115, 42
- Angle measurements
  - AOA estimation method. *See* AOA estimation method
  - monopulse technique, 701–703
  - sequential lobing, 700–701
- Angle of arrival (AOA), 685
  - estimation method. *See* AOA estimation method
  - fluctuations, 138
- Angular frequency, 6
- Angular selectivity, 309, 310
- AN/MPQ-39 C-band phased array radar, 45
- AN/MPQ-64 sentinel, 40
- Annapolis Microsystems, 474
- AN nomenclature, 36–37
- AN/SPQ-9A, 46
- AN/SPQ-9B ship-based TWS radar, 47
- AN/SPS-48 radar, 39
- AN/SPS-49(V) radar, 38
- AN/SPY-1 radar, 47–48
- Antenna, 4. *See also* Radar antennas
  - bistatic configurations, 18–20
  - dwelt time, 88
  - isotropic, 310–311
  - monostatic configurations, 18–20
  - mounting error, 682
  - one-dimensional pattern, 14
  - pattern of, 14
  - phased array. *See* Phased array antenna reflector, 322–326
  - sidelobes, 14
- Anti-air warfare (AAW), 38
- AN/TPQ-36 firefinder radar, 48
- AN/TPQ-37 firefinder radar, 48
- AN/TPS-75 air defense system, 40
- AN/TPY-2 systems, 42
- AOA. *See* Angle of arrival (AOA)
- AOA estimation method, 702–704
  - centroiding
    - binary integration approach, 703–704
    - ML approach, 703, 704
  - monopulse
    - multiple unresolved targets, 707–708
    - single target, 704–707
- AOA fluctuations. *See* Angle of arrival (AOA), fluctuations

- Aperture, 312, 314  
 defined, 314  
 efficiency, 316, 323  
 taper, 314  
 errors, 316
- API. *See* Application programming interface (API)
- Application programming interface (API), 477
- Applicationspecific integrated circuits (ASIC), 462, 474, 475, 480
- Approximation, 82
- AR model. *See* Autoregressive (AR) model
- Array factor (AF), 327, 328, 330, 338
- Array(s)  
 antenna technology, 90  
 defined, 326  
 elements, 333–335
- Artillery locating radars, 48
- ASIC. *See* Applicationspecific integrated circuits (ASIC)
- Aspect angle, 239  
 of RCS, 249–250, 252, 253, 257, 261, 264, 266
- ASR-9, 667
- ASR-9 airport surveillance radar, 49
- ASR-12 airport surveillance radars, 667
- Atmosphere  
 anomalous, refraction and, 130, 134–137  
 ducting/trapping, 135–136  
 subrefraction, 135  
 superrefraction, 135  
 attenuation of radar signals in, 121–123  
 gases, attenuation and, 124–125  
 layers, and radar propagation analysis, 120–121  
 standard, refraction and, 130, 131–134  
 effective earth radius and, 134
- Atmospheric absorption, 117, 121
- Atmospheric clutter  
 frozen precipitation, 199–200  
 models, 205  
 rain reflectivity, average, 196–199  
*versus* frequency band, 197  
 temporal spectra, 200
- Atmospheric loss, 68–69
- Atmospheric refraction, of  
 electromagnetic waves, 15–17.  
*See also* Refraction  
 cloud attenuation as, 16  
 radar technology in, 16
- Atmospherics, 118
- Atmospheric turbulence, 118, 137–138
- Atmospheric volumetric scattering, 118, 121–122, 168
- ATR. *See* Automatic target recognition (ATR)
- Attenuation  
 of electromagnetic waves, 121–123  
 circular polarization, 126  
 dust and, 129  
 fog and, 127–128  
 hail and, 128–129  
 one-way, 122  
 rain rate and, 125–126, 127  
 smoke and, 130  
 snow and, 128–129  
 water vapor and, 124–125  
 frequency at sea level, 15
- Autocorrelation function (ACF), 166, 187, 533  
 of sea return, 194, 195
- Autocorrelation sequence, of phase code, 812
- Automated gain control (AGC), 408
- Automatic target recognition (ATR), 36
- Automotive collision avoidance radars, 53
- Autoregressive (AR) model, 656
- AWACS. *See* Air Force E3A Sentry (AWACS)
- Azimuth angle, 27
- B**
- Backprojection, of image formation, 873
- Backscatter coefficient, 168
- Backscatter cross section, 221
- Backscatter reflectivity, 177–178
- Ballistic missile defense (BMD) radars  
 applications of, 41–43
- Ballistic missile early warning system (BMEWS), 382
- Ballistic Research Laboratory (BRL), 177
- Band-pass filter, 391, 395–396
- Bandwidth, of transmit signal, 431
- Barker codes  
 biphasic, 817–818  
 longest, compressed response for, 818  
 polyphasic, 824, 825
- Barker phase coded waveform, 809
- Baseband filter, 795
- Batch estimator, 757
- BAW devices. *See* Bulk acoustic wave (BAW) devices
- Bayesian approach, 562
- Bayliss function, 321
- BBS synthesizer. *See* Broad-band synthesizer (BBS)
- BDTI Benchmark Suites, 484
- Beam-limited case, scattering coefficients, 169–170
- Beam shape loss, 91
- Beamwidth, 13, 236  
 defined, 312  
 factor, 316
- Benchmarks, signal processor sizing and, 483–485
- Bernstein estimator, 704
- Bilinear transformation, 526
- Binary integration, 550, 584, 703–704
- Biphase-coded pulse, 30
- Biphase-coded waveforms, 788, 809, 811–812, 816
- Biphase codes  
 Barker, 817–818  
 MPS codes, 818–819, 820–821
- Bisection bandwidth, 464
- Bistatic antenna configurations, 18–20
- Bistatic propagation, 119
- Bistatic radar cross section, 221
- BIT functions. *See* Built-in-test (BIT) functions
- BLAS – LINPACK – LAPACK – ScaLAPACK series, 485
- Blind Doppler frequencies, 634
- Blind speeds, and staggered PRF, 634–637
- Blind zone  
 map, 660  
 pulse-Doppler processing, 660
- BMD. *See* Ballistic missile defense (BMD) radars
- BMEWS. *See* Ballistic missile early warning system (BMEWS)
- Boltzmann's constant, 404
- Boundary admittance, 148
- Bragg scattering, 194
- Brewster's angle, 149, 150
- BRL. *See* Ballistic Research Laboratory (BRL)
- $B_{rms}$ . *See* Rms bandwidth ( $B_{rms}$ )
- Broad-band synthesizer (BBS), 444, 445
- Brute-force algorithm, 471
- Built-in-test (BIT) functions, 392
- Bulk acoustic wave (BAW) devices, 795
- C**
- CA-CFAR. *See* Cell-averaging (CA)-CFAR
- Canadian RADARSAT 2 system, 52
- Cartesian coordinates, 10, 87, 709, 719
- Cartesian space, 748
- Cassegrain configuration, 325
- Cathode-to-body voltage, 363
- Causal, 524
- C-band mixer, 430
- CBE. *See* Cell Broadband Engine (CBE)
- CDF. *See* Cumulative distribution function (CDF)

- Cell-averaging (CA)-CFAR, 593, 597–599  
 CFAR loss, 601–603, 610  
 performance, 600  
 in heterogeneous environments, 603–607  
 in homogenous environment, 600–601  
 ROC for, 616–617  
 threshold, 598, 600
- Cell Broadband Engine (CBE), 475
- Cell under test (CUT), 595, 596  
 clutter boundaries and, 607
- Censored (CS)-CFAR, 613–614, 615  
 combining greatest-of with, and ordered statistics CFAR, 615–616  
 ROC for, 616–617
- Centroid tracker, 694
- CFA. *See* Crossed-field amplifiers (CFA)
- CFAR. *See* Constant false alarm rate (CFAR)
- CFAR loss, 69
- CFLOP. *See* Complex floating-point operations (CFLOP)
- Channelized receivers, 392, 395–396
- Chip, 438
- Chirp pulse, 30
- Chirp waveform. *See* Linear frequency modulation (LFM)
- Chi-square, 558, 559, 560, 578, 579
- Chi-square of degree 2, 254, 256
- Circularly polarized, EM wave, 11
- Circular polarization, 214  
 attenuation, 126  
 scattering matrix for, 223–224
- Circular random process, 557
- Circulator, 394
- Clear region, 295
- Closely spaced targets, 715
- Clutter, 4, 590  
 atmospheric. *See* Atmospheric clutter  
 attenuation, 637, 638  
 backscatter coefficient of, 168  
 boundaries, 600  
 CA-CFAR performance and, 606–607  
 GOCA-CFAR and, 618  
 SOCA-CFAR and, 618  
 cancellation, 421  
 characteristics of  
 atmospheric clutter. *See* Atmospheric clutter  
 millimeter wave clutter, 200–202  
 overview of, 172  
 surface clutter. *See* Surface clutter  
 defined, 165  
 detect discrete target, 76  
 fill pulses, 664  
 interference, 105  
 mapping, 665–667  
 millimeter wave, 200–202  
 models, 202–205  
*versus* noise signals, 165–169  
 polarization scattering matrix, 171  
 power spectra, 190–192  
 radar performance in, 202  
 reduction, effect of phase noise on, 424–425  
 region, 295  
 scattering coefficients, 169–171  
 statistical behavior of, 76  
 surface. *See* Surface clutter  
 volume, 77–78
- Clutter, moving radar  
 altitude line (AL), 298–299  
 distribution, 299–300  
 hyperbolic isovelocity contours, 299  
 range-velocity distribution, 299, 300, 301  
 Doppler bandwidth, 296, 297  
 Doppler shift of, 296–297  
 ambiguities in, 301  
 radar-to-ground, 298  
 main lobe clutter (MLC), 298–299  
 range ambiguity, 300–301  
 sidelobe clutter (SLC), 298  
 spectrum elements, 297–299  
 velocity ambiguity, 301–302
- Clutter-to-noise ratio (CNR), 295, 887
- CMOS. *See* Complementary metal oxide semiconductor (CMOS)
- CNR. *See* Clutter-to-noise ratio (CNR)
- Coarse resolutions, 841
- Cobra Judy system, 42
- Cognitive radar, 378
- Coherent demodulation, 402–403
- Coherent detector, 564, 565, 566, 568
- Coherent integration, 67, 189, 536–537, 549, 559
- Coherent-on-receive system, 353
- Coherent oscillator (COHO), 431, 433
- Coherent processing interval (CPI), 69, 88, 264, 419, 502, 548, 550, 551, 552, 627
- Coherent system, 23, 419  
 local oscillator (LO) signal, 24
- COHO. *See* Coherent oscillator (COHO)
- Coincidence algorithm, 662–663
- Coincidence detection. *See* Binary integration
- COMBIC. *See* Combined Obscuration Model for Battlefield-Induced Contamination (COMBIC)
- Combined Obscuration Model for Battlefield-Induced Contamination (COMBIC), 158
- Commercial off-the-shelf (COTS) programmable processors, 462  
 open modular architectures of, 476–478
- Complementary metal oxide semiconductor (CMOS), 410
- Complex floating-point operations (CFLOP), 465
- Computer simulation in error analysis, 316–317
- Conditional CRLB, 707
- Conical scan, 320, 677
- Connectorized components, 446
- Constant acceleration estimator, 721  
 filtering, 726–727
- Constant false alarm rate (CFAR), 69, 96, 460, 532, 593, 717  
 adaptive, 618–619  
 algorithms, selection of, 616–618  
 architecture of, 595–597  
 cell averaging. *See* Cell-averaging (CA)-CFAR  
 detection  
 processing, 666  
 theory, overview of, 590–592  
 loss, 69, 601–603  
 robust, 607  
 censored CFAR, 613–614  
 greatest-of CA-CFAR, 608–612  
 ordered statistics CFAR, 614–615  
 smallest-of CA-CFAR, 608, 612–613  
 trimmed mean-CFAR, 613–614  
 target masking and, 590  
 threshold, 595  
 vs. Neyman-Pearson threshold, 601
- Constant gamma model, 174
- Constant phase area, 230
- Constant velocity (CV), 724  
 estimate, 720  
 filtering, 722–726  
 target, 646–648
- Constructive interference, 9, 13, 51.  
*See also* Interference
- Continuoustime white noise acceleration (CWNA), 730  
 NCV filtering with, 736–739  
 NCV motion model with, 748
- Continuous wave (CW), 20, 222, 352, 844  
 pulse, 775  
 match filtered response for, 781  
 radars, 394
- Converted measurement filter, 760
- Convolution sum, 524

- Cooley-Tukey FFT algorithm, 521  
 Coordinate systems, 709  
 Corner reflector, simple target, 248, 249  
 Corner reflectors, 226, 235  
 “Corner-turn” memories, 476  
 Corporate feeds, 354, 355  
   vs. distributed feeds, 354, 355  
 Correlation lag, 534  
 Correlation length, 258, 259  
 Cosine, 92  
 COTS. *See* Commercial off-the-shelf (COTS) programmable processors  
 COTS 6U VME boards, 476  
 COTS 6U VME signal processor, 477–478  
 Covariance matrix, 541  
 Covariance of estimate, 722  
 CPI. *See* Coherent processing interval (CPI)  
 Cramèr-Rao lower bound (CRLB), 687–688, 775  
 Creeping waves, 226  
 Critical angle, 149  
 CRLB. *See* Cramèr-Rao lower bound (CRLB)  
 Cross-correlation function, 533  
 Crossed-field amplifiers (CFA), 353, 364  
 Crossed-field tubes vs. linear beam tubes, 357–359, 358–359  
 Cross range resolution, SAR, 838, 839, 841, 844, 845–846  
   stripmap, 848  
 Cross-track range, 838, 840, 842, 857–860, 862, 864  
 Crowbar, 374  
 Crystal reference oscillator, 440–441  
 Crystal video receiver, 393  
 CS-CFAR. *See* Censored (CS)-CFAR  
 CTT ASM/050-1636-123A amplifier, 452  
 CTT RF amplifiers, 452  
 Cumulative distribution function (CDF), 185–186  
 CUT. *See* Cell under test (CUT)  
 CV. *See* Constant velocity (CV)  
 CW. *See* Continuous wave (CW)  
 CWNA. *See* Continuous-time white noise acceleration (CWNA)
- D**  
 1-D, CFAR window. *See* One-dimensional (1-D), CFAR window  
 2-D. *See* Two-dimensional (2-D) system  
 D/A converter. *See* Digital-to-analog (D/A) converter  
 Data association, 713–716, 717  
 Data collection, SAR, 852–856  
   phase information, 854–855  
   range variation, 855–856  
   stop-and-hop model, 854  
 Datacube, radar, 502–503  
   algorithms act in, 503  
 Data processing, 461  
 Data rates, signal processor sizing and, 485–487  
 DC. *See* Direct current (DC)  
 DCT. *See* Discrete cosine transforms (DCT)  
 2-D data set. *See* Two-dimensional (2-D) data set  
 DDS. *See* Direct digital synthesizer (DDS)  
 Dechirp-on-receive, LFM, 847  
 Decibels (dBi), 313  
 Decorrelation models, 583  
 Decorrelation time, 187–189  
   for rain backscatter, 200  
 Delta beam, 320  
 Demodulation  
   analog coherent detection  
     implementation and mismatch errors, 403–404  
   coherent, 402–403  
   noncoherent, 400–402  
 Depressed collector, 374  
 Depression angle, 173  
 Despeckling, 168  
 Destructive interference, 9, 12, 13.  
   *See also* Interference  
 Detection, 95, 547  
   criterion, 109–111  
   fundamentals  
     closed-form solutions, 106  
     concept of threshold, 95–96  
     detection for nonfluctuating target, 106–107  
     probabilities of, 96–97  
     swerling 1 target model, 107–108  
   statistics, 548, 550, 560  
   theory, 590–592  
 Detector, 4  
   loss, 566  
 DFT. *See* Discrete Fourier transform (DFT)  
 Dielectric permittivity, 213  
 Dielectric resonant oscillator (DRO), 441  
 Differential path length, 327  
 Diffraction, 11–15, 140–142, 226.  
   *See also* Interference  
   coefficient, 141  
   extreme cases of, 12  
   in multi-element antenna, 13  
 Diffuse scattering, 17–18, 153–154  
 Digital compressor, 795–796  
 Digital filter, 523–532, 795–796  
   characteristics of, 525–528  
   design of, 525–528  
   FIR filters, 525–526  
   implementation of, 528–530  
   of LSI, 524  
 Digital receivers, 395  
 Digital signal processing (DSP), 392, 459–460  
   correlation as, 538–540  
   data collection, 502–503  
   digital filtering, 523–532  
   Fourier analysis, 506–522  
   integration of, 536–538  
   matched filters, 540–543  
   overview, 495–496  
   quantization, 504–506  
   random signals, 532–535  
   sampling, 496–503  
   z transform, 522–523  
 Digital-to-analog (D/A) converter, 438  
 Digital up/down frequency conversion, 414  
 Dihedrals, 235, 884, 885  
 Diode detector, 400, 401  
 Diode limiters, 396  
 Dipole moments, 225  
 Dirac delta function, 498, 777, 871, 873  
 Direct current (DC), 350  
 Direct digital in-phase/quadrature (I/Q) sampling, 412–414  
 Direct digital synthesizer (DDS), 438–439, 444  
 Directivity, 62, 312–313, 316  
   beamwidth and, 313  
   gain and, 313  
   sidelobe levels and, 314  
 Direct synthesizer (DSX), 444–445  
 Dirichlet function, 508  
 Discrete cosine transforms (DCT), 485  
 Discrete Fourier transform (DFT), 28, 464, 470, 499, 514–516, 549, 628, 643, 795  
   matched filter and filterbank  
     interpretations of pulse-Doppler processing with, 652–653  
   methods  
     for doppler and range rate measurements, 697–698  
     interpolation methods, 698–699  
 Discrete ray tracing, 147  
 Discrete-time Fourier transform (DTFT), 294, 506–509, 567, 628, 697, 795  
   of constant-velocity target, 646–648  
 Discrete white noise acceleration (DWNA)  
   NCA model and, 749  
   NCV filtering with, 730–736  
   NCV motion model and, 748

- Dispersive analog filters, 794–795
- Displaced phase center antenna (DPCA)  
processing, 642–644
- Distributed feeds, 354, 355  
vs. corporate feeds, 354, 355
- Divergence factor, multipath, 151–152
- D layer, ionosphere, 138
- Doppler beam sharpening (DBS), for  
SAR imaging, 860–870  
derivation, 860–864  
example, 866–868  
image formation, 864–865  
limitations, 868–870  
spatial frequency, 863–864
- Doppler bins, 82, 100
- Doppler cell, 98
- Doppler effect, 23
- Doppler filter bandwidth, 841
- Doppler filtering, 841
- Doppler frequency, 195
- Doppler loss, 684
- Doppler processing, 66, 402, 717  
clutter mapping, 665–667  
Doppler shift, 626  
moving target detector (MTD),  
667–668  
moving target indication (MTI),  
629–631  
blind speeds and staggered PRFs,  
634–637  
figures of merit, 637–640  
from moving platform, 641–644  
performance, limitations to,  
640–641  
pulse cancellers, 631–634  
overview, 625–626  
pulse-Doppler processing. *See*  
Pulse-Doppler processing  
pulsed radar Doppler data acquisition,  
627–629  
pulse pair processing (PPP), 668–673  
Doppler shift, 23–24, 274–276, 294–295,  
626, 805, 808, 816–817  
of clutter (moving radar), 296–297  
ambiguities in, 301  
radar-to-ground, 298  
as function of velocity and  
frequency, 626  
impacts of, on pulse compression  
waveform, 807  
measurement of radar, 28  
ratio of, 804  
unambiguous measurement of, 24–25
- Doppler spectrum, 30  
clear region, 295  
DTFT, 294  
elements of, 293–294  
of fluctuating targets, 267–269  
for range bin, 294  
SNR in, 651–652  
and straddle loss, sampling, 648–651  
transition region, 295
- Doppler tolerance, 788, 791, 816–817,  
827–828  
defined, 801  
of P4 code, 829
- Double-balanced mixer, 430
- Double-delay filter, 424
- Douglas sea number, 181
- Down-range resolution, 845
- DPCA condition, 642–643
- DPCA processing. *See* Displaced phase  
center antenna (DPCA)  
processing
- DRO. *See* Dielectric resonant oscillator  
(DRO)
- Drop-size distribution model, 125
- DSP. *See* Digital signal processing (DSP)
- DSX. *See* Direct synthesizer (DSX)
- DTFT. *See* Discrete-time Fourier  
transform (DTFT)
- Dual polarized radars, 409
- Ducting, 16  
anomalous atmosphere, 135–136  
sea reflectivity and, 184–185
- Duplexer, function of, 391
- Dust, and attenuation, 129
- Duty cycle, 350–351
- Dwell time, 31, 33, 88, 502, 548, 627
- Dwell-to-dwell frequency change,  
439–440
- Dwell-to-dwell stagger  
pulse-Doppler processing, 659
- DWNA. *See* Discrete white noise  
acceleration (DWNA)
- Dynamical motion model, 728
- Dynamic range, 496, 504  
receiver, 406  
coupling issues, 409  
gain control, 408–409  
sensitivity time control, 407–408  
SFDR, 411, 412, 413  
of signal-following ADC, 411–412
- E**
- Early/late gate tracker, 693–694
- East-North-Up coordinates, 709
- Echo amplitude, 251, 259, 261
- Echo area, 219
- Eclipsed, 660
- ECM. *See* Electronic countermeasures  
(ECM) system
- Edge diffraction, 231, 232–234
- Edge waves, 226
- EED. *See* Electro-explosive devices  
(EED)
- EEMBC, 484
- Effective earth radius, 134
- Effective number of bits (ENOB), 473
- EKF. *See* Extended Kalman filter (EKF)
- E layer, ionosphere, 139
- Electric field, 5, 213
- Electric permittivity, 212–213
- Electro-explosive devices (EED), 384
- Electromagnetic (EM) waves, 4, 59, 211  
atmospheric attenuation, 15  
atmospheric refraction, 15–17  
attenuation of, 121–123  
characteristics of, 212  
diffraction, 11–15  
electric, *E*, field, 5  
frequency of, 6–7  
fundamentals, 212–214  
intensity of, 10  
interaction with matter, 11–18  
magnetic, *B*, field, 5  
phase of, 7–9  
physics of, 5  
polarization of, 10–11, 214–215  
propagation of, 4  
factor, 118–119  
paths and regions, 119–120  
reflection, 17–18, 215–219  
superposition of, 9–10  
transmission of, 156–158  
types of, 8  
wavelength of, 6
- Electromagnetic fields, 6
- Electromagnetic interference (EMI), 5,  
294, 824
- Electromagnetic velocity vector, 6
- Electronically scanned array (ESA), 14,  
80, 88, 848
- Electronic countermeasures (ECM)  
system, 5, 362, 716, 717
- Electronic warfare (EW) systems,  
7, 370  
receivers, 392
- Elevation angle, 27
- Elliptic IIR filter, 527
- EMI. *See* Electromagnetic  
interference (EMI)
- EM waves. *See* Electromagnetic (EM)  
waves
- End-region scattering, 226, 231–232
- Energy conservation equation, 314
- Engineering Refractive Effects Prediction  
(EREPS), 159
- ENOB. *See* Effective number of bits  
(ENOB)
- Envelope detector, 400

- Equivalence operations, phase-coded waveforms, 812
- EREPS. *See* Engineering Refractive Effects Prediction (EREPS)
- Erlang density, 574
- Error correction filter, 796
- ESA. *See* Electronically scanned array (ESA)
- Estimators, 685–686  
types of, 686
- European Communications Office, 159
- Evaporation duct, 136
- EW. *See* Electronic warfare (EW) systems
- EW bands, 8
- Exciters  
components  
amplifiers, 451–452  
assembly approaches, 446–448  
frequency dividers, 450–451  
frequency multipliers, 450  
mixers, 448–449  
stable oscillators, 440–444  
switches, 449–450  
synthesizers, 444–446  
design considerations  
transmit signal, 429–437  
waveform generation, 437–440  
internal components of, 434  
overview, 417–418  
performance issues, 418–429  
phase noise, 419–421  
clutter reduction, effect on, 424–425  
imaging, effect on, 428–429  
pulse-Doppler processing, effect on, 425–428  
self-coherence effect and, 422–424  
spectral folding effects and, 421–422  
purpose of, 419  
timing and control circuits, 452–454
- Exponential PDF, 253, 254, 255
- Exponential PDF, 557
- Extended Kalman filter (EKF), 753, 755–756, 759–760
- Extended targets, defined, 692
- Extinction efficiency, 129
- F**
- False alarm rate (FAR), 553–554, 591–592. *See also* Constant false alarm rate (CFAR)
- False alarms, 95, 552, 553–554  
average probability of, 599  
clutter boundaries and, 607  
defined, 97–98  
impact of, 592–593  
noise PDF and, 97–100  
probability of, 96–111, 592–593
- Fan beam, 38
- FAR. *See* False alarm rate (FAR)
- Faraday shield, 215
- Fast convolution, 528, 795  
approach, 471
- Fastest Fourier Transform in the West (FFTW) library, 483, 485
- Fast Fourier transform (FFT), 28, 67, 88, 460, 485, 496, 521, 628, 643, 795, 841  
algorithm, 470, 656, 697
- Fast switching synthesizer (FSS), 444, 445
- Fast time, 502  
SAR data acquisition, 842
- FCC. *See* Federal Communication Commission (FCC)
- FCR. *See* Fire control radar (FCR)
- FDS. *See* Fractional Doppler shift (FDS)
- Federal Communication Commission (FCC), 7
- Feed horn, 323, 324, 325
- Fermat's minimum path, 229
- Ferrite limiters, 396
- FFT. *See* Fast Fourier transform (FFT)
- FFTW library. *See* Fastest Fourier Transform in the West (FFTW) library
- Field of view (FOV), 317, 334, 691
- Field programmable gate arrays (FPGA), 395, 454, 474, 523
- Filterbank, 537
- Filtered state estimate, 719
- Fine resolution. *See* High resolution
- Finite impulse response (FIR) filters, 395, 460, 496, 525–526, 631
- Finite pulse train, 280–283  
modulated, 281–283
- FIR. *See* Finite impulse response (FIR) filters
- Fire-and-forget mode, 44
- Fire control radar (FCR), 37, 46–47
- Firefinder, 90
- First-order canceller, 631
- Fixed point vs. floating point, 480–482
- Flash point, 229
- F1 layer, ionosphere, 139
- F2 layer, ionosphere, 139
- FLOPS, counting  
choosing efficient algorithms, 470–472  
general approach, 464–468  
mode-specific formulas, 468–470
- Fluctuating targets, 247, 578–581  
Doppler spectrum of, 267–269  
vs. non-fluctuating targets, 580–581
- FM. *See* Frequency modulation (FM)
- FMCW. *See* Frequency modulated continuous wave (FMCW)
- Focal length to diameter ( $f/D$ ) ratio, 323–324
- Fog  
attenuation and, 127–128  
types of, 127
- Foliage penetration (FOPEN) SAR systems, 836
- Fourier analysis, 506–522  
DFT, 514–516  
DTFT, 506–509  
fast Fourier transform, 521  
reciprocal spreading, 508  
spatial frequency, 513–514  
straddle loss, 515–516, 517–518  
summary of, 521–522  
windowing, 509–513, 516–518
- Fourier spectrum, 30
- Fourier transform, 187, 276–277  
matched filter and, 778–779
- Fourier uncertainty principle, 784–785
- Fourth-degree chi-square PDF, 254, 255, 256
- FOV. *See* Field of view (FOV); Field of view (FOV)
- FPGA. *See* Field programmable gate arrays (FPGA)
- Fractional Doppler shift (FDS), 804
- Frank codes, 824, 825–827, 829
- Free-running oscillator, 352–353
- Frequency  
agility, 262, 559, 580–581, 708  
dependence, of RCS, 249–250  
diversity, 581  
dividers, for exciters, 450–451  
Doppler shift as function of, 626  
downconversion  
double, 398  
and mixers, 397–399  
single, 398  
of electromagnetic waves, 6  
pulling, 379
- Frequency modulated continuous wave (FMCW), 49, 361, 371, 377
- Frequency modulation (FM), 371, 419
- Frequency multipliers, for exciters, 450
- Fresnel reflection coefficient, 148–150
- Frozen precipitation, 199–200
- FSS. *See* Fast switching synthesizer (FSS)
- Furuno FAR2817 X-band radars, 47
- G**
- Gain, 313. *See also* Directivity  
antenna vs. amplifier, 313
- Gain control  
receiver dynamic range and, 408–409
- Gain loss, 330, 332–333  
phase-shifter bits and, 330

- Gamma density, 560, 574  
 Gamma PDF, 256  
 Gap cells, 596  
   self-masking and, 604  
 Gases, attenuation and, 124–125  
 Gating, 763  
   typical threshold values for, 764  
 Gaussian Clutter Power Spectrum  
   improvement factor for, 639  
 Gaussian noise, 557, 775. *See also*  
   Circular random process  
 Gaussian PDF, 97  
 Gaussian spectra, 190, 192  
 GCMLD. *See* Generalized censored mean  
   level detector (GCMLD)  
 Gedae by Gedae, Inc., 483  
 Generalized censored mean level detector  
   (GCMLD), 616  
   ROC for, 619  
 Generalized likelihood ratio test  
   (GLRT), 708  
 General-purpose processors, 474  
 Georgia Tech Research Institute (GTRI),  
   45, 177  
   empirical model, 202–205  
   coefficients for, 203  
   sea clutter model equations, 204  
 Ghosts, 663  
 Giga, 7  
 Gigabit Ethernet, 477  
 Glint, 678, 690  
 Glistening surface, 152  
 GLRT. *See* Generalized likelihood ratio  
   test (GLRT)  
 GMTI radars. *See* Ground MTI (GMTI)  
   radars  
 GOCA-CFAR. *See* Greatest-of CA-CFAR  
   (GOCA-CFAR)  
 GPR. *See* Ground penetration radars  
   (GPR)  
 GPU. *See* Graphical processing units  
   (GPU)  
 Graphical processing units (GPU), 475  
 Grating lobes, 330–331, 349  
   element spacing and, 331, 332  
 Grazing angle, 144, 150, 169  
   clutter surface and, 172, 173  
   dependence on, land reflectivity and,  
   177–178  
   effect of, on PDF, 193  
 Greatest-of CA-CFAR (GOCA-CFAR),  
   608–612, 618  
   CFAR loss associated with, 610  
   ROC associated with, 609–610,  
   616–617  
 Green's function, 217  
 Ground MTI (GMTI) radars, 463  
 Ground penetration (GPEN) SAR  
   systems, 838  
 Ground penetration radars (GPR), 53  
 Ground plane, 143, 299, 879, 881, 887  
 Group delay, matched filter, 794  
 Gs. *See* Guard cells (Gs)  
 GTRI. *See* Georgia Tech Research  
   Institute (GTRI)  
 Guard cells (Gs), 595, 596  
   self-masking and, 604  
 Gunn oscillators, 360–361  
 Gyrotrons, 360
- H**
- Hail, and attenuation, 128–129  
 Hard-tube modulator, 372  
 Hardware metrics, of radar signal  
   processor, 462–464  
 Harry Diamond Laboratory, 177  
 HCE-CFAR. *See* Heterogeneous clutter  
   estimating (HCE)-CFAR  
 Herley-CTI, Inc., 442, 444  
 Hertz, 7  
 Heterodyne receiver, 394–395  
 Heterogeneous clutter estimating  
   (HCE)-CFAR, 618  
 HF. *See* High frequency (HF)  
 High frequency (HF), 118, 430  
 High-frequency optics region,  
   226–227  
 High-frequency scattering  
   edge diffraction, 232–234  
   end-region scattering, 231–232  
   multiple-bounce scattering,  
   235–236  
   phasor addition, 227–229  
   specular scattering, 229–231  
 High grazing angle region, clutter  
   surface, 174  
 High-order filter, 436  
 High Performance Computing (HPC)  
   Challenge, 483, 484  
 High PRF mode, 661  
 High-range resolution (HRR)  
   systems, 787  
 High resolution, 843  
 High voltages (HV), 347  
 Hilbert transformer, 413–414  
 Hittite Microwave Corp. HMC C014  
   mixer, 448  
 Homodyne receiver, 394  
 Horizon, defined, 134  
 Horizontally polarized, EM wave, 11  
 Hot spot, 229  
 HPC Challenge. *See* High Performance  
   Computing (HPC) Challenge  
 HPCS Benchmarks, 484  
 HPEC challenge, 484  
 HRR systems. *See* High-range resolution  
   (HRR) systems  
 Huffman coded waveform, 787  
 Huygen's principle, 12, 140. *See also*  
   Diffraction  
 Huygen's wavelet, 217  
 HV. *See* High voltages (HV)
- I**
- IBM PowerPC microprocessors, 476  
 IBM "Roadrunner" system, 479  
 IC technology. *See* Integrated circuit (IC)  
 Ideal (noise-free) matched filter output,  
   693–694  
 IEEE dictionary. *See* Institute of Electrical  
   and Electronics Engineers (IEEE)  
   dictionary  
 IEEE P754 32-bit format, 481  
 IF. *See* Intermediate frequency (IF)  
 IFM receivers. *See* Instantaneous  
   frequency measurement (IFM)  
   receivers  
 IID. *See* Independent and identically  
   distributed (IID)  
 IIR filters, 526–527  
 IIR high-pass filters. *See* Infinite impulse  
   response (IIR) high-pass filters  
 Imaging, 34–36  
   effect of phase noise on, 428–429  
 Imaging, SAR, 468–469, 856–874  
   ambiguity, 879–880  
   CNR, 887  
   coordinate systems, 856–857  
   DBS, 860–870  
   derivation, 860–864  
   example, 866–868  
   image formation, 864–865  
   limitations, 868–870  
   foreshortening, 880  
   layover, 880  
   man-made returns, 884–886  
   matched filter imaging, 871–873  
   NAR in, 875, 876  
   PSR, 856, 865  
   linear collection, 857–860  
   shadowing. *See* Shadows, imaging  
   SNR, 886–887  
   speckle, 881–884  
   survey of, 873–874  
 IMM estimator. *See* Interacting multiple  
   model (IMM) estimator  
 Impact ionization avalanche transit time  
   (IMPATT) diodes, 360–361  
 IMPATT. *See* Impact ionization  
   avalanche transit time  
   (IMPATT) diodes

- Improvement factor, 637, 638–640  
 for Gaussian Clutter Power Spectrum, 639
- Incident field, 215
- Independent and identically distributed (IID), 561, 591
- Index of refraction, 213
- InfiniBand, 477
- Infinite impulse response (IIR) high-pass filters, 633
- Infinite pulse train, 279–280
- Initial phase, 6
- Injection-lock, 353
- Injection-prime, 353
- In-phase (I) frequency value, 844
- Instantaneous AGC, 408–409
- Instantaneous frequency, vs. time for LFM, 790
- Instantaneous frequency measurement (IFM) receivers, 392, 395
- Institute of Electrical and Electronics Engineers (IEEE) dictionary, 219  
 RCS definition, 219–220
- Instrumentation, radar, 45–46
- Integrated circuit (IC), 454
- Integrated power conditioner, 369
- Integrated sidelobe ratio (ISR), 794
- Integration, 536–538, 548–552, 559, 570–572, 584  
 binary, 550, 584  
 coherent, 536–537, 549, 559  
 combination of, 550–552  
 gain, 536, 549  
 noncoherent, 537–538, 549–550, 559, 570–572, 575, 576  
 of nonfluctuating target, 570–572
- Integration angle, in SAR, 845, 847–848, 849
- Intel microprocessors, 478, 479
- Intel's Math Kernel Library (MKL), 485
- Intensity, of electromagnetic wave, 10
- Interacting multiple model (IMM)  
 estimator, 743  
 implementation of  
 combination of state estimates, 745–746  
 mode conditioned estimates, 744  
 model likelihood computations, 744–745  
 mode probability update, 745  
 state mixing, 744
- Interference, 95  
 constructive, 9  
 destructive, 9  
 forms of, 5  
 other than noise, 105–106  
 power, 598  
 region, 120
- Interferometric processing, 884
- Interferometric SAR, 35
- Interferometry, 702
- Intermediate frequency (IF), 4, 360, 430, 434, 776  
 oscillator, 437  
 selection of, 399–400  
 signal, 391
- International Telecommunications Union (ITU), 7, 159
- Interpulse period (IPP), 20
- Intrapulse, pseudorandom biphasic modulation, 437–438
- Intrapulse LFM. *See* Intrapulse linear frequency modulation (LFM)
- Intrapulse linear frequency modulation (LFM), 438–439
- Inverse methods, image formation survey, 873
- Inverse synthetic aperture radar (ISAR), 45. *See also* Synthetic aperture radar (SAR)  
 image, 46  
 turntable range, 46
- Ionosphere, 121, 138–140
- IPP. *See* Interpulse period (IPP)
- ISAR. *See* Inverse synthetic aperture radar (ISAR)
- Isodoppler contour, 299
- Isorange contour, 299
- Isotropic antenna, 310–311  
 defined, 310  
 power density of, 310  
 radiation intensity from, 310
- ISR. *See* Integrated sidelobe ratio (ISR)
- ITU. *See* International Telecommunications Union (ITU)
- J**
- Jamming signals, 5, 78  
 preselection effect on rejection of, 397
- K**
- Kalman algorithm, 728
- Kalman filters, 461, 718, 719, 728–729, 737, 741  
 as predictor-corrector algorithm, 729
- Keller cone, 232–233, 234
- Kinematic motion models, 746  
 NCA motion model, 749  
 NCV motion model, 747–749  
 nearly constant speed motion model, 750–751  
 Singer motion model, 749–750
- Kinematic state estimation, 678
- KLIX WSR-88D NEXRAD weather radar, 671–672
- Klystrons, 348, 361–362
- Knife edge effect, 141
- K-point DFT, 697
- L**
- Land clutter  
 clutter frequency spectra, 190–192  
 decorrelation time, 187–189  
 spatial variations, 192–193  
 temporal variations, 185–186
- Land reflectivity  
 frequency bands, 178–180  
 grazing angle, 177–178
- Latency, 462–463
- L-band frequency, 15
- Leading-edge (LE) diffraction, 233
- Leading window, 596, 597
- Least squares estimate (LSE), 722
- LE diffraction. *See* Leading-edge (LE) diffraction
- Left-handed circular (LHC), 150, 223
- LEIBE MPM. *See* Microwave Propagation Model (LEIBE MPM)
- LFM. *See* Linear frequency modulation (LFM)
- LFM waveform. *See* Linear frequency modulated (LFM) waveform
- LHC. *See* Left-handed circular (LHC)
- Light, speed of, 5
- Likelihood ratio (LR), 554–556
- Likelihood ratio test (LRT), 554–556, 562
- Linear detector, 58, 537, 563, 572–573
- Linear frequency modulated (LFM)  
 waveform, 695, 730, 774, 787–788  
 ambiguity function for, 802  
 vs. biphasic MLS coded waveform, 823–825  
 compressed response, 791–792  
 match filtered response for, 792  
 measurements with, 756  
 NCV tracking with, 736  
 peak sidelobe ratio of, 793–794, 797  
 range-Doppler coupling, 803–805  
 spectral interpretation of, 806–807  
 Rayleigh resolution, 792–793  
 sidelobe  
 reduction in, 797–800  
 structure of, 805  
 spectrum of, 791  
 summary of, 808  
 Taylor weighted, straddle loss  
 reduction associated with, 800  
 time-domain description of, 789–790

- time for, instantaneous frequency  
  *versus*, 790
  - V-LFM, 808
  - Linear frequency modulation (LFM), 30, 433, 847
    - chirps, 627
  - Linearity, 523
  - Linearly polarized, EM wave, 11
  - Linear polarization, 214
    - scattering matrix for, 222–223
  - Linear shift-invariant (LSI), 523
    - spectral representations of, 524
  - Line-of-sight (LOS) region, 119–120, 558
  - LNA. *See* Low-noise amplifier (LNA)
  - LO. *See* Local oscillator (LO)
  - Load balancing, 482
  - Local oscillator (LO), 360
    - selection of, 399–400
    - signal, 23, 391
      - coherent system, 24
  - Log amplifiers, 401
  - Logarithmic receiver, 176
  - Log detector, 98
  - Log-likelihood ratio test, 554, 568
  - Log-normal distribution, 176, 256, 257
  - Log-video, 98
  - Longbow radar, 44–45
  - Long-pulse illumination, 222
  - LOS region. *See* Line-of-sight (LOS) region
  - Lower-power radar systems, 396
  - Lower sideband (LSB), 432
  - Low grazing angle region, clutter surface, 174
  - Low-noise amplifier (LNA), 339, 356, 391, 395
  - Low power density (LPD), 340, 341
  - Low PRF mode, 661
  - Low-voltage differential signaling (LVDS), 410
  - LPD. *See* Low power density (LPD)
  - LRT. *See* Likelihood ratio test (LRT)
  - LSB. *See* Lower sideband (LSB)
  - LSE. *See* Least squares estimate (LSE)
  - LSI. *See* Linear shift-invariant (LSI)
  - LVDS. *See* Low-voltage differential signaling (LVDS)
- M**
- Macro component, surface boundary, 146
  - Magnetic field, 5, 213
  - Magnetic permeability, 213
  - Magnetron, 348, 358, 359–360
  - Mahalanobis distance, 763
  - Main beam, 13
    - Main lobe, 13, 782
      - shape of, 784
      - width, range resolution and, 784
  - Maneuver index, 731
  - Man-made returns, in SAR imaging, 884–886
  - Manual gain control, 408
  - Maple, 481
  - Marcum's Q function, 100, 564
  - Marcum targets, 257
  - Marine navigation radar, 51–52
  - Markovian switching coefficients, 742–743
  - Masking, 600, 693
    - mutual, 601, 604–605
    - self, 603–604
  - Massachusetts Institute of Technology
    - Lincoln Laboratories (MIT/LL), 177
  - Master oscillator-power amplifier (MOPA), 353, 429
  - Matched filter, 530, 540–542, 567–568
    - for continuous-time signals, 542
    - defined, 774
    - derivation of, 779–780
    - form of, 776
    - Fourier transform and, 778–779
    - implementations of, 794–796
    - phase-coded waveform and, 812–813
    - point target model, 776–777
    - radar range equation, 775–776
    - relationship between radar range equation and, 780
    - response
      - for phase codes, 812–813
      - properties of, 782
      - for simple pulse, 781
    - response for LFM waveform, 792
    - SNR, radar performance and, 775
  - Matched filter imaging, 871–873
    - concept, 871
    - of near-range point targets, 872
  - MathCAD, 481
  - Mathematica, 481
  - MathWorks, Inc., the, 483
  - MATLAB, 101, 481, 527
  - Maximum length sequence (MLS), 810, 819, 822–823
    - vs.* compressed LFM waveform, 823–824
  - Maximum likelihood (ML) estimators, 592, 686, 719
  - Maximum MSE (MMSE), 733–734
  - Maxwell, James Clerk, 212
  - Maxwell's equation, 5, 214, 216
  - MCAEKF. *See* Measurement covariance adaptive extended Kalman filter (MCAEKF)
  - MCRLB. *See* Modified Cramèr-Rao lower bound (MCRLB)
  - MDD. *See* Minimum detectable Doppler (MDD)
  - MDV. *See* Minimum detectable velocity (MDV)
  - Mean, 533–534
    - square, 533–534
  - Mean time between failures (MTBF), 366, 381
  - Measurement covariance adaptive extended Kalman filter (MCAEKF), 759
  - Measurement-to-track data association, 713–716, 717, 760–761
    - formation of new track, 762
    - measurement validation and gating, 762–763
    - nearest neighbor (NN) filter, 764
    - probabilistic data association filter (PDAF), 765–766
    - strongest neighbor (SN) filter, 764–765
  - Measurement validation, 763–764
  - Median filters, 530
  - Medium PRF radar, 661
    - in range and velocity ambiguities, 302–303
  - MEM. *See* Microelectro-mechanical systems (MEM)
  - Mercury Computer Systems, 477–478
  - MESFET. *See* Metal semiconductor field-effect transistor (MESFET)
  - Mesosphere, 120–121
  - Message passing interface (MPI), 477
  - Metal semiconductor field-effect transistor (MESFET), 364–365
  - Method-of-moments (MoM), 147
  - MFA. *See* Multiple frame assignment (MFA)
  - MHT. *See* Multiple hypothesis tracking (MHT)
  - Micro component, surface boundary, 146
  - Microelectro-mechanical systems (MEM), 326
  - Microwave filters, 435–436
  - Microwave power modules (MPM), 363, 369–370
    - components of, 369–370
  - Microwave Propagation Model (LEIBE MPM), 158
  - Microwave tubes
    - crossed-field tubes, 358–359
    - linear beam tubes, 357–358

- Millimeter wave (MMW), 347  
 amplitude fluctuations and, 138  
 clutter, 200–202  
 surface electrical and physical parameters at, 147
- Millions of instructions per second (MIPS), 463
- Minimum detectable Doppler (MDD), 658
- Minimum detectable radar cross section, 72
- Minimum detectable velocity (MDV), 638
- Minimum mean squared error (MMSE), 534, 722, 728
- Minimum peak sidelobe (MPS) codes, 774, 818–819, 820–821  
 lengths, and corresponding peak sidelobe levels, 819
- Minimum variance (MV) estimators, 686
- Minimum variance unbiased (MVU) estimator, 686
- MIPS. *See* Millions of instructions per second (MIPS)
- Miss, 553
- Missile support radars, 46–47
- MITEQAMF-4B-02000400-20-33P-LPN amplifier, 451
- MITEQ Inc., 445
- Miteq LNS series synthesizers, 445
- MITEQ model LNS60806580 frequency synthesizer, 445, 446  
 phase noise of, 446
- MITEQ MX2M010060 passive frequency multiplier, 450
- MIT/LL. *See* Massachusetts Institute of Technology Lincoln Laboratories (MIT/LL)
- Mixer output frequencies, 431–432
- Mixers, 430  
 for exciters, 448–449  
 frequency downconversion and, 397–399
- Mk-86 Gunfire Control system, 46
- MKL. *See* Intel's Math Kernel Library (MKL)
- ML. *See* Maximum likelihood (ML)
- ML approach, 703, 704
- ML estimators. *See* Maximum likelihood (ML) estimators
- MLS. *See* Maximum length sequence (MLS)
- MMIC. *See* Monolithic microwave integrated circuits (MMIC)
- MMSE. *See* Minimum mean squared error (MMSE)
- MNR. *See* Multiplicative noise ratio (MNR)
- Modes, diffraction, 141
- Modified Cramèr-Rao lower bound (MCRLB), 707, 708
- Moding, 360
- Modulators, 371–373  
 active-switch, 372–373  
 line-type, 371–372
- M-of-n detection. *See* Binary integration
- MoM. *See* Method-of-moments (MoM)
- Moments, 533–534
- Monolithic microwave integrated circuits (MMIC), 364
- Monopulse, 27, 320–322, 409, 677, 701–703  
 angular position determination and, 320  
 AOA estimation  
 multiple unresolved targets, 707–708  
 single target, 704–707  
 error signal, 320–321
- Monostatic antenna configurations, 18–20
- Monostatic cross section, 221
- Monostatic propagation, 119
- Monte Carlo simulations, 730, 766–767
- Moore, Gordon, 478
- Moore's law, 459, 560  
 influence, on radar signal processor implementation, 478–480
- MOPA. *See* Master oscillator-power amplifier (MOPA)
- MOTR. *See* Multiple-object tracking radar (MOTR)
- Moving radar, 641–642
- Moving radar, range-Doppler spectrum of, 296–303  
 clutter  
 altitude line (AL), 298–299  
 distribution, 299–300  
 Doppler bandwidth, 296, 297  
 Doppler shift of, 296–297, 301  
 main lobe clutter (MLC), 298–299  
 range ambiguity, 300–301  
 sidelobe clutter (SLC), 298  
 spectrum elements, 297–299  
 velocity ambiguity, 301–302  
 range and velocity ambiguity, 300–303
- Moving target detector (MTD), 667–668
- Moving target indication (MTI), 28, 283, 378, 402, 497, 629–631  
 blind speeds and staggered PRFs, 634–637  
 figures of merit, 637–640  
 filters. *See* MTI filters  
 from moving platform, 641–644  
 performance, limitations to, 640–641  
 processing, 424–425  
 pulse cancellers, 631–634  
 visibility factor, 640
- Moving targets, pulse-Doppler detection of, 658–659
- MPI. *See* Message passing interface (MPI)
- MPM. *See* Microwave power modules (MPM)
- MPS codes. *See* Minimum peak sidelobe (MPS) codes
- MRSIM. *See* Multispectral Response Simulation (MRSIM)
- MTD. *See* Moving target detector (MTD)
- MTI. *See* Moving target indication (MTI)
- MTI filters, 460  
 effect of, 630  
 figures, 637–640  
 clutter attenuation, 637, 638  
 improvement factor, 637, 638–640  
 minimum detectable velocity (MDV), 638  
 subclutter visibility, 637  
 usable Doppler space fraction (UDSF), 638
- MTT. *See* Multiple target tracking (MTT)
- Multicore processor, 475
- Multilook processing, speckle, 882–884
- Multipath  
 angle errors, 155  
 classification error, 155–156  
 defined, 142  
 divergence factor, 151–152  
 Fresnel reflection coefficient, 148–150  
 propagation paths, 143  
 roughness factors, 152–155  
 diffuse scattering, 153–154  
 specular scattering, 152–153  
 superposition, 144–145  
 surface boundary and, 146–148
- Multiple-bounce scattering, 226, 235–236
- Multiple-dwell detection principles, 108
- Multiple frame assignment (MFA), 763
- Multiple hypothesis tracking (MHT), 763
- Multiple model filtering, 741–746
- Multiple-object tracking radar (MOTR), 45
- Multiple target tracking (MTT), 716  
 performance assessment of, 76–767
- Multiplicative noise ratio (MNR), 888
- Multispectral Response Simulation (MRSIM), 159
- Mutual target masking, 601, 604–605  
 censored CFAR, 613–614  
 ordered statistics CFAR, 614–615  
 smallest-of CA-CFAR, 608, 612–613  
 trimmed mean-CFAR, 613–614
- MV estimators. *See* Minimum variance (MV) estimators
- MVU estimator. *See* Minimum variance unbiased (MVU) estimator

**N**

Nallatech, 474

Narrowband system, 435

NASA Tracking and Data Relay Satellite System (TDRSS), 487

National Telecommunications and Information Administration (NTIA), 376

spectrum efficiency (SE) and, 376

National Weather Service, 670

NATO Seasparrow AAW missiles, 43

Naval Research Laboratory (NRL), 177

Navy E2C AEW system, 46

NCA filtering. *See* Nearly constant acceleration (NCA) filtering

NCV filtering. *See* Nearly constant velocity (NCV) filtering

NCV tracking. *See* Nearly constant velocity (NCV) tracking

Nearest neighbor (NN) filter, 764

Nearly constant acceleration (NCA) filtering, 730, 739–741

DWNA and, 749

Nearly constant speed motion model, 750–751

Nearly constant velocity (NCV) filtering

with CWNA, 736–739

with DWNA, 730–736

Nearly constant velocity (NCV) tracking

with LFM waveforms, 736

motion model, 747–749

with CWNA, 748

with DWNA, 748

state vector for, 746

NEES. *See* Normalized estimation error squared (NEES)

Nested codes, 810

Neyman-Pearson criterion, 553–554, 561, 571

Neyman-Pearson (NP) detector, 591, 594–595

threshold *vs.* CFAR threshold, 601

NLFM waveforms. *See* Nonlinear frequency modulated (NLFM) waveforms

NLSE. *See* Nonlinear least-squares estimate (NLSE)

NN filter. *See* Nearest neighbor (NN) filter

Noise, 25–26

clutter signals *vs.*, 165–169

defined, 64

at Doppler shifts, 295

effects, on precision and accuracy in radar measurements, 679–681

figure, 65, 404–405

power receiver, 404–406

quantization, 505

statistical models of, 557

thermal receiver, 24, 64–65

threshold detection, of signal, 26

Noise-equivalent backscatter coefficient, 887

Noncentral gamma-gamma density, 267

Noncoherent demodulation, 400–402

Noncoherent integration, 67, 537–538, 549–550, 559, 570–572, 575, 576, 684

gain, 575, 577

Noncoherent system, 23

*vs.* coherent system, 352

Noncontact radar, 49

Nonfluctuating targets, 247, 561–562, 570–572, 580, 581, 584

defined, 561–562

noncoherent integration of, 570–572

*vs.* fluctuating targets, 580, 581

Nonlinear frequency modulated (NLFM) waveforms, 785

Nonlinear least-squares estimate (NLSE), 757–759

Nonlinear systems, shift-varying and, 530–532

Nonrecurring engineering effort (NRE), 474

No return areas (NRA), in SAR imaging, 875

Normalized estimation error squared (NEES), 725–726, 767

Normalized frequency, 507

Northrop Grumman Norden Systems, 46

Nose-view scattering center image, 239, 241

Notably biased estimate, 706

NP detector. *See* Neyman-Pearson (NP) detector

*N*-pulse cancellers, 634

NRE. *See* Nonrecurring engineering effort (NRE)

NRL. *See* Naval Research Laboratory (NRL)

NTIA. *See* National Telecommunications and Information Administration (NTIA)

Null hypothesis, 552

Nyquist criterion, 498

Nyquist rate, 188, 498, 501

Nyquist sampling, 24

theorem, 496, 497–501, 795

**O**

Observed SNR, 685

Ogive tip diffracted field, 219

OLA method. *See* Overlap-add (OLA) method

Onboard *versus* offboard processing, 487–488

One-dimensional (1-D), CFAR window, 595

One-step smoothed estimate, 719

One-way attenuation, 122

fog and, 127–128

rain rate and, 125–126, 127

OpenCL, 475

Open modular architectures, of COTS processors, 476–478

Optimal detection, 552–557

Optimum detector, 564

for coherent receiver, 563

for nonfluctuating radar signals, 561–562

for nonfluctuating radar signals with coherent integration, 566–570

for nonfluctuating target with noncoherent integration, 570–572

Ordered statistics (OS)-CFAR, 614–615

combining greatest-of with, and censored CFAR, 615–616

ROC for, 616–617

Order statistics filter, 530

OS-CFAR. *See* Ordered statistics (OS)-CFAR

Oscillators, 359–361

gyrotron, 360

magnetron, 359–360

solid-state, 360–361

OTH. *See* Over-the-horizon (OTH) radars

OTH radar. *See* Over-the-horizon (OTH) radars

Output frequencies, 435

Overlap-add (OLA) method, 471–472

Over-the-horizon (OTH) radars, 17, 121

applications of, 40–41

**P**

PA. *See* Power amplifier (PA)

PAG. *See* Power-aperture-gain product (PAG)

Paired echo theory, 380–381

Parallel feed systems, 354

corporate feeds, 354

distributed feeds, 354

Parallel plate waveguide, 135

Parametric estimation approach, track filtering, 720–722

constant acceleration filtering, 726–727

constant velocity filtering, 722–726

limiting memory in, 721

Parks-McClellan algorithm, 526, 633

Parseval's theorem, 780

- Passive arrays, 353, 354  
 architectures, 339, 340  
 disadvantages of, 339  
 vs. active array architectures, 340
- Passive phased array, 339, 350
- Pave Paws, 42
- PCI Express, 477
- PCPEM. *See* Personal Computer Parabolic Equation Model (PCPEM)
- PDAF. *See* Probabilistic data association filter (PDAF)
- PDF. *See* Probability density functions (PDF)
- PDR. *See* Phase-derived range (PDR)
- PDRO. *See* Phase-locked dielectric resonator oscillator (PDRO)
- Peak detector, 400
- Peak sidelobe ratio (PSR), 793
- PEC. *See* Perfect electric conductor (PEC)
- Pencil beam, 39
- Penetration, depth of, 156–158
- Perfect electric conductor (PEC), 215
- “Perfect model,” 721
- Periodic system calibration, 682
- Personal Computer Parabolic Equation Model (PCPEM), 159
- PFA. *See* Polar formatting algorithm (PFA)
- PFN. *See* Pulse-forming network (PFN)
- Phase, of electromagnetic waves, 7–9
- Phase-coded pulse, 30
- Phase-coded waveforms, 788  
 Barker, match filtered response for, 809  
 biphas-coded waveforms, 811–812  
 equivalence operations, 812  
 matched filter and, 812–813  
 phase codes, 810  
 polyphase-coded waveforms, 811–812  
 properties of, 808–810  
 spectrum of, 813–816  
 structure of, 808–810
- Phase codes, 810  
 equivalence operations, 812  
 match filtered response of, 812–813  
 summary of, 829–830
- Phase comparison monopulse, 702–703
- Phased array antenna, 14, 326–338  
 advantage of, 326  
 characterization of, 353–354  
 issues for, 91–92
- Phased array radar, 349–350
- Phase-derived range (PDR), 45
- Phase drift, 641
- Phase errors  
 on directivity pattern, 316, 317  
 vs. amplitude errors, 316
- Phase-locked dielectric resonator oscillator (PDRO), 442–443
- Phase-locked loop (PLL) bandwidth, 443
- Phase-locked oscillators (PLO), 440  
 for stable local oscillator, 442–443
- Phase noise, 419–421  
 clutter reduction, effect on, 424–425  
 imaging, effect on, 428–429  
 plot, 421  
 pulse-Doppler processing, effect on, 425–428  
 self-coherence effect and, 422–424  
 spectral characteristics, 420–421  
 spectral folding effects and, 421–422  
 spectrum, 440
- Phase quantization error, 329, 330  
 phase-shifter bits and, 330
- Phase shifter, 328–330  
 switched line length, 329
- Phase variation, 312  
 antenna size on, 312
- Phasor addition, 227–229
- Phasor sum, 226
- PHEMT. *See* Pseudomorphic high-electron mobility transistor (PHEMT)
- Pilot pulse, 796
- Plane wave, 213, 311, 327
- Plan position indicator (PPI) displays, 401, 838
- Plateau region, surface clutter, 173, 174
- PLL bandwidth. *See* Phase-locked loop (PLL) bandwidth
- PLO. *See* Phase-locked oscillators (PLO)
- Point scatterers, 228
- Point spread response (PSR), for SAR imaging, 856, 865. *See also* Doppler beam sharpening (DBS), for SAR imaging  
 linear collection, 857–860  
 along-track invariance, 589  
 cross-track variance, 859  
 properties of, 860
- Point target model, 776–777
- Polar formatting algorithm (PFA), 873
- Polarization, 214–215, 836  
 of electromagnetic waves, 10–11  
 measurement of radar, 28–29
- Polarization scattering matrix (PSM), 28, 171  
 for circular polarization, 223–224  
 for linear polarization, 222–223
- Poles, 523
- Police speed measuring radars, 52–53
- Polyphase-coded waveforms, 811–812
- Polyphase codes, 810  
 Barker, 824, 825  
 Frank codes, 824, 825–827  
 P1 code, 827  
 P2 code, 827  
 P3 code, 827–829  
 P4 code, 827–829  
 Doppler tolerance of, 829
- Poseidon Scientific, 441, 442
- Power  
 PPP measurements of, 669–670  
 from target, 62–64
- Power amplifier (PA), 339, 347, 364
- Power-aperture form, of RRE, 80
- Power-aperture-gain product (PAG), 350, 368
- Power-aperture product, 79, 350
- Power-aperture space, 319
- Power density, 10  
 transmission of, 10
- Power law spectra, 190, 192
- Power sources, 356–370  
 amplifiers, 361–364  
 microwave power modules (MPM), 369–370  
 oscillators, 359–361  
 solid-state devices, 364–369
- Power spectral density (PSD), 65, 166, 187, 427
- Power spectrum, in random signal, 533–534
- Power supplies, 373–375  
 high voltage, 349, 373–374  
 for solid-state amplifiers, 374–375
- Poynting vector, 214
- PPI. *See* Plan position indicator (PPI) displays
- PPP. *See* Pulse pair processing (PPP)
- PPS. *See* Pulses per second (PPS)
- Precision and accuracy, in radar measurements, 678–681  
 effects of noise on, 679–681  
 error sources, 678–679, 682–683, 684  
 performance considerations and, 681–683  
 resolution and sampling density and, 681  
 signal propagation and, 682  
 in target shooting, 678
- Pre-T/R tubes, 396
- PRF. *See* Pulse repetition frequency (PRF)
- PRI. *See* Pulse repetition interval (PRI)
- Principles of Modern Radar: Basic Principles*, 3
- Probabilistic data association filter (PDAF), 765–766

- Probability density function (PDF), 96, 166, 185, 253, 427, 532–533, 552, 583, 596, 679, 687. *See also* Swerling models  
of amplitude voltage, 258  
chi-square of degree 2, 254, 256  
of clutter, 583  
cumulative distribution function and, 186  
effect of grazing angle on, 193  
exponential, 253, 254, 255, 256, 257  
fourth-degree chi-square, 254, 255, 256  
gamma, 256  
log-normal distribution, 256, 257  
one-parameter, 256  
Rayleigh, 253, 254, 256  
two-parameter, 256  
Weibull, 256, 257
- Probability of detection, 96–111, 598  
average, 599
- Probability of false alarm, 96–111
- Process control radars, 48–49
- Programmable DSP module, 474
- Prolate spheroid, 230
- Propagation, electromagnetic waves.  
*See also* Multipath  
atmospheric refraction. *See* Refraction  
attenuation. *See* Attenuation, of  
electromagnetic waves  
bistatic, 119  
diffraction. *See* Diffraction  
factor, 118–119  
ionosphere, exploiting. *See* Ionosphere  
monostatic, 119  
paths, 119–121  
regions, 119–121  
turbulence. *See* Atmospheric turbulence
- PSD. *See* Power spectral density (PSD)
- Pseudomorphic high-electron mobility transistor (PHEMT), 365
- Pseudorandom biphasic modulation, intrapulse, 437–438
- PSM. *See* Polarization scattering matrix (PSM)
- PSR. *See* Peak sidelobe ratio (PSR); Point spread response (PSR)
- Ptolemy system, 483
- Pulse  
biphase-coded, 30  
chirp, 30  
compression, 30, 74–75, 222, 371  
gain, 788  
waveform. *See* Pulse compression  
waveforms  
frequency modulation of, 847  
phase-coded, 30  
width, 20
- Pulse cancellers, MTI, 631–634  
frequency response of, 632
- Pulse compression waveforms  
amplitude modulation, 787  
defined, 773  
Doppler modulation in, 807  
LFM waveform, 787–788  
matched filter, 774–782  
phase-coded waveforms, 788
- Pulse-Doppler processing, 644, 696  
advantages of, 646  
blind zones, 660  
for detection of moving targets, 645  
metrics for, 657–659  
with DFT, matched filter and filterbank  
interpretations of, 652–653
- Doppler spectrum  
SNR in, 651–652  
and straddle loss, sampling, 648–651
- DTFT, of constant-velocity target, 646–648
- dwelt-to-dwell stagger, 659  
effect of phase noise on, 425–428  
fine doppler estimation, 653–655  
modern spectral estimation in, 656–657
- PRF regimes and ambiguity resolution, 660–664  
transient effects, 664–665
- Pulse-Doppler spectrum, 665
- Pulsed radar, 348–349
- Pulsed radar Doppler data acquisition  
data matrix and Doppler signal model, 627–628  
generic Doppler spectrum for single  
range bin, 628
- Pulsed waveform, 20
- Pulse-forming network (PFN), 371–372
- Pulse-limited case, scattering  
coefficients, 170
- Pulse pair processing (PPP), 668–673  
for doppler and range rate  
measurements, 699  
power, measurements of, 669–670
- Pulse repetition frequency (PRF), 20–21, 70, 89, 190, 348, 350, 418, 468, 627  
regimes, advantages and disadvantages  
of, 661–662  
regimes and ambiguity resolution, 660–664  
regimes in airborne radar, advantages  
and disadvantages of, 662  
staggered, blind speeds and, 634–637
- Pulse repetition interval (PRI), 20, 89, 486, 502, 548, 549, 627  
timing, 418
- Pulses per second (PPS), 21
- Pulse-to-pulse decorrelation, 558, 579, 580
- Pulse-to-pulse stagger, 635, 636
- Pushing factors, 379
- Pythagorean theorem, 857
- Q**
- Q. *See* Quadrature (Q)
- QRD. *See* Q-R decomposition (QRD)
- Q-R decomposition (QRD), 485
- Quadratic phase, LFM waveform and, 791
- Quadratic phase error (QPE), 863
- Quadrature (Q), 98  
components, 420  
frequency value, 844
- Quadrature codes, 810, 824
- Quantization, 496, 504–506  
binary representations of numeric  
data, 502  
error, 505  
noise, 505
- R**
- RACEway (ANSI/VITA 5–1994), 477
- RACEway protocols, 476
- Radar(s)  
air defense systems, 40  
airport surveillance, 49  
altimeters, 53–54  
artillery locating, 48  
automotive collision avoidance, 53  
bands, 8  
basic configurations, 18  
BMD, 40–41  
classification of, 376  
cloud attenuation as, 16  
coherent system, 23  
concepts of, 4–5  
datacube, 502–503  
design, 557  
equation, 169  
exciters. *See* Exciters  
functions of, 33–36  
imaging of, 34–36  
instrumentation of, 45–46  
marine navigation, 51–52  
measurements of, 27–32  
military applications, 36–37  
multiple functions of, 47–48  
noise detection, 25–26  
noncoherent system, 23  
over-the-horizon search, 40–41  
overview, 3–4  
police speed measuring, 52–53  
process control, 48–49  
satellite mapping, 52  
search/detect, 33

- Radar(s) (*cont.*)
- search mode
    - overview, 87–89
    - phased array antenna issues, 91–92
    - search-and-track, 93–94
    - search regimens, 92–93
    - search time, 90–91
    - search volume, 90
    - track-while-scan, 93
  - semiactive seekers in, 43
  - target identification of, 48
  - three-dimensional search, 39–40
  - track, 33–34
  - transmission/reception process, 5
  - two-dimensional search, 37–39
  - wake vortex detection, 51
  - weather, 49–51
- Radar-absorbing material (RAM), 18
- Radar antennas, 309–343
- architectures of, 339–343
    - active array, 339–341
    - passive array, 339
    - subarray, 341–343
  - beamwidth of, 312
  - directivity for, 313
  - directivity pattern of, 312
  - on performance, 317–319
  - radiation pattern of, 311–312
    - angular dependence of, 311–312
  - sidelobes of, 313–314
- Radar cross section (RCS), 10, 18, 19–20, 45, 62, 64, 94, 168, 174, 317, 425, 496, 665, 677, 775
- aspect angle. *See* Aspect angle, of RCS
  - complex targets. *See* Radar cross section (RCS), of complex targets
  - customary notation, 222
  - decorrelation, 558–559
  - estimation, 699–700
  - IEEE RCS definition, 219–220
  - intuitive derivation for scattering cross section, 220–222
  - polarization scattering matrix (PSM)
    - for circular polarization, 223–224
    - for linear polarization, 222–223
  - simple target. *See* Radar cross section (RCS), of simple targets
  - solving for, 72
  - statistical models of, 558–560
    - extended, 560
    - Swerling models. *See* Swerling models
- Radar cross section (RCS), of complex targets
- correlation, 258, 259–263
  - echo amplitude, 259, 261
  - length, 259
  - decorrelation of, 259–263
    - frequency agility, 262
  - distribution, 253–258, 259
  - scatterers, 251–252
  - statistical models for, 253–263
- Radar cross section (RCS), of simple targets
- aspect angle of, 249–250
  - conducting spheres, 248
  - corner reflector, 248, 249
  - frequency dependence of, 249–250
- Radar detection
- algorithms, 553
  - scheme, 560–561
- Radar measurements, 751
- angle measurements
    - AOA estimation method. *See* AOA estimation method
    - monopulse technique, 701–703
    - sequential lobing, 700–701
  - coordinate systems, 709
  - doppler and range rate measurements, 696
    - DFT interpolation methods, 698–699
    - DFT methods, 697–698
    - pulse pair processing, 699
  - hypothesis, 552–553
  - with LFM waveforms, 756
  - overview, 677–678
  - parameter estimation
    - Cramèr-Rao lower bound (CRLB), 688–688
    - estimators, 685–686
    - Gaussian case, precision and resolution for, 688–690
    - signal and target variability, 690
  - phase measurement, 695–696
  - precision and accuracy, 678–681
    - effects of noise on, 679–681
    - error sources, 678–679, 682–683, 684
    - performance considerations and, 681–683
    - resolution and sampling density and, 681
    - signal propagation and, 682
    - in target shooting, 678
  - radar signal model, 683–685
  - range measurements
    - resolution and sampling, 690–693
    - split-gate and centroid, 693–695
  - RCS estimation, 699–700
  - of reduced dimension, surveillance radars with, 756–757
  - in sine space, 754–756
  - in stabilized coordinates, 752–754
- Radar range equation (RRE), 26, 88, 118, 317–318
- atmospheric loss, 68–69
  - average power, 83–84
  - average power form of, 73–74
  - clutter, 76–78
  - decibel form of, 72–73
  - as dependent variable, 72
  - dwelt time, 83–84
  - energy form of, 775–776
  - graphical example, 75–76
  - matched filter and, relationship between, 780
  - monostatic, 119
  - multiple-pulse effects, 66–67
  - one way equation, 78–79
  - overview, 59–61
  - power-aperture form of, 80
  - power density at a distance R, 61–62
  - received power from target, 62–64
  - receive loss, 69
  - search form of, 79–80, 318–319
  - signal processing loss, 69–72
  - signal-to-noise ratio and, 66
  - summary of losses, 67–68
  - target RCS effect, 84
  - track form of, 80–83
  - for tracking, 318
  - transmit loss, 68
- Radar receivers. *See* Receiver(s)
- RADARSAT 2, resolution modes, 52
- Radar signal model, 683–685
- Radar signal processor
- algorithm metrics, 464
  - counting FLOPS
    - choosing efficient algorithms, 470–472
    - general approach, 464–468
    - mode-specific formulas, 468–470
  - fixed point *versus* floating point, 480–482
  - hardware metrics, 462–464
  - implementation technology
    - analog-to-digital conversion, 472–473
    - comparison of, 474
    - COTS technology and modular open architectures, 476–478
    - Moore’s law, influence of, 478–480
    - processor technologies, 473–475
  - major elements of, 459
  - overview, 459–460
  - sizing
    - benchmarks, 483–485
    - considerations in estimating timing, 482–483
    - data rates, 485–487

- onboard *versus* offboard processing, 487–488
- software tool impacts, 485
- structure, 460–462
- Radar signals
  - nonfluctuating, 561–562
    - detector for, 561–562, 566–570
    - performance for, 563–566
    - threshold detection of, 560–584
    - unknown parameters of, 561
- Radar spectrum engineering criteria (RSEC), 376, 377, 378
- Radar tracking algorithms
  - kinematic motion models, 746
    - NCA motion model, 749
    - NCV motion model, 747–749
    - nearly constant speed motion model, 750–751
    - Singer motion model, 749–750
  - measurements, 751
    - with LFM waveforms, 756
    - of reduced dimension, surveillance radars with, 756–757
    - in sine space, 754–756
    - in stabilized coordinates, 752–754
  - measurement-to-track data association, 760–761
    - formation of new track, 762
    - measurement validation and gating, 762–763
    - nearest neighbor (NN) filter, 764
    - probabilistic data association filter (PDAF), 765–766
    - strongest neighbor (SN) filter, 764–765
  - performance assessment of, 766–767
  - target tracking
    - data association, 713–716, 717
    - detection processing, 717
    - functional areas, 717–718
    - in modern radar systems, 716, 717
    - parameter estimation, 717
    - track filtering. *See* Track filtering
- Radar video signal, 391–392
- RADC. *See* Rome Air Development Center (RADC)
- Radial velocity, 677
- Radii of curvature, 230
- Radio-acoustic sounding systems (RASS), 50
- Radio frequency (RF), 4, 138, 184, 347, 349, 350, 351, 431, 434, 776
  - bands, 8
  - hardware, 682
  - oscillator, 347
  - phase shifters, 349, 350
  - power, 350, 351
  - preselection, 396–397
  - signal, 393
  - subassembly, 447
    - with SMT assembly technique, 447–448
- Rain rate
  - equivalent, snow *vs.*, 129
  - one-way attenuation and, 125–126, 127
- Rain reflectivity
  - atmospheric clutter and, 196–199
    - versus* frequency band, 197
- RAM. *See* Radar-absorbing material (RAM)
- Ramp rate, 790
- Random phase errors, 316, 317
- Random processes, 532
- Random signals, 532–535
  - autocorrelation function, 533
  - cross-correlation function, 533
  - moments and, 533–534
  - power spectrum, 533–534
  - probability density functions, 532–533
  - time averages, 535
  - white noise, 534–535
- Random tracking index, 731
- Random variable (RV), 679
- Range, 27–28
  - ambiguity, 22
  - bins, 502
  - coverage, 629
  - frequency, 514
  - gates, 502, 691
  - measurements
    - resolution and sampling, 690–693
    - split-gate centroid method, 693–695
  - migration, 469, 548, 628
  - rate, 677
  - resolution. *See* Range resolution
  - sampling, 21–22
  - window, 684, 690
- Range-Doppler coupling, 695, 803–805
  - spectral interpretation of, 806–807
- Range-Doppler coupling coefficient, 736
- Range-Doppler imaging, SAR as, 839–842
  - azimuth, 840–841
  - for coarse resolutions, 841
  - cone angle, 840
  - Doppler filter bandwidth, 841
  - Doppler filtering, 841
  - dwelt time, 841
  - velocity vector, 842
- Range-Doppler spectrum
  - for moving radar, 296–303
    - clutter. *See* Clutter, moving radar
    - range and velocity ambiguity, 300–303
    - for stationary radar, 295–296
  - Range migration algorithm (RMA), 873
  - Range-profiling, 439
  - Range resolution, 29, 690–692, 773, 782
    - computation of, 785
    - defined
      - by Rayleigh criterion, 783–784, 785–786
      - in terms of mainlobe width, 784
    - degraded/reduced, 784
    - improved/enhanced, 784
    - requirements of, 782–783
    - two point targets, 785–786
    - waveform bandwidth and, relationship between, 784–785
    - Woodward constant, 784
- RASS. *See* Radio-acoustic sounding systems (RASS)
- Rayleigh criterion, 783–784, 785–786
  - for resolution, 844
- Rayleigh distributed interference, 591, 592
- Rayleigh distribution, 557, 563, 569
  - of noise, 105
- Rayleigh PDF, 98, 253, 254, 256
- Rayleigh (peak-to-null) Doppler resolution, 627
- Rayleigh scattering, 225
- Rays
  - bending of, 131
  - path of, 131, 132
- RCS. *See* Radar cross section (RCS)
- Real-beam ground mapping (RBGM), 837–838
- Real floating-point operations (RFLOP), 465
- Received phase, 419
  - measurement of, 419–420
- Receive loss, 69
- Receiver circuits, 4
- Receiver/exciter (REX), 418
- Receiver operating characteristics (ROC), 96, 556, 602
  - for CFAR algorithms, 617–618
  - for generalized censored mean level detector, 619
- Receiver operating curves, 102–103
- Receiver(s)
  - analog-to-digital data conversion, 409–414
    - digital up/down frequency conversion, 414
  - direct digital coherent detection implementation, 412–414
  - spurious-free dynamic range, 412

- Receiver(s) (*cont.*)  
 channelized, 395–396  
 crystal video, 393  
 demodulation  
   analog coherent detection  
     implementation and mismatch  
       errors, 403–404  
   coherent, 402–403  
   noncoherent, 400–402  
 digital, 395  
 dynamic range, 406  
   coupling issues, 409  
   gain control, 408–409  
   sensitivity time control, 407–408  
 functions, 392  
   frequency downconversion and  
     mixers, 397–399  
   LO and if frequencies, selection of,  
     399–400  
   receiver protection, 396  
   RF preselection, 396–397  
 homodyne, 394  
 instantaneous frequency measurement,  
   395  
 major elements, 392  
 noise power, 404–406  
 overview, 391–392  
 radar video signal, 391–392  
 superheterodyne, 394–395  
 superregenerative, 393  
 types, 392–396  
 Reciprocal spreading, 508  
 Reciprocity theorem, 171  
 Reconfigurable hardware  
   modules, 474  
 Rectangular gating, 763  
 Rectangular window, 512  
 Reference oscillator, 440  
 Reference window, CFAR  
   target returns in, 603  
 Reference windows, 596  
 Reflection, of electromagnetic waves,  
   17–18  
 Reflection coefficient, 143, 144  
   multipath  
     angle errors, 155  
     classification error, 155–156  
     divergence factor, 151–152  
     Fresnel reflection coefficient,  
       148–150  
     roughness factors, 152–155  
 Reflector antennas, 322–326  
   parabolic, 322–326  
 Refraction, 118, 130  
   anomalous, 134–137  
   effective earth model and, 134  
   index of, 130  
   Snell's law and, 131, 132  
   standard, 130  
   standard atmosphere and, 131–134  
 Refractive index, 130  
 Relative phase, waves, 9  
 Resolution, 843–844  
   cross-range, 845–846  
   down-range resolution, 845  
   fine range resolutions, 846  
   integration angle, 845  
   measurement of radar, 29–32  
     concept of, 30  
     frequency of, 32  
     range in, 29  
   pulse, frequency modulation of, 847  
   range. *See* Range resolution  
   Rayleigh criterion for, 844  
   and sampling, 851–852  
   short pulses, 846  
   spatial, 843  
   stepped frequency waveform,  
     846–847  
 Resonance region, 174  
 Resonant region scattering, 225–226  
 Resource manager, 93  
 REX. *See* Receiver/exciter (REX)  
 RF. *See* Radio frequency (RF)  
 RFLOP. *See* Real floating-point  
   operations (RFLOP)  
 RHC. *See* Right-handed circular (RHC)  
 Richards, M. A., 303  
 Rician PDF, 100, 564, 570  
 Right-handed circular (RHC), 150  
   components, 223  
 RMA. *See* Range migration algorithm  
   (RMA)  
 Rms. *See* Root mean square (rms)  
 Rms bandwidth ( $B_{rms}$ ), 689  
 RMSE. *See* Root mean squared error  
   (RMSE)  
 Rms time duration, ( $\tau_{rms}$ ), 689  
 ROC. *See* Receiver operating  
   characteristics (ROC)  
 Rome Air Development Center  
   (RADC), 191  
 Root mean squared error (RMSE), 682,  
   687, 725  
 Root mean square (rms), 173  
   noise, 27  
 Root sum of squares (rss), 682  
 Roughness factors, multipath, 152–155  
 Rough surface theory, 173  
 RRE. *See* Radar range equation (RRE)  
 RSEC. *See* Radar spectrum engineering  
   criteria (RSEC)  
 Rss. *See* Root sum of squares (rss)  
 RV. *See* Random variable (RV)
- ## S
- Sampled signals, vector representation of,  
 501  
 Sampling, 496  
   interval for, 497  
   nonbaseband signals, 501  
   Nyquist theorem, 496, 497–501  
 SAR. *See* Synthetic aperture radar (SAR);  
   Specific absorption rate (SAR)  
 Satellite mapping radars, 52  
 Saturation, 505  
 SAW. *See* Surface acoustic wave (SAW)  
 S-band frequency, 15  
 SBC. *See* Single board computers (SBC)  
 SBO. *See* Shoe-box oscillator (SBO)  
 SBX. *See* X-Band (SBX) radar  
 Scalloping loss, 91, 333  
 Scan-to-scan decorrelation, 558, 578, 580  
 Scattered field, 215, 218–219  
 Scattered power density, 220  
 Scattering, 17, 224  
   atmospheric volumetric, 118,  
     121–122, 168  
   coefficients, 169–171  
   diffuse, 153–154  
   specular, 152–153  
   diffuse, 17–18  
   high-frequency optics region, 226–227  
   Rayleigh scattering, 225  
   resonant region scattering, 225–226  
   specular, 17–18  
 SC-cut crystal oscillator, 440  
 SC-cut quartz crystal oscillator. *See*  
   Stress-compensatedcut (SC-cut)  
   quartz crystal oscillator  
 Schwartz inequality, 780  
 SCI (IEEE 1596–1992), 477  
 Scintillation, 678, 690  
 SCR. *See* Signal-to-clutter ratio (SCR);  
   Silicon-controlled rectifiers (SCR)  
 SE. *See* Spectrum efficiency (SE)  
 Sea clutter, 193  
   correlation properties, 194–195  
   GTRL, model equations, 204  
   sea spikes, 195–196  
   spatial variations, 196  
   spectral properties, 195  
 Search mode, radar, 33  
   overview, 87–89  
   phased array antenna issues, 91–92  
   search-and-track, 93–94  
   search regimens, 92–93  
   search time, 90–91  
   search volume, 90  
   track-while-scan, 93  
 Search radars, and low frequency,  
   318–319

- Sea reflectivity, 180  
 angular and frequency dependencies, 182–183  
 ducting, 184–185  
 GTRI empirical model and, 203  
 physical parameters affecting, 181
- Sea spikes, 195–196
- Sea states, 181  
 physical properties for various, 147–148
- Second-degree non-central chi square (NCCS2), 559
- Self-coherence effect, phase noise and, 422–424
- Self-masking, target, 603–604
- Semiactive seekers, 43
- Sensitivity time control (STC), 395  
 receiver dynamic range and, 407–408
- Sensor measurement vector, 720
- Sensor-noise only (SNO) covariance, 733
- Sequential lobing, 320, 700–701
- Serial RapidIO, 477
- SFDR. *See* Spurious-free dynamic range (SFDR)
- Shadow region, 120
- Shadows, imaging, 877–879  
 cross-range extent of, 277  
 length of, 277, 878  
 RF energy, 275, 276  
 size and shape of, 878  
 solid objects, 276, 277  
 width of, 277
- Sheared ridge, 804
- Shift-invariant, 523
- Shift register, 822
- Ship-based standard missile (SM), 43
- Shnidman's equation, 581–583  
 vs. Albersheim's equation, 582–583
- Shoe-box oscillator (SBO), 442
- Short-time pulse, 846
- Shuttle Imaging Radar-C (SIRC), 469
- Shuttle Imaging Radars (SIR), 52
- Sidelobe clutter, 298
- Sidelobes, 14, 226, 782, 792  
 performance of, LFM waveform and, 793–794  
 range measurement and, 693  
 reduction in LFM waveform, 797–800  
 structure of LFM waveform, 805  
 time, 800
- Sidelooking airborne radar (SLAR), 838
- Sifting property, 498
- Signal-plus-noise PDF, 100–102
- Signal-plus-noise-to-noise ratio, 685
- Signal Processing Designer by CoWare, Inc., 483
- Signal processing exercise, SAR imaging, 842–843  
 data acquisition, 843  
 image formation, 843  
 synthesis, 842
- Signal processing loss, 69–72
- Signal processor, 4
- Signal quantization, 678
- Signal-to-clutter ratio (SCR), 59, 189, 422  
 determination of, 425–427
- Signal-to-interference-plus-noise-ratio (SINR), 590  
 CA-CFAR performance and, 600  
 CFAR loss and, 601–602
- Signal-to-interference ratio (SIR), 59, 189, 427, 630
- Signal-to-noise ratio (SNR), 14, 25–26, 59, 189, 411, 495, 679, 717, 773  
 in Doppler spectrum, 651–652  
 loss, 566  
 loss associated with Taylor weighting function, 798  
 radar performance and, 775  
 radar range equation and, 66, 775–776
- Signal-to-noise ratio (SNR), 318, 548, 556, 564, 886–887
- Signal-to-quantization noise ratio (SQNR), 473, 505
- Signal variability, 690
- Signal windowing techniques, 693
- Sign-magnitude, 504  
 encoding, 504
- Silicon-controlled rectifiers (SCR), 372
- Simple pulse  
 ambiguity surface for, 802  
 match filtered response for, 781  
 spectrum of, 785
- Simulink, 483
- Simultaneous lobing technique, 701
- Sinc function, 278
- Sinc response, 31
- Sine space, 330  
 measurements in, 754–756
- Singer motion model, 749–750
- Single board computers (SBC), 462
- Single canceller, 631
- Single-pole single-throw (SPST) RF switch, 449
- Single-pulse signal-to-noise ratio (SNR), 88
- Single range bin, generic Doppler spectrum for, 628
- Single-sideband frequency converter, 432–433
- Single-sideband phase noise, 420
- Single-transmit pulse, timing for, 453
- Singular value decomposition (SVD), 485
- SINR. *See* Signal-to-interference-plus-noise-ratio (SINR)
- SIR. *See* Shuttle Imaging Radars (SIR); Signal-to-interference ratio (SIR)
- SIRC. *See* Shuttle Imaging Radar-C (SIRC)
- Sizing, signal processor  
 benchmarks, 483–485  
 considerations in estimating timing, 482–483  
 data rates, 485–487  
 onboard *versus* offboard processing, 487–488  
 software tool impacts, 485
- Skin depth, 156–158
- Skip, 17
- Skirt region, 295
- Skirts of filter, 435
- Slant plane, 879, 881, 887
- Slant range, 855  
 azimuth extent, 841  
 cross-track range and, 838  
 DBS image, 861, 862, 864  
 fine resolutions, 853  
 layover, 880  
 PSR, 857–858, 860  
 SNR, 886
- SLAR. *See* Sidelooking airborne radar (SLAR)
- Sliding window estimator, 721, 757
- Slow AGC, 408
- Slow time, 502  
 SAR data acquisition, 842
- SM. *See* Ship-based standard missile (SM)
- Smallest-of CA-CFAR (SOCA-CFAR), 608, 612–613, 618  
 CFAR loss associated with, 610, 613  
 ROC for, 616–617
- Smoke, and attenuation, 130
- SMT devices. *See* Surface mount technology (SMT) devices
- Snell's law, 131, 132, 215
- SN filter. *See* Strongest neighbor (SN) filter
- SNO covariance. *See* Sensor-noise only (SNO) covariance
- Snow, and attenuation, 128–129  
*versus* equivalent rainfall rate, 129  
 types, 129
- SNR. *See* Signal-to-noise ratio (SNR)
- Solid-state active-aperture arrays, 368–369  
 high-power density, 368  
 low-power density, 368

- Solid-state amplifiers, 364–367, 369  
 analog, 366  
 class of operation of, 366–367  
 Solid-state devices, 364–370  
 advantages of, 365–366  
 drawbacks of, 366  
 vs. vacuum tube devices, 364,  
 365–366  
 Solid-state power amplifiers  
 (SSPA), 371  
 Solid-state technology, 356, 364, 367  
 Solid-state Transmitter/Receiver modules,  
 367–368  
 Space-based radars, 140  
 Space-fed feed system, 354, 355  
 Space-time adaptive processing (STAP),  
 96, 402, 460, 468, 503, 642, 717  
 Spatial distributions, land clutter,  
 192–193  
 Spatial Doppler signal, 627  
 Spatial frequency, 7, 513–514, 863–864  
 Spatial locality, 464  
 Spatial resolution, 843  
 SPEC. *See* Standard Performance  
 Evaluation Corporation (SPEC)  
 commercial benchmarks  
 Specific absorption rate (SAR), 384  
 Speckle, 881–884  
 multilook processing, 882–884  
 Speckle-reduction procedure. *See*  
 Multilook processing, speckle  
 Spectral folding effects  
 phase noise and, 421–422  
 Spectral width, 50, 669, 699  
 Spectrum efficiency (SE), 376  
 Spectrum engineering, 376, 377  
 Spectrum management, 376  
 activities of, 376  
 Specular point, 229  
 Specular scattering, 17, 152–153, 226,  
 229–231  
 Specular spike, 236  
 Speed of light, 5  
 Spherical coordinates, 27, 709  
 Spherical waves, 213  
 intensity of, 10  
 Spikes, sea, 195–196  
 Split-gate centroid method, 693–695  
 Split-gate tracker, 693–694  
 Spook-9, 46  
 Spotlight SAR collection, 847–848  
 SPST RF switch. *See* Single-pole  
 single-throw (SPST) RF switch  
 Spurious-free dynamic range (SFDR),  
 411, 412, 413  
 SQNR. *See* Signal-to-quantization noise  
 ratio (SQNR)
- Square law detector, 98, 400, 537, 563,  
 572–575, 592, 598  
 Neyman-Pearson, 592, 594–595  
 for nonfluctuating target, 573–575  
 SSPA. *See* Solid-state power amplifiers  
 (SSPA)  
 Stabilized coordinates, measurements in,  
 752–754  
 Stable local oscillator (STALO), 441–442  
 phase-locked oscillators for, 442–443  
 phase noise, 424  
 Staggered PRFs, blind speeds and,  
 634–637  
 Stagger ratio, 635  
 STALO. *See* Stable local oscillator  
 (STALO)  
 Standard missile, 43  
 Standard Performance Evaluation  
 Corporation (SPEC) commercial  
 benchmarks, 483  
 STAP. *See* Space-time adaptive processing  
 (STAP)  
 State estimate, 719  
 Stationary phase point, 229  
 STC. *See* Sensitivity time control (STC)  
 Steering vector, 566  
 Stepped chirp, 788  
 Stepped frequency waveforms, 788,  
 846–847  
 Stochastic state estimation, 719,  
 728–730  
 CWNA, nearly constant velocity  
 filtering with, 736–739  
 DWNA, nearly constant velocity  
 filtering with, 730–736  
 LFM waveforms, nearly constant  
 velocity tracking with, 736  
 multiple model filtering for highly  
 tracking maneuvering targets,  
 741–746  
 nearly constant acceleration filtering,  
 739–741  
 Stop-and-hop model, 627, 854  
 “Stove pipe” aircraft, 239–243  
 Straddle loss, 515–516, 516–518, 684,  
 782, 786–787  
 reduction, LFM waveform and, 800  
 sampling Doppler spectrum and,  
 648–651  
 Stratosphere, 120  
 Streaming processing, 460  
 Stress-compensatedcut (SC-cut) quartz  
 crystal oscillator, 433  
 Stretch processing, 473, 787  
 LFM, 847  
 Stripmap SAR, 14, 847  
 Strongest neighbor (SN) filter, 764–765
- Subarray architecture, 341–343  
 advantage of, 341–342  
 analog time delay units (TDUs) in,  
 341–343  
 overlapped, 343  
 Subclutter visibility, 637  
 Subreflector, 324, 325  
 Subrefraction, anomalous atmosphere,  
 135  
 Sum beam, 320  
 Summation point, defined, 311  
 Superheterodyne receivers, 394–395  
 Superposition  
 of electromagnetic waves, 9–10.  
*See also* Interference  
 multipath, 144–145  
 Superrefraction, anomalous  
 atmosphere, 135  
 Superregenerative receiver, 393  
 Surface  
 clutter. *See* Surface clutter  
 diffraction, 118  
 intervisibility, 118  
 multipath, 118  
 reflectivity, 169  
 wave  
 effects, 226  
 scattering, 226  
 Surface acoustic wave (SAW)  
 devices, 795  
 oscillators, 438, 443–444  
 Surface boundary, and multipath, 146–148  
 Surface clutter, 77, 202–205  
 general dependencies, 172–175  
 temporal and spatial variations,  
 175–177  
 value data, experimental programs  
 land reflectivity, 177–180  
 sea reflectivity, 180–185  
 variability of  
 land clutter, 185–193  
 sea clutter, 193–196  
 Surface mount technology (SMT) devices,  
 446–448  
 Survey, of image formation, 873–874  
 SVD. *See* Singular value decomposition  
 (SVD)  
 SW0. *See* Swerling 0 (SW0)  
 Sweep rate, 790  
 Swerling models, 263–267, 559–560, 578,  
 579, 580  
 analyzing detection performance, 264  
 concept, 263  
 correlation model, 266  
 CPI, 264  
 detection performance of, 580  
 extension strategy, 267

PRF, 263–264  
 pulse-to-pulse decorrelation, 264, 266  
 scan-to-scan decorrelation, 264,  
 265, 266  
 Swerling 0 (SW0), 103  
 Swerling 2 target, 700  
 Swerling 1 target model, 107–108  
 Switches  
   for exciters, 449–450  
 Synthesizers, 444–446  
 Synthetic aperture radar (SAR), 28, 165,  
 530, 549, 596, 782, 835–837.  
   *See also* Imaging, SAR  
   advantage, 836  
   beamwidth, 838  
   data collection, 852–856  
   geometry for, 35  
   as large synthetic antenna aperture,  
   837–839  
   overview, 835  
   processing, 402, 459  
   as range-Doppler imaging, 839–842  
   sampling requirements, 849–851  
     along-track sampling limit, 850  
     pulsed waveform, 849  
   SAR imaging vs. optical imaging, 835,  
   836, 837  
   as signal processing exercise, 842–843  
 Synthetic wideband waveforms, 788  
 System noise temperature, 405

**T**

Tangential signal sensitivity (TSS), 401  
 Target  
   detection, strategies for, 548–552  
   masking, 600  
     mutual, 601, 604–605  
     self, 603–604  
   motion model, 719  
   position, 27  
   RCS. *See* Radar cross section (RCS)  
   reflectivity. *See* Target reflectivity  
   tracking. *See* Target tracking  
   variability, 690  
   visibility, 640  
 Target motion resolution (TMR), 45  
 Target reflectivity  
   EM wave, 211  
   characteristics of, 212  
   fundamentals, 212–214  
   polarization, 214–215  
   reflection, 215–219  
   examples, 236–243  
   high-frequency scattering  
     edge diffraction, 232–234  
     end-region scattering, 231–232  
     multiple-bounce scattering, 235–236

  phasor addition, 227–229  
   specular scattering, 229–231  
 RCS. *See* Radar cross section (RCS)  
 scattering regimes, 224  
   high-frequency optics region,  
   226–227  
   Rayleigh scattering, 225  
   resonant region scattering, 225–226  
 Target tracking  
   data association, 713–716, 717  
   detection processing, 717  
   functional areas, 717–718  
   in modern radar systems, 716, 717  
   parameter estimation, 717  
   track filtering. *See* Track filtering  
 Taylor aperture tapers, 316  
 Taylor function, 315, 321  
 Taylor weighting function  
   defined, 797  
   Rayleigh resolution associated  
     with, 798  
   SNR loss associated with, 798  
   straddle loss reduction, 800  
 TDRSS. *See* NASA' Tracking and Data  
   Relay Satellite System (TDRSS)  
 TDU. *See* Time delay units (TDU)  
 TE diffraction. *See* Trailing-edge (TE)  
   diffraction  
 TEMPER. *See* Tropospheric  
   Electromagnetic Parabolic  
   Equation Routine (TEMPER)  
 Temporal locality, 464  
 Terrain Integration Rough Earth Model  
   (TIREM), 158  
 Texas Instruments, Inc. (TI), 474  
 THAAD. *See* Theater High Altitude Air  
   Defense (THAAD)  
 Theater High Altitude Air Defense  
   (THAAD), 42, 43  
 Thermal noise, 25  
   receiver, 64–65  
 Thermosphere, 121  
 Three-dimensional search, radar, 39–40  
 Three-pulse canceller, 631–634  
 Threshold detection, 553–554, 560–584  
   concept of, 95–96  
 Thumbtack ambiguity surface, 817  
 Thunderstorms, 198  
 Time-bandwidth product, 696, 791, 793,  
   799–800, 804, 805, 810, 823  
 Time delay units (TDU), 337, 338  
 Time sidelobes, 800  
 Timing and control circuits, for exciters,  
   452–454  
 Timing jitter, 453  
 TIREM. *See* Terrain Integration Rough  
   Earth Model (TIREM)

TKMOD5C, 158  
 TM-CFAR. *See* Trimmed mean  
   (TM)-CFAR  
 TMR. *See* Target motion resolution  
   (TMR)  
 Toeplitz matrices, 541  
 Tomographic methods, image formation  
   survey, 873  
 T/R. *See* Transmit/receive (T/R) module  
 Track filtering, 34, 678, 713–716, 719  
   converted measurement filter, 760  
   extended Kalman filter (EKF),  
   759–760  
   nonlinear least squares estimation,  
   757–759  
   overview, 713  
   parametric estimation, 720–722  
     constant acceleration filtering,  
     726–727  
     constant velocity filtering, 722–726  
     limiting memory in, 721  
   stochastic state estimation, 728–730  
     CWNA, nearly constant velocity  
     filtering with, 736–739  
     DWNA, nearly constant velocity  
     filtering with, 730–736  
     LFM waveforms, nearly constant  
     velocity tracking with, 736  
     multiple model filtering for highly  
     tracking maneuvering targets,  
     741–746  
     nearly constant acceleration filtering,  
     739–741  
 Tracking, 678. *See also* Target tracking  
   radar application of, 46–47  
 Track partitioning, 763  
 Trailing-edge (TE) diffraction, 233  
 Transient effects, pulse-Doppler  
   processing, 664–665  
 Transition region, 295  
 Transmission bands, 125  
 Transmit loss, 68  
 Transmit/receive (T/R) module, 350, 356  
 Transmit signal, 429–437  
   bandwidth of, 431  
 Transmitters, 4  
   configurations for, 352–356  
   cooling of, 382–383  
   design, 376–378  
   efficiency, 351  
   operation of, 381–384  
   safety in, 383–384  
   parameters of, 350–351  
   power source of, 356  
   classification of, 356  
   reliability of, 381–382  
   MTBF and, 381–382

- Transmitters (*cont.*)  
 on spectral purity, 378–381  
 nontime-varying errors, 380–381  
 time-varying errors, 379–380
- Trapping, anomalous atmosphere,  
 135–136
- Traveling waves, 226
- Traveling-wave tube (TWT), 348, 363,  
 370, 374  
 amplifiers, 433  
 in microwave power modules, 370
- TRF receiver. *See* Tuned radio frequency  
 (TRF) receiver
- Trihedrals, 235, 249, 885
- Trimmed mean (TM)-CFAR, 613–614
- $T_{rms}$ . *See* Rms time duration, ( $\tau_{rms}$ )
- Troposphere, 120
- Tropospheric Electromagnetic Parabolic  
 Equation Routine (TEMPER),  
 159
- T/R tubes, 396
- TSS. *See* Tangential signal sensitivity  
 (TSS)
- Tube amplifiers, 361–364  
 crossed-field, 364  
 linear beam, 361–364
- Tuned radio frequency (TRF)  
 receiver, 393
- Turbulence, atmospheric, 118, 137–138
- Two-dimensional (2-D) data set, 596
- Two-dimensional (2-D) system, 37
- Two-dimensional search, radar, 37–39
- Two-pulse MTI canceller, 631–634  
 frequency response, 636–637
- Two's complement encoding, 504
- TWT. *See* Traveling-wave tube (TWT)
- U**
- UAV. *See* Unmanned aerial vehicles  
 (UAV)
- UAV radars. *See* Unmanned aerial  
 vehicles (UAV)
- UDSF. *See* Usable Doppler space fraction  
 (UDSF)
- UHF. *See* Ultra high frequency (UHF);  
 Ultra high frequency (UHF)
- Ultra high frequency (UHF), 135, 561
- UMOP. *See* Unintentional modulation of  
 pulse (UMOP)
- Unambiguous Doppler coverage, 629
- Unambiguous range, 23, 629
- Underflow, 505
- Unintentional modulation of pulse  
 (UMOP), 378
- Unmanned aerial vehicles (UAV),  
 370, 480
- Upper sideband (USB), 432
- U.S. Firefinder system, 90
- U.S. Military's Common Data Link  
 (CDL), 487
- U.S. Standard Atmosphere, 131
- Usable Doppler space fraction  
 (UDSF), 638
- USB. *See* Upper sideband (USB)
- V**
- Vacuum electron device (VED), 371
- Vacuum tube power booster, 370
- Variance, 533–534, 685–686
- Vector Signal Image Processing Library  
 (VSIPL), 477–478, 485
- VED. *See* Vacuum electron device (VED)
- Velocity  
 ambiguity, 301–302  
 constant velocity (CV). *See* Constant  
 velocity (CV)  
 Doppler shift as function of, 626  
 radial, 677
- Versa module europe (VME), 476
- Very high frequency (VHF), 135
- VHF. *See* Very high frequency (VHF)
- Video filtering, 404
- Virtual sources, 140
- V-LFM, 808
- VME. *See* Versa module europe (VME)
- VME (IEEE P1014–1987), 477
- VME64 (IEEE P1014 Rev D), 477
- “Voltage domain” approach, 469–470
- “Voltage reflectivity,” 683
- Voltage standing wave ratio (VSWR),  
 367, 447
- Volume  
 clutter, 77–78  
 reflectivity, 169
- VSIPL. *See* Vector Signal Image  
 Processing Library (VSIPL)
- VSWR. *See* Voltage standing wave ratio  
 (VSWR); Voltage standing wave  
 ratio (VSWR)
- W**
- Wake vortex detection radars, 51
- Water concentration, 127  
 fog *versus*, 128
- Water vapor, attenuation and, 124–125
- Wave  
 height, 181  
 impedance, 214
- Waveforms  
 bandwidth, range resolution and,  
 784–785  
 biphasic-coded, 788
- CW, 20  
 design methods, 693  
 filtered response, 782  
 generation  
 dwell-to-dwell frequency change,  
 439–440  
 intrapulse, pseudorandom biphasic  
 modulation, 437–438  
 intrapulse linear frequency  
 modulation (LFM), 438–439
- Huffman coded, 787
- interpulse modulation, 787–788
- linear frequency modulated, 787–788
- modulations, 774
- phase-coded, 788
- polyphase-coded, 811–812
- pulse compression, 787–788. *See also*  
 Pulse compression waveforms
- pulsed, 20
- stepped frequency, 788
- synthetic wideband, 788
- Wavelength, of electromagnetic  
 waves, 6
- Wavelet transforms, 485
- Wavenumber, 213, 513. *See also* Spatial  
 frequency
- Weather radars, 49–51
- Weibull distribution, 105, 175–176,  
 186, 194  
 PDF, 256, 257
- Wenzel Associates, 440, 441
- White noise, 65, 534–535, 779  
 acceleration error, 730
- Wideband phased array, 335–338
- Wideband STAP-GMTI radar, 466–467
- Windowing, 509–513
- Woodward constant, range  
 resolution, 784
- WSR-88D (NEXRAD) radar, 50
- WSR-88D Next-Generation Radar  
 (NEXRAD) radar, 670
- X**
- X-band pulsed magnetron, 359
- X-band radar, 433
- X-Band (SBX) radar, 42
- Xilinx, 474
- XPatch, 158
- Z**
- Zeros, 523
- Zero-mean error, 687
- Zero padded signal vector, 652
- Zero padding, 516, 648
- Zero-velocity filter, 664–667
- Z transform, 522–523

# Principles of Modern Radar: Basic Principles

*Principles of Modern Radar: Basic Principles* is a comprehensive and modern textbook for courses in radar systems and technology at the college senior and graduate student level; a professional training textbook for formal in-house courses for new hires; a reference for ongoing study following a radar short course; and a self-study and professional reference book.

*"Principles of Modern Radar engages the radar student, the new radar practitioner, and even the experienced radar designer through its focus on modern radar fundamentals, problem sets stretching these fundamentals, and advanced treatments of signal processing and tracking. That it achieves these results with clear readability and precise mathematics is even more remarkable."*

- Dr. John Milan, radar consultant; formerly 36 years with ITT Gilfillan, IEEE AESS Radar Systems Panel

*Principles of Modern Radar* focuses on four key areas:

- BASIC CONCEPTS, such as the radar range equation and threshold detection;
- RADAR SIGNAL PHENOMENOLOGY, such as radar cross section models, clutter, atmospheric effects, and Doppler effects;
- DESCRIPTIONS OF ALL MAJOR SUBSYSTEMS OF MODERN RADARS, such as the antenna, transmitter, receiver, including modern architectural elements such as exciters, and advanced signal processors; and:
- SIGNAL AND DATA PROCESSING BASICS, from digital signal processing (DSP) fundamentals, through detection, Doppler processing, waveforms and pulse compression, basic imaging concepts, and tracking fundamentals.

While several established books address introductory radar systems, *Principles of Modern Radar* differs from these in its breadth of coverage, its emphasis on current methods (without losing sight of bedrock principles), and its adoption of an appropriate level of quantitative rigor for the intended audience of students and new professional hires.

The manuscript for this book was reviewed by over 50 volunteer professionals (see Acknowledgments) in academia, military, and commercial enterprises. Their extensive comments, corrections, and insights ensure that *Principles of Modern Radar* will meet the needs of modern radar educators and students around the world. Written and edited by world-renowned radar instructors and critically reviewed by users before publication, this is truly a "radar community-driven" book.

## BOOKS OF RELATED INTEREST

*Principles of Modern Radar: Advanced Radar Techniques and Applications* (ISBN 978-1-891121-53-1)

Edited by William Melvin and James A. Scheer

*Pocket Radar Guide: Key Radar Facts, Equations, and Data* (ISBN 978-1-891121-08-1)

By G. Richard Curry



Raleigh, North Carolina  
www.scitechpub.com

ISBN 978-1-891121-52-4

